Short-Term Physical, Chemical and Biological Variability on the Scotian Shelf

B.J.W. Greenan, B. Petrie, G. Harrison,
and N.S. Oakey

Ocean Sciences Division
Maritimes Region
Fisheries and Oceans Canada

Bedford Institute of Oceanography
P.O. Box 1006
Dartmouth, Nova Scotia
Canada B2Y 4A2

2002

Canadian Technical Report of Hydrography and Ocean Sciences 218

Fisheries and Oceans Canada | Pêches et Océans Canada

Canada

102-02987/

Canadian Technical Report of
Hydrography and Ocean Sciences 218

2002

SHORT-TERM PHYSICAL, CHEMICAL AND BIOLOGICAL VARIABILITY ON THE SCOTIAN SHELF

by

B. J. W. Greenan, B. Petrie, G. Harrison,
and N. S. Oakey

Ocean Sciences Division
Maritimes Region
Fisheries and Oceans Canada

Bedford Institute of Oceanography
P. O. Box 1006
Dartmouth, Nova Scotia
Canada B2Y 4A2

© Minister of Supply and Services 2002

Cat. No. Fs 97- 18/218E ISSN 0711-6764

Correct Citation for this publication:

Greenan, B.J.W., B. Petrie, G. Harrison, and N. S. Oakey. 2002. Short-term physical, chemical and biological variability on the Scotian Shelf. Can. Tech. Rep. Hydrogr. Ocean. Sci. 218:xi + 106 pp.

TABLE OF CONTENTS

ABSTRACT	IV
TABLE CAPTIONS	VIII
FIGURE CAPTIONS	VIII
1. INTRODUCTION	1
2. FALL 2000 MOORINGS	3
3. SEAWIFS SCALE ANALYSIS	12
4. HISTORICAL DATA ANALYSIS	14
5. SUMMARY	24
ACKNOWLEDGMENTS	25
REFERENCES	26
TABLES	27
FIGURES	28
APPENDIX A: EPSONDE STATION PROFILES	76
APPENDIX B: ADCP TIME SERIES	88

ABSTRACT

Greenan, B.J.W., B. Petrie, G. Harrison, and N. S. Oakey. 2002. Short-term physical, chemical and biological variability on the Scotian Shelf. Can. Tech. Rep. Hydrogr. Ocean. Sci. 218:xi + 106 pp.

Daily to weekly timescale variability on the Scotian Shelf is studied using a combination of historical data sets and new field data collected in the Fall 2000. The intent of this study is to improve the understanding of the relationship between the physical forcing mechanisms and the response of the chemical and biological fields on these short time scales. This is accomplished through the use of a newly developed mooring platform (SeaHorse) that uses surface wave energy to enable the instrument to climb down the mooring wire and then float upwards while sampling the water column. This provides bi-hourly profiles of CTD and chlorophyll at one location over month-long periods. Results from the Fall 2000 deployment indicate a subsurface chlorophyll maximum below the pycnocline during the first part of the time series. An event occurred in mid-October during which the temperature, salinity and density iso-surfaces rise approximately 25 m in the water column. During the peak of this event, a small bloom begins as nutrients are brought into the upper part of the water column. SeaWiFS ocean color satellite images prove to be valuable in providing a spatial context for chlorophyll concentrations, however, the lack of temporal resolution due to poor quality images means that this data set provides limited information for short-term chlorophyll variability. Using SeaHorse CTD data and ADCP current measurements, a trend of decreasing Richardson number in the ocean mixed layer with increasing surface wind stress has been demonstrated.

One historical data set studied was that of the Canadian Atlantic Storms Program 1985-86 (CASP). The CASP instrument array on the Scotian Shelf consisted of current meters with temperature and conductivity cells, thermistor chains and bottom pressure gauges with temperature sensors. At any single site, the CASP program provided a low-resolution array of ocean currents and hydrographic properties over a 4-month winter period. This data set indicates that wind forcing can contribute substantially to mixing, upwelling and stratification during this period of the year. The duration of upwelling events ranged from several days to a month with strong coherence at all the mooring sites.

Direct measurements of dissipation of turbulent kinetic energy were studied using an existing data set from 1990. The range of wind speeds encountered during this experiment was small and made it difficult to determine if any relationship exists between surface wind stress and turbulent mixing rates.

RÉSUMÉ

Greenan, B.J.W., B. Petrie, G. Harrison, and N. S. Oakey. 2002. Short-term physical, chemical and biological variability on the Scotian Shelf. Can. Tech. Rep. Hydrogr. Ocean. Sci. 218:xi + 106 pp.

La variabilité quotidienne et hebdomadaire sur la plate-forme néo-écossaise est étudiée en combinant des jeux de données historiques et nouveaux recueillis sur le terrain pendant l'automne 2000. Cette étude vise à mieux comprendre la relation entre les mécanismes physiques de forçage et la réaction des agents chimiques et biologiques pour ces courts intervalles. Cette expérience est réalisée en se servant de la plate-forme d'amarrage nouvellement construite (SeaHorse) qui utilise l'énergie des vagues de surface pour permettre à l'instrument de descendre le long du câble d'amarrage avant de remonter à la surface en raison de sa flottabilité tout en échantillonnant la colonne d'eau. Ce procédé fourni des profils de conductivité, de température, de profondeur (CTD) et de chlorophylle toutes les deux heures à un endroit donné, pour des périodes d'un mois. Les résultats obtenus au cours du déploiement de l'automne 2000 indiquent la présence d'une valeur maximale de la chlorophylle sous la pycnocline pendant la première partie de la série chronologique. Un phénomène s'est produit à la mi-octobre pendant lequel les isosurfaces de température, de salinité et de densité se sont élevées d'environ 25 m dans la colonne d'eau. Pendant le maximum d'intensité de ce phénomène, un bloom se développe à measure que les sels nutritifs sont emportés dans la partie supérieure de la colonne d'eau. Des images satellite de la couleur de l'océan recueillies au moyen du SeaWiFS se sont avérées utiles pour l'obtention d'un contexte spatial des concentrations de chlorophylle. Cependant, en raison de l'absence de résolution temporelle résultant d'une faible qualité des images, ce jeu de données fournit peu de renseignements sur la variabilité à court terme de la chlorophylle. À l'aide des données de CTD du SeaHorse et des mesures des courants à l'ADCP, on a réussi à démontrer une tendance à la baisse du nombre de Richardson dans la couche de mélange océanique lorsqu'augmente la tension du vent à la surface.

Un jeu de données historiques du Programme canadien d'étude des tempêtes de l'Atlantique 1985-86 (PCETA) a été examiné. Le réseau d'instruments du PCETA sur la plate-forme néo-écossaise comprend des courantomètres contenant des cellules de conductivité et de

température, des séries de thermistances et des manomètres de fond avec des capteurs de température. À chacun des sites, le PCETA fournissait une représentation à faible résolution des courants océaniques et des propriétés hydrographiques pendant une période hivernale de quatre mois. Ce jeu de données indique que la force d'entraînement du vent peut contribuer de manière importante au mélange, à la remontée et à la stratification de l'eau pendant cette période de l'année. Les remontées duraient de plusieurs jours à un mois avec une forte cohérence à tous les sites d'amarrage.

Des mesures directes de la dissipation d'énergie cinétique turbulente ont été étudiées en se servant d'un jeu de données existantes de 1990. La plage de vitesse des vents pendant cette expérience était peu étendue ce qui n'a pas facilité la détermination d'une relation entre la tension du vent à la surface et les taux de mélange turbulent.

Table Captions

Table 1: Correlations\slopes between alongshore wind stress and currents at CASP Station 3. Correlations are in lower left half, slopes in upper right.

Figure Captions

Figure 1: Map of Scotian Shelf showing the fixed stations (open circles) and monitoring sections (plus signs) which are part of the AZMP. Station 2 on the Halifax Section is the site of SeaHorse and ADCP moorings deployed in the Fall 2000. The 100 and 200 m isobaths are drawn as thick and thin solid lines, respectively. Canadian Atlantic Storms Program (CASP) mooring locations are marked with solid circles.

Figure 2: The SeaHorse mooring profiler uses surface wave energy and a one-way cable clamp to climb down the mooring wire. The photograph shows SeaHorse being prepared for deployment. The schematic includes the Sea-Bird 19 CTD.

Figure 3: Time series of water temperatures measured with Minilog recorders at fixed depths spaced 6 m apart on the mooring wire.

Figure 4: Contour plot of the seven temperature time series recorded with Vemco Minilogs. The Minilogs were spaced 6 m apart starting at 15 m depth and ending at 51 m.

Figure 5: NOAA AVHRR sea surface temperature for the period surrounding the cooling event captured by the Minilog temperature recorders.

Figure 6: Temperature, salinity, density (sigma-t) and chlorophyll at Sta. 2, September 30 – October 18, 2000.

Figure 7: Typical Station 2 (Halifax Section) temperature and salinity profile from the Sea-Bird model 19 CTD. The "spikes" in salinity are caused by different response functions of the temperature and conductivity sensors.

Figure 8: (Upper panel) Along-shore (60°T) wind stress calculated using Sable Island wind data. Positive (negative) stress is upwelling (downwelling) favorable.

Figure 9a: Temperature time series from selected depths at Sta. 2. Gaps indicate that the SeaHorse failed to rise to the top of the mooring during a sampling cycle.

Figure 9b: Salinity time series from selected depths at Sta. 2. Gaps indicate that the SeaHorse failed to rise to the top of the mooring during a sampling cycle.

Figure 9c: Density time series from selected depths at Sta. 2. Gaps indicate that the SeaHorse failed to rise to the top of the mooring during a sampling cycle.

Figure 10: Average top 1 m chlorophyll, temperature, salinity and density from the SeaHorse profiles. In nearly all cases, the top 1 m corresponds to the 7-8 m interval below the sea surface.

Figure 11a: Depth of selected temperature surfaces.

Figure 11b: Depth of selected salinity surfaces.

Figure 11c: Depth of selected density surfaces.

Figure 12a: Spectra of vertical amplitude for selected temperature isopleths. Note that the amplitude corresponds to that associated with the harmonic component at each frequency.

Figure 12b: Spectra of vertical amplitude for selected salinity isopleths. Note that the amplitude corresponds to that associated with the harmonic component at each frequency.

Figure 12c: Spectra of vertical amplitude for selected density isopleths. Note that the amplitude corresponds to that associated with the harmonic component at each frequency.

Figure 13: Top panels: vertical profiles of nitrate and chlorophyll concentrations taken during AZMP cruises to Halifax Line – Station 2. Five dates were selected to bracket the Seahorse deployment of 30 September - 18 October. Bottom panel: column integrals of nitrate and chlorophyll concentrations for same stations. Note: there were no chlorophyll samples for the 7 October station occupation.

Figure 14: Contour plots of nitrate concentrations (upper panel) concentration gradients (lower panel) at Halifax Line – Station during 2000. Vertical lines in both figures between days 270 and 300 represent the Seahorse deployment period.

Figure 15: Integrated chlorophyll from 7-120 m depth as measured by the WetLabs fluorometer on the SeaHorse.

Figure 16a: Nitrate field created from the SeaHorse salinity data using the relationships derived from ship-based CTD and nutrient profiles from September 30, October 7, 17 and 25.

Figure 16b: Silicate field created from the SeaHorse salinity data using the relationships derived from ship-based CTD and nutrient profiles from September 30, October 7, 17 and 25.

Figure 17: Time series of the depth of the 32.5 isohaline and the integrated offshore Ekman flux.

Figure 18: Progressive vector diagram for selected ADCP bins. Each cross marker denotes five days elapsed time

Figure 19: Vertical shear in the water column calculated using RDI ADCP. This includes only ADCP data within 15 minutes of SeaHorse CTD profiles.

Figure 20: Contour plot of buoyancy frequency calculated from the SeaHorse CTD profiles.

Figure 21: Gradient Richardson number calculated by combining ADCP and CTD data from the two moorings at Station 2.

Figure 22: Histograms of Richardson number estimates at four depth intervals for the period 30 Sep – 18 Oct, 2000 at Station 2, Halifax Section. Statistics are included in the legend of each histogram.

Figure 23: Time series of wind stress from Sable Island and Richardson number at Station 2 derived from SeaHorse CTD and ADCP data. The Richardson number represents an average for the depth range of 7-20 m.

Figure 24: Boxplot of Richardson number for the 7-20 m depth range. The data has been binned in 0.05 Pa intervals of wind stress. The horizontal line in the middle of the box is the median, the top of the box is the 3rd quartile, and the bottom is the 1st quartile. If the notches in the sides of two boxes do not overlap, then the medians are significantly different at the 5% level.

Figure 25: SeaWiFS near-surface chlorophyll images for May 1, 1999 1657 UTC (upper panel) and April 6, 2000 1631 UTC (lower panel).

Figure 26: Time series of near-surface chlorophyll average (open circles), standard deviation (dash-dot line) and maximum values (dash line) in a 20 by 20 pixel area centered on Station 2. *In situ* surface chlorophyll measurements at Station 2 are shown as solid circles.

Figure 27: Correlation field from the SeaWiFS images from 1998-1999. The pixel at the centre of the field is at the Station 2 location.

Figure 28: Correlation of near-surface chlorophyll with centre pixel, located at Station 2, as a function of separation. The solid line is a least squares fit of $e^{-\lambda r}$, where $1/\lambda$ is the e-folding scale.

Figure 29: Temperature, salinity and density fields from CASP moorings 1, 2, 3 and 6.

Figure 29 Continued: Temperature, salinity and density from CASP moorings 7, 8, 10 and 11.

Figure 30: Time series of the deepest temperature and salinity records from instruments along the 100 m isobath.

Figure 31: Superimposed time series of the deepest temperature and salinity records from instruments along the 100 m isobath.

Figure 32: Comparison of the temperature, salinity and density fields from mooring 3 with the alongshore wind stress calculated from Sable Island observations.

Figure 33: Comparison of density variability at Sta. 3, 110 m with the alongshore wind stress calculated from Sable Island observations. The density (stress) data have been filtered with a 25 h (5 d) running mean filter.

Figure 34: Time series of alongshore current from station 1, 12 m (solid line) and wind stress (broken line, upper panel). Alongshore current versus stress for the first half of the record (solid dots) and second half (triangles). Both data sets have been filtered with a 5 day running mean filter.

Figure 35: The alongshore currents at Sta. 3, (16, 50, 70 and 110 m, upper panel) and with the mean removed (lower panel). The alongshore wind stress (dotted line) is also plotted in the lower panel. All records had a 25 hour running mean filter applied.

Figure 36: Histogram of Richardson numbers for mooring 3.

Figure 37: Richarson numbers at mooring 3 are plotted against the total and alongshore stress. Six-hour median values (solid black dots) and median of these values in 0.1 Pa bins (grey dots) are also shown. The broken grey line and the number is the Richardson number calculated from the mean density and current shears.

Figure 38: Averaged salinity from 0 to 65 m for Sta. 6, 2, 7, 8 and 10.

Figure 39: (top) Individual profiles have been stacked side-by-side to provide a contour plot of EPSONDE data. The two left-hand panels are temperature and salinity; the middle panels are dissipation of TKE (ε) and mass diffusivity ($K\rho$); the right hand panels are dissipation of thermal variance (χ) and heat diffusivity (Kt). (bottom) bootstrap estimated mean and confidence intervals for the station.

Figure 40: Time series of wind stress calculated using Shearwater winds (top left panel). Time series of ε for 5 m bins in the ocean mixed layer (lower left panels). Depth-integrated dissipation of TKE versus the wind speed cubed (upper right panel, dashed line represents fit of data from Oakey and Elliott, 1982). Scatter plots of wind stress and ε for the various bins (lower right panels).

1. INTRODUCTION

Phytoplankton cells are the fundamental source of energy on which life in the ocean is based. These cells use the sun's energy to convert carbon dioxide, water and dissolved salts into organic compounds, a process known as photosynthesis. The traditional view of the production cycle on the continental shelf features a spring bloom followed by a period of low production. The spring bloom begins with the increase of light levels and the onset of stratification in shelf waters whose nutrient concentrations have built up during the winter. The ocean stratification and weak winds during the summer limit the diffusion of nutrients into the euphotic zone from the nutrient-rich waters below. The low production throughout the summer is followed by a fall bloom driven by an infusion of nutrients into the upper layer that is a consequence of increased meteorological forcing. The fall bloom is typically less intense than the spring bloom due to the decreasing light levels during this time period. The annual cycle of primary productivity thus has a large, low frequency component. However, there is increasing evidence that the production cycle has significant variability on shorter time scales. The time scale of the fluctuations investigated by this study range from daily to weekly. We hypothesize that these high frequency events may be of critical importance in determining the annual cycle of production. The objective of this study is to improve our understanding of the relationship between physical forcing and short-term fluctuations of chlorophyll biomass and the implications of this for primary productivity on the Scotian Shelf.

Primary production is the amount of carbon fixed by organisms through photosynthesis. Most methods to estimate marine primary productivity require information on chlorophyll. Estimates of chlorophyll in the upper ocean for the Canadian East coast are available as biweekly composites of SeaWiFS satellite images from the Biological Oceanography Section of the Ocean Sciences Division, BIO. The images cover the period September 1997 to present. The chlorophyll concentrations for the central Scotian Shelf, which includes Emerald Basin and Station 2 (Halifax Line, fixed station of Atlantic Zonal Monitoring Program; Figure 1), show significant temporal variability. The median concentration is 1.6 mg/m^3, with a range of 8 and a standard deviation of 1.5 mg/m^3. While much of this variability is caused by spring and fall blooms, the biweekly differences indicate that there is a significant high frequency component.

The average biweekly difference over the entire period is 0.4 mg/m^3, with a maximum of 4.5 and a standard deviation of 1.4 mg/m^3. This leads to the suggestion that there is significant variability at high frequencies that could have implications for the integrated total production.

Nutrients must be available to account for the production either through recycling in the euphotic zone or through advection and diffusion into the upper layer from nutrient-rich deeper waters. Petrie and Yeats (2000) have shown that vertical diffusion makes a significant contribution to the nutrient supply throughout the year, averaging about 1500 mol/s of nitrate for the central Scotian Shelf. In fact, vertical diffusion dominates horizontal and vertical advection in all but the winter months when nitrate builds up in the upper layer, as a consequence of vertical mixing and convection, and subsequently is depleted during the spring bloom. Advective and diffusive components could account for about 30 to 100% of the total monthly production with the remainder provided through recycling (B. Petrie, G. Harrison and P. Yeats, in prep.). Estimates of the vertical diffusion of nutrients require knowledge of the eddy diffusivity and the nutrient gradient. Petrie and Yeats (2000) have calculated an annual average vertical eddy diffusion coefficient that is based on the annual harmonics. Monthly eddy diffusivities derived for the central Scotian Shelf (Umoh 1992; Umoh and Thompson 1994) exhibit an annual cycle, generally stronger in fall and winter and weaker in spring and summer. However, the vertical eddy diffusion is likely to vary on shorter time scales, forced by meteorological events such as storms or oceanographic phenomena such as internal waves. This could lead to an enhanced flux of nutrients into the euphotic zone and pulses in primary production.

Given the importance of the relationship between vertical mixing and nutrient supply, field measurements on the Scotian Shelf are in progress to study these processes. This report provides background information that build upon existing data sets and will serve as the basis for a planned field experiment at Station 2 on the Halifax Section (44.2667N, 63.3167W, Depth 143 m, Figure 1). This sampling is part of the northwest Atlantic Zonal Monitoring Program (AZMP). The AZMP is a comprehensive monitoring program that has been designed for the northwestern Atlantic with the aim of increasing the Department of Fisheries and Ocean's (DFO) capacity to understand, describe, and forecast the state of the marine ecosystem and to quantify the changes in the oceans and the predator–prey relationships of marine resources (Therriault et

al, 1998). In Section 2, data from two previous field experiments are analysed in the context of the current study. In Section 3, SeaWiFS satellite ocean colour for the period 1997-2000 will be used to describe spatial correlation of chlorophyll biomass on the Scotian Shelf. The results of a deployment of two moorings at Station 2 in the Fall 2000 are given in Section 4. A summary of these various data sets is provided in Section 5.

2. FALL 2000 MOORINGS

Two moorings were deployed at Station 2 on the Halifax Section (Figure 1) on September 30th, 2000. The first mooring consisted of a SeaHorse profiling platform (Fowler et al., 1997; Hamilton et al., 1999) with a payload that included a Sea-Bird model 19 CTD and a WetLabs fluorometer (Figure 2). The second mooring included a RDI Workhorse ADCP at mid-depth (~80 m) in a streamlined sub-surface float (SUBS). Above the ADCP were seven Vemco Minilog temperature recorders spaced six metres apart starting at a SUBS float at 15 m depth. The SeaHorse mooring was recovered on October 17th, 2000 and returned to BIO for scheduled servicing. This deployment provided good quality data, however, the SeaHorse clamp appeared to be binding on the cable at the bottom bumper and this caused the clamp motor to draw a large current in order to move the clamp to the open position. Some engineering modifications were carried out and this mooring was re-deployed at the same site on November 9th, 2000. Both of the moorings were recovered on November 22nd, 2000. The Minilog and ADCP instruments provided good quality data for the complete deployment. The CTD pump hose became disconnected during the second SeaHorse deployment and, therefore, no conductivity or fluorometer data are available for this period. This failure of the CTD mounting has led to a series of modifications being contracted to Brooke Ocean Technology prior to the spring 2001 field deployment.

The Vemco Minilogs recorded water temperature every 15 minutes with 0.1°C resolution. The Minilogs were placed on the mooring wire in locations that would include both the ocean mixed layer (OML) and water below the pycnocline throughout the deployment period. These time

series (Figure 3) demonstrate a gradual cooling of the surface layer as heat is lost to the atmosphere during this time of year. The increasing strength and frequency of storms also mixes the warm surface layer with the cold intermediate layer below. This is evident as the temperature records for the deeper Minilogs show a significant increase in temperature throughout November. The lack of vertical structure in temperature in the OML produces a record at 15 m with very little high frequency variability. This is also apparent in the latter part of the 21 m record as the OML deepens below that level. At depths below 39 m, there is little variability for the first few weeks of October when that part of the water column is well below the pycnocline. The most intriguing event captured by these temperature recorders is a cooling that occurs in the upper 30 m around October 15th. This cooling is potentially caused by a coastal upwelling event. The deeper recorders do not show evidence of this event because of the low temperature gradient at and below these depths. A more integrated view of the seven time series is shown in Figure 4. This contour plot clearly shows that the cooling event caused the isotherms to rise by approximately 25 m over the period of several days before relaxing back to the original state. There is some evidence of this event in a 6-day series of NOAA AVHRR sea surface temperature (SST) satellite images (Figure 5). The image from October 15th shows a tongue of water approximately 9°C extending off the coast south of Halifax and at certain locations along the eastern shore of Nova Scotia. These satellite images suggest that coastal upwelling, not horizontal advection, is responsible for the cooling event captured in the Minilog temperature records. SeaWiFS ocean color imagery was not available for the period of this event. Figure 4 also demonstrates the cooling and deepening of the OML to about 50 m in the period of late October and early November as the warm OML water mixes with the colder water below. After this, the OML shallows to approximately 40 m by the end of the record. The Minilog time series (Figure 3) at depths of 39-51 m capture an abrupt change in the water temperature on October 16th. This temperature jump occurs in about 8 hours as 3.8°C intermediate layer water is replaced by water at 5.8°C.

Vertical profiles of temperature, conductivity and chlorophyll fluorescence were collected with the SeaHorse mooring at Station 2 (Figure 6). The SeaHorse cycled between 7 and 120 m every 2 hours. A Sea-Bird 19 CTD with an integrated WetLabs fluorometer was mounted as a payload on the SeaHorse profiling platform. The manufacturer's calibration was used to convert the

fluorometer readings into chlorophyll concentrations. Only two casts (16 observations at AZMP standard depths) measuring *in situ* chlorophyll were available for intercomparison with the fluorescence sensor estimates. The squared correlation of these two methods was 0.78 with an average offset of 0.1 and standard deviation of 0.45. In the configuration used at Station 2, the SeaHorse ascended in the water column at a rate of 0.5 m/s. The model 19 CTD has a sampling rate of 2 Hz and, therefore, provided 0.25 m resolution of the measured parameters. It became evident during the analysis of data from this deployment that the model 19 is less than optimal for such sampling. This instrument has a pumped conductivity cell, however, water is not pumped over the temperature sensor. This leads to difficulty in matching the response of the two sensors since they do not sample the same water parcel simultaneously. Often the solution to this type of problem is to find an optimal lag of the conductivity channel relative to the temperature channel. The problem encountered with the model 19 is that with a sampling rate of 2 Hz it is impossible to "match" the sensor response because each sample is 0.25 m apart, which is much larger than the spatial difference in response would be expected to be. An example of the spiking caused by this problem is shown in Figure 7. In order to use such data for further analysis, we applied a low-pass filter to the temperature and conductivity signals to reduce the salinity "spikes".

Throughout the period of the SeaHorse deployment, temperature was highest near the surface, decreased to minimum values of 4-6°C at roughly 60 m, and increased to 8-10°C at 120 m. The salinity was lowest, about 30, at the surface and increased essentially monotonically to about 34.5 at 120 m. This is a characteristic fall profile for the inner Scotian Shelf. The near surface waters largely originate from the Gulf of St. Lawrence; the deeper waters from the continental slope. In 2000, the subsurface slope waters were dominated by Warm Slope Water.

During the first half of the mooring period, some weak, low frequency events are evident in the thermocline and the halocline (Figure 6). There is a general deepening of the shallow mixed layer from September 30 until October 9. The chlorophyll record shows higher concentrations between 30 and 40 m during this period. These appear to be slightly deeper than the pycnocline. In the middle of the record, there is a sharp downward displacement evident in temperature and salinity. This is followed by a fairly steady rise of the temperature and salinity isobaths

throughout the water column. The rise peaks about 2 days before the end of the record and is followed by a relaxation of the thermo-, halo- and pycnoclines. At the peak (21:00 October 16), there is a burst of higher chlorophyll concentrations with a maximum value of 2.2 $\mu g\ l^{-1}$. The data in Figure 6 indicate a potential upwelling event occurred between October 12th and the 18th. The density of the upper layer appears to have increased due to mixing that occurred during the upwelling. The elevated chlorophyll concentrations near the ocean surface could have been a consequence of upwelling and mixing of nutrients up into the near-surface layer during this event. A plot of the along-shore wind stress from Sable Island during this period (Figure 8, upper panel) indicates that the conditions were upwelling favorable for the period 11-16 October; this period had a combination of both large wind stress and long duration. This corresponds well with the timing of the results from the SeaHorse. The Halifax harbour SST trend (Figure 8, lower panel) is also consistent with an upwelling event showing a significant decrease during the latter part of the upwelling period as cooler water from below is brought to the surface near-shore to replace the surface layer advected away from the coast.

SeaHorse CTD temperature, salinity and density time series at selected depths are shown in Figure 9a-c. The 10 and 20 m series are in the mixed layer for most of the period, show a gradual cooling until October 10 when the temperature decrease accelerates in response to the shallowing of the thermocline. The 30 m time series is from the high-gradient region and consequently shows considerably more variability. At 70 m, near the minimum temperature region, the variability is considerably lower. Below 70 m, temperatures rise during the last half of the record indicating an inflow of warmer slope water to this region of Emerald Basin. The salinity response is quite consistent over all depths largely because of its monotonic increase from the surface to the bottom. The outstanding feature of the record is the overall increase of salinity at all depths from October 9 until nearly the end of the record. The deep salinity rises to above 34.5, consistent with an increase of Warm Slope Water in the Basin. Near surface densities increase substantially towards the end of the record indicating upwelling and/or vertical mixing; maximum values occur on October 15-16 corresponding to the surface increase of chlorophyll.

Figure 10 shows the top 1 m average (generally corresponding to between 7 and 8 m below the sea surface, but always less than 10 m) of chlorophyll, temperature, salinity and density from each profile. The broad chlorophyll peak is centered around October 16 and is coincident with the lowest temperatures and highest densities.

In addition to the low frequency variability there are events with shorter periods (Figure 6, 11). A major component of the variability of temperature and salinity, and consequently of density, consists of high frequency oscillations at semi-diurnal tidal periods. Amplitudes of several meters are evident in the salinity records. These are likely internal waves caused by the principal lunar component M2. There is evidence also of occasional bursts at roughly twice the M2 frequency with amplitudes of about 1 m. These higher harmonic internal waves have been seen at the shelf break in temperature records (Petrie 1975, amplitudes to nearly 30 m) and in Batfish tows (H. Sandström, pers. comm., typical amplitudes of 3 m). Below the pycnocline, chlorophyll displays a pattern consistent with temperature and salinity, having significant variability at the M2 frequency (isoline at 0.2 mg m^{-3} in Figure 6). Above this level, the chlorophyll high frequency variability does not correlate as well with the semi-diurnal tidal period because changes in production depend on light and nutrient fields, which may not have a direct relationship with the varying physical fields.

To examine the magnitude of these higher-frequency phenomenon, we have constructed the time series of depth of selected isotherms, isohalines and isopycnals (Figure 11). For all 3 variables the high frequency oscillations come in bursts. For example, there are semi-diurnal waves evident from the 13th to the 15th of October (T=8°C, S=34, sigma-t=26.5) that have peak-to-peak amplitudes of about 15 m. Quarter-diurnal energy with peak-to-peak amplitudes of about 3 m is evident between October 3rd and 6th in the T=6°C, S=32 and sigma-t=25 isolines.

Spectra of selected isopleths indicate a range of 1 to 2 m for the semi-diurnal (M2) amplitudes over the entire record (Figure 12). All three variables show the highest amplitudes generally occur near the bottom. At the M4 frequency, the range is about 0.5 to 1 m.

On five occasions (September 12 and 30, October 7, 17 and 25), bracketing the Seahorse deployment, discrete water samples were collected at Station 2 for determination of chlorophyll and nutrient (nitrate, phosphate, silicate) concentrations in the water column. Nitrate profiles were similar, i.e. low and relatively a uniform concentrations in the upper ~25 m and a strong nitracline below (25-50 m), for the dates leading up to and following 17 October when there was a significant increase in concentrations at all depths (Figure 13). These elevated concentrations coincided in time with the observed vertical upward displacement of cooler and saltier water in the Seahorse record between 14-18 October. Station 2 was sampled 24 times over the year and on at least one other occasion, a pronounced vertical displacement of nutrient concentrations was observed. Not only were concentrations elevated during these "events" but vertical concentration gradients were also elevated near surface (Figure 14).

Coincident with the elevated surface nitrate concentrations on October 17th was a significant change in the vertical structure of chlorophyll (Figure 13). Prior to the event, surface chlorophyll concentrations were low and a pronounced subsurface maximum was evident (at ~25-35 m). On the 17th and the following sampling date (25th), maximum chlorophyll concentrations were observed at the surface. This was consistent with the Seahorse fluorescence data showing a subsurface maximum leading up to the 12-18th event after which concentrations peaked near surface. An increase in nutrient concentrations in surface waters would be expected to not only influence the vertical structure of chlorophyll but also the absolute amount of biomass produced. Nitrate concentrations were integrated over the upper 50 m (approximates the biologically-mediated nutrient consumption zone) as well as chlorophyll (surface to max depth). Nitrate integrals showed the expected pattern with concentrations significantly elevated during the 17 October event, and decreasing to pre-event levels afterwards. Chlorophyll integrals, on the other hand, were not higher on the 17th than prior to or after the event, suggesting that the elevated surface concentrations may have resulted from a vertical displacement rather than a net synthesis of biomass. On the other hand, the SeaHorse estimates of Chlorophyll a (Figure 6) indicate that the subsurface maximum had disappeared on roughly the 9th of October. This argues that the increase centered around the 17th could not have been merely an upwelling of the subsurface maximum. Integrated chlorophyll estimates from the fluorometer on SeaHorse (Figure 15) show a peak value of 40 mg m^{-2} at the beginning of the record and then dropping off to about 25-30 for

the rest of the period until the event on the 17th; which again has a peak value near 40 mg m^{-2}. A comparison of the AZMP and SeaHorse integrated chlorophyll results on September 30th and October 17th demonstrates similar results for both methods, which is encouraging. If we assume that these data represent the area roughly described by a radius equal to an RMS current times 8 days (Oct 17-25), then these findings do not support the idea that the decrease in nitrate following the event was due to biological consumption unless the phytoplankton biomass was grazed by herbivorous micro- and meso-zooplankton at a rate matched by the chlorophyll increase. Mesozooplankton biomass collected during the same time frame does not support this explanation, however they may not respond to the Chl increase on such a short time scale. Microzooplankton, which are more likely to be able to respond, were not collected. Another explanation is that perhaps the strength of the upwelling was greatest in the area of Station 2 and the excess chlorophyll was advected from the region.

Based on Sept. 30, Oct. 7, 17 and 25, CTD and nutrient profiles, nitrate and silicate were highly correlated (r^2 = 0.88, 0.83) with salinity for values greater than 31 (Figure 16). For salinity values less than 31, a constant nutrient concentration was used. These relationships allowed the salinity field to be transformed into nutrient fields. These proxy nutrient fields are quite suggestive. They indicate an inflow of higher nutrient waters at depth through the latter half of the mooring period. Secondly, between the 15th and 17th of October, the 2 μM nitrate contour is uplifted to nearly the top of the SeaHorse profile. If this nitrate were converted into chlorophyll, it should yield concentrations of about 2 μg Chl l^{-1}; this is about the peak concentration of chlorophyll that is observed. This suggests that physical processes that bring nutrients into the euphotic zone could drive small-scale (in time and space) phytoplankton blooms.

Wind is a potential cause for some of the variability seen in this 2.5 week deployment of the SeaHorse profiler. In particular earlier studies, e.g. Sandstrom (1980) and Petrie et al. (1987), indicated that coastal upwelling was an effective process for bringing underlying waters to the surface. The depth of the 32.5 isohaline from SeaHorse is plotted (Figure 17) along with the integrated offshore Ekman flux that is calculated from the alongshore component of the wind stress. The latter is determined from Sable Island wind data. The depth of the salinity isohaline deepens from about 60 m at the start of the record to about 70 m halfway through. Then it rises

to about 40 m at the end of the record. The variation of the Ekman flux over the same period is qualitatively similar, i.e. an overall downwelling tendency for the first half of the record, a stronger upwelling tendency for the last half. From mid-record until the end, the Ekman flux changes by about 400,000 m^2. Station 2 is roughly 25 km off the coast. If the upwelling were spread equally over this distance then the vertical movement would be about 16 m, accounting for roughly half of the observed vertical excursion of the isolines. However, for a straight coastline, the strength of the upwelling is not uniform offshore, but decays with a spatial scale given by the internal Rossby radius. For the inner Scotian Shelf this is typically less than 10 km. On the other hand, the observations reported by Petrie et al. (1987) indicated that upwelling was enhanced in this area off Halifax. Moreover, Donohue (2000) has found enhanced upwelling at this location in his modeling of this process. Petrie (1983) found that shelf break upwelling can bring water into Emerald Basin and could contribute to the observed shallowing of the isohalines in the inner Basin. It appears that coastal upwelling contributes significantly to the observed variability.

The SeaHorse and ADCP moorings at Station 2 were located within several hundred metres of each other. The ADCP recorded a vertical profile of water currents every 15 minutes with vertical bins of 2 m depth. A progressive vector diagram (Figure 18) of six bins spanning the range of depths measured by the ADCP demonstrates that the mean flow at all depths is to the southwest with the magnitude decreasing with depth. Each cross marker on the plots indicates five days of elapsed time. In the records close the surface, the direction of the flow changes substantially during the period around October 15th. This is coincident with the increased alongshore wind stress during this period and the rising of the T, S and density surfaces are Station 2. At the deeper bins, the flow does not change direction during this period but does appear to slow down. Time series of current speed and direction have been compiled for all ADCP bins in Appendix B. These plots have been divided into three time periods (30 Sep – 17 Oct; 18 Oct – 4 Nov; 5 Nov – 22 Nov) to allow sufficient resolution in the time axis to discern sub-diurnal variability. It is evident from these time series that there is a strong coherence at all depths measured.

Combining the SeaHorse and ADCP data sets provides an opportunity to estimate the gradient Richardson number, which is an indicator of potential mixing. The vertical shear in the water column was computed using a first difference technique for those profiles which were within 15 min of a SeaHorse CTD profile (Figure 19). Values of shear below the precision of the ADCP were removed from the data set. The contour plot indicates that shear was mainly enhanced at the base of the OML and was particularly strong at the beginning of the upwelling event that occurred near the end of the SeaHorse deployment. The buoyancy frequency, N^2, calculated using the SeaHorse CTD data, is elevated in the area of the strong gradients at the base of the mixed layer (Figure 20). The buoyancy frequency reaches its highest values during the period October 10-14th, just prior to the upwelling event. Some negative values of N^2 are evident in the OML because the low gradients in this region make it difficult to calculate this quantity properly. In addition, the spikes in the density derived from the Sea-Bird 19 CTD causes problems as well (see Figure 7).

The data from individual CTD profiles were matched with ADCP data corresponding in time to produce an estimate of *Ri* in 2 m vertical bins. The contour plot of these results (Figure 21) indicates a "background" *Ri* value in the range of 1 to 5. Higher values of *Ri* tend to be concentrated at the base of the mixed layer where strong gradients are likely to suppress mixing. Critical *Ri* values ($Ri < 0.25$) are most evident in the OML while there are small intermittent pockets below the pycnocline. It is interesting to note that the upwelling event that occurs around October 15th is not readily evident in the *Ri* plot, which suggests that the potential for vertical mixing of the water column does not change substantially during this event. The Richardson number estimates were grouped in 4 bins (7-20 m, 21-40 m, 41-60 m, 61-80 m) and plotted as histograms (Figure 22). The upper limit of the first bin is 7 m because the SeaHorse does not profile any higher than this. The upper bin approximates the ocean mixed layer (OML) and shows a substantially different character from the other three bins. In the OML, approximately 35% of the *Ri* estimates are less than 0.25, 67% are less than 1.0, and the median value of all estimates in this bin is 0.49, indicating a strong potential for mixing in this region of the water column. In the lower three bins the distribution of *Ri* peaks close to 1 and at values greater than 5. The median values in these bins range from 3 to 4 indicating more limited mixing potential than observed in the OML.

A time series plot in Figure 23 compares wind stress estimated using Sable Island winds with the average Richardson number for the 7-20 m depth range of the ocean mixed layer. The two *Ri* value that go off the scale have values less than 80. During the period of October 5-9, the wind stress is low relative to other parts of the time series and the corresponding *Ri* values are higher. In the period following this, the wind stress increases during two events (with a low period between) and *Ri* values remain low for this extended period of time. Similar time series plots for layers below the mixed layer do not show evidence of a strong correlation between the surface wind stress and estimated *Ri*.

The data for the 7-20 m range are binned in 0.05 Pa intervals and shown in a boxplot (Figure 24). This plot demonstrates a trend of decreasing median *Ri* with increasing wind stress, as might be expected. The median values for the group above 0.2 Pa is significantly different from those at $\tau < 0.1$ Pa, based on the boxplot notches that represent the confidence intervals on the medians. To our knowledge this has not been shown before because of the logistical difficulty of obtaining long-term simultaneous CTD and current measurements with good temporal and spatial resolution. This has important implications for ocean modelers who often use *Ri* as a proxy for mixing rates. The inter-quartile range also decreases with increasing wind stress indicating there is less variability at high values of τ. However, the small number of observations available for these cases of high τ may have some role in this. A planned field experiment will measure the rate of dissipation of turbulent kinetic energy directly and allow comparison with *Ri* to determine if a strong relationship exists between these two parameters.

3. SeaWiFS SCALE ANALYSIS

A first-year objective of this project was to determine the spatial scale of ocean colour variability at Station 2 in order to give an indication of how representative point measurements at this location are of surrounding areas. Figure 25 shows two examples of SeaWiFS images: the first

from May 1, 1999 features fairly uniform chlorophyll concentrations and complete data coverage for the entire Scotian Shelf; the second, from April 6, 2000 has less data return, considerably more spatial variability, and spikes evident in the image, particularly near areas where there were no data because of cloud cover. A total of 334 SeaWiFS ocean colour images, satisfying the criteria they contain at least some data from the area around Station 2, were examined for the period 1998-1999. These images formed the base data set, however, a large number had erroneous points associated with scattered clouds and low satellite angle. Images were classified as good, fair and poor based on data return and the number of spikes that could be seen in the images. A total of 90 images were selected as "good" images and used in a correlation analysis over a 20 by 20 pixel (approximately 34 by 34 km) box centered on Station 2. Obvious spikes were removed from each image. Often this amounted to a single extreme value that exceeded all others in the field by more than a factor of 10. It is interesting to note that during the two-year period studied there were approximately 3 SeaWiFS passes each day over the Scotian Shelf and of this total only 90 images were of "good" quality in the area of Station 2. Assuming the distribution of errors is roughly uniform, this means that SeaWiFS can only provide ocean colour information at a temporal resolution similar to the bi-weekly *in-situ* measurements carried out as part of the AZMP. The strong advantage of SeaWiFS is the high spatial resolution (~1.5 km) with bi-weekly composites providing almost complete coverage of the Scotian Shelf.

The time series of the average, maximum and standard deviation of chlorophyll in the 20 by 20 box indicate that the mean did not vary substantially in 1998 but showed greater variability in 1999 (Figure 26). The standard deviation was generally less than 1 mg m^{-3} and the peak value from these images was about 8 mg m^{-3}. The *in situ* and SeaWiFS estimates of near-surface chlorophyll concentrations are in close agreement, thus providing some confidence in the SeaWiFS imagery in the area surrounding Station 2. Correlations of all pixels within the box were calculated relative to the centre pixel, which corresponded to the site of the fixed station. The minimum correlation was 0.52, the average was 0.85 with a standard deviation of 0.09 (Figure 27). There was not strong evidence of anisotropy in the correlation field even though the Nova Scotian Current is thought to flow through this area in roughly a northeast to southwest direction. The correlations have been combined independent of direction (Figure 28) and fitted to an exponential, $A_0e^{-\lambda r}$. The constant A_0 was set equal to 1, representing a perfect correlation at 0

distance, $1/\lambda$ is the e-folding scale, and r is the distance from Station 2, the central pixel in the field, to the other pixel used to compute the individual correlation. The results of that analysis indicated an e-folding scale of 82 km.

The analysis indicates that chlorophyll observations collected at Station 2 are representative over a broad area. An expanded spatial analysis of the data set is warranted since the scale of variability was considerably larger than the 20 by 20 pixel box. In addition, it would be useful to add the past year's (2000) data , and to examine the images that were classified as fair to determine if they can be added to the data set. These additional calculations would add confidence to the present computation.

4. HISTORICAL DATA ANALYSIS

4.1 Analysis of CASP Mooring Data

The Canadian Atlantic Storms Program 1985-86 (CASP) instrument array consisted of current meters with temperature and conductivity cells, thermistor chains and bottom pressure gauges with temperature sensors (Figure 1). The analysis of this data set was carried out to provide support to the finding from the Fall 2000 mooring that coastal upwelling plays an important role in the physics of Scotian Shelf. Moorings 1 and 9 were located on the 60 m isobath, moorings 6, 2, 7, 8 and 10 on the 100 m isobath, and moorings 3, 4 and 11 on the 175, 220, and 155 isobaths, respectively. Mooring 5 at 225 m was equipped only with a bottom pressure recorder. Lively (1988) provides an extensive data report of this field program; Anderson and Smith (1989) describe the characteristics of the monthly mean flows, the diurnal tide K_1, the response to wind forcing through spectral analysis, and inertial period motions. At any single site, the CASP program provided a low-resolution array of ocean currents and hydrographic properties in comparison to the SeaHorse-ACDP deployment in the fall 2000 (see Section 4). On the other hand, this is a 4-month data set of observations similar to the ones that have been collected in the

present observation program. Their analysis can provide insight for the higher resolution data, and can reveal important processes that contribute to mixing and subsequently to primary production. There are three distinct advantages of the CASP data: they are already in hand; they cover a longer continuous time span and a greater area than we could expect for a single deployment of the SeaHorse-ADCP combination.

Contoured time series of temperature (T), salinity (S) and density (σ_t) were created using the observations from discrete depths and linear interpolation (Figure 29). The data were smoothed with a 24 h running mean filter before contouring. The most complete data set was collected at mooring 3 with all instruments providing full records of T and conductivity (C). In this case the deepest conductivity cell was at 110 m while the temperature record extends to the bottom through a sensor on a bottom pressure gauge. At other mooring sites, failure of T and/or C sensors at various times provided more limited records (moorings 4, 5 and 9 are not shown in Figure 29 due to lack of data at these sites). The temperature at mooring 3 features seasonal cooling from about 6°C to 0°C over the span of the record in a layer from 16 m (shallowest instrument) to about 75 m. At the same time, the upper layer salinity is increasing from about 31 and the beginning of the record to about 31.5 near the end. The shallowing of the 32 isohaline is another manifestation of the increase. Density increases by more than 1 kg m^{-3}. At depth, there are a number of events from several to more than 10 days duration that are characterized by an upward movement of warm (8-10°C), salty (33-34) water. These events are reflected in the σ_t contours as vertical intrusions of denser water.

The hydrographic variability at mooring 3 is seen at the other sites as well. In particular, for moorings on the 100 m isobath (sites 6, 2, 7, 8 and 10), seasonal cooling is observed at shallower depths; salinity also appears to increase at 2, 7, 8 and 10 but not at 6. The deep intrusions of warmer, saltier water are coherent from site to site. Mooring 11, the deepest site on the eastern end of the array, did not have the vertical coverage of instruments that mooring 3 did; nonetheless, the intrusions of warm, salty water are evident. The last event, beginning roughly on March 15, at mooring 11 has the 32-salinity water reaching 11m, the depth of the shallowest instrument. Salinity and density increase during the mooring period but with significant variability occurring throughout. The cooling occurs at mooring 1 and there are indications of

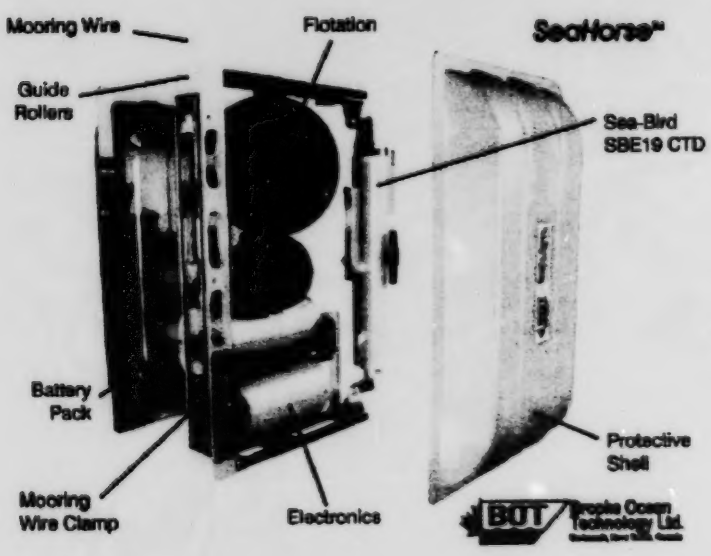

Figure 2: The SeaHorse mooring profiler uses surface wave energy and a one-way cable clamp to climb down the mooring wire. The photograph shows SeaHorse being prepared for deployment. The schematic includes the Sea-Bird 19 CTD.

the deep-water intrusions as well. Mooring 9 had current meters only at 9 and 50 m; the T and S observations at these depths were nearly copies of those at mooring 1, at 12 and 45 m.

The overall coherence of the hydrographic time series is illustrated in Figure 30, where T and S from the deepest records along the 100 m isobath are shown. The major events, featuring large increases in T and S, line up quite well from mooring to mooring. However, superposition of the temperature data reveals some interesting variations in the temperature response (Figure 31). For the first half and the last 3 weeks of the temperature time series, the variations of temperature appear to be nearly in phase at the 5 sites along the 100 m isobath. The leading edges of the two large events from the end of January to mid-March are approximately in phase, however, the trailing edge decreases first in the east then progressively later westward. Comparison of the data from Sta. 10 and 6 indicates that the decrease at mooring 10 leads that at mooring 6 by 4 to 9 days. Similar behaviour is seen in the salinity time series from approximately 70 m.

The most likely process that could cause the variability described above is wind-driven upwelling. This phenomenon has been studied by Hachey (1937) and Petrie et al. (1987) but their data were confined to summer months. Sandstrom (1980) related sea level changes at Halifax to the alongshore wind, the component responsible for the most of the sea level variability. Schwing (1989) examined the wind-forced response of bottom pressure measured by the CASP array, complemented with records from permanent tide gauges at North Sydney, Halifax and Yarmouth. This provided extensive coverage of the inner half of the Scotian Shelf. Schwing found that alongshore wind stress (positive to NE, 60°T) was by far the most important contributor to bottom pressure variability in the subtidal band. The response consisted of local and non-local components. Local forcing was the more important factor west of Halifax, non-local forcing to the east. Together they accounted for 90% of the subtidal bottom pressure variance. Consequently, the along-shore wind stress component has been examined in this study as a probable cause of the recorded T, S and σ_t variability. The comparison between wind and hydrographic variability for mooring 3 indicates a relationship between positive stress and upwelling (Figure 32 and Figure 33). Positive stress generally corresponds to upward movement of temperature and salinity isopleths. The other mooring sites behave similarly, i.e. upwelling is a general response along the coast. However, it is also apparent that the T and S response is not

directly proportional to the strength of the alongshore stress. The connection between upwelling and wind is more complicated than the simple picture implied by this discussion. Nonetheless, it is useful to calculate the integrated offshore Ekman flux for the mooring period using:

$$\Sigma(\tau_{along}/\rho f)\Delta t$$

where τ_{along} is the alongshore wind stress, ρ is the seawater density, f is the Coriolis parameter and t is time. This calculation estimates that 15×10^6 m^2 of water was transported offshore per meter of coastline during the CASP observation period. This is 4 times the area between the coast and mooring site 3. The offshore Ekman flux could make a major contribution to alter the hydrographic field.

There is also evidence of the wind directly affecting currents. In Figure 34, the time series of alongshore current from Station 1, 12 m, the site closest to the coast, and wind stress have a correlation of 0.54 for the first half of the record. For the last half, the records are less correlated, r = 0.27. This is also illustrated in the lower panel of the figure. At Station 3, the currents tend to be stronger than at Station 1 with a mean flow to the southwest (Figure 35). The southwesterly current is largest near the surface and decreases towards the bottom. The mean currents are in geostrophic balance with cross-isobath density gradients (Smith and Schwing, 1991). In the lower panel of Figure 35, the alongshore current, with the mean for the entire record removed, has been plotted together with the alongshore wind stress. The correlations of current with stress are low, ranging from 0.06 to 0.17 (see Table 1). However, the plot and table indicate that the currents are highly correlated and quite uniform over the range of instrument depths. For example, the linear regression of the alongshore flows at 16 and 50 m has a correlation of 0.88 and a slope of 0.86 (U_{50m} = intercept + slope*U_{16m}). The coherent variability at the deeper instrument has a reduced amplitude compared to that at shallower depths.

To address the mixing that occurred during CASP we used the temperature, salinity and velocity observations to calculate Richardson numbers. The Richardson number, *Ri*, is an indication of the potential for vertical mixing to occur. In a shear flow, its value is the square of the Brunt-Vaisala frequency divided by the vertical shear of the horizontal current. For $Ri<0.25$, Kelvin-Helmholtz instabilities will develop and mixing will occur (Turner, 1973). The Richardson number is:

$$Ri = -g\frac{\partial \rho}{\partial z}\Big/\rho\left(\frac{\partial u}{\partial z}\right)^2$$

where g is the gravitational acceleration, z is vertical distance, and u is the mean velocity. The spacing between the current meters at Sta. 3 ranges from 20 to 40 m, a very large gap for the estimation of this parameter. Nonetheless low values, but not necessarily less than 0.25, could indicate that mixing is occurring. In Figure 36, we show the histogram of *Ri* for the three instrument pairs. The 16-50 m depth range has a larger percentage of values in the lower bins, indicating that mixing is more likely there than for the deeper depth ranges. The percentage distributions for the two deeper ranges are quite similar.

There is considerable shear in the mean flow that could affect the potential for mixing to occur (Figure 35). Consequently, "background" Richardson numbers were calculated from the record average mean current shear and density gradient at mooring 3. The values were 4.6, 8.2 and 8.6 for the 16 to 50, 50 to 70, and 70 to 110 m depth ranges. The time series of *Ri* for the entire record is very noisy; however, there appears to be a qualitative relationship between the wind stress and the Richardson number, particularly for the shallowest depth range (Figure 37). In this range, there is the tendency for lower *Ri* at higher total and alongshore stress. This tendency is less evident for the 50-70 m range and is not consistent at all for the deepest range. The number of values where wind stress exceeds 0.3 Pa is small. Above 0.5 Pa, medians of *Ri* have been calculated from all of the values and plotted at a stress of 0.6 Pa. It appears that wind stress affects the shallower depths and that higher values lead to lower *Ri* and a greater chance for vertical mixing.

Smith (1989) showed that some of the vertical current shear arises from inertial period motions, and that the inertial response can persist after the wind stress ceases. Thus high current shears, and potentially lowered *Ri*, can occur during periods of reduced atmospheric forcing. This could account for some of the scatter in the data displayed in Figure 37.

We can make some qualitative conclusions concerning the upwelling and mixing processes occurring during the CASP observation program. There is a tendency for the Richardson

number, particularly in the 16 to 50 m depth range, to approach critical values for mixing during periods of stronger winds. Stronger winds generally mean stronger alongshore winds that can cause upwelling. Upwelling increases the vertical stratification in the lower half of the water column (Figure 29), thus inhibiting mixing there. This may account for the poor relationship between wind stress and *Ri* in the 70-110 m layer (Figure 37). It appears that in the upper half of the water column, the increased current shear during an upwelling event dominates the potential for increased vertical density stratification as more dense, deeper waters move upwards, leading to reduced *Ri*. The opposite appears to happen in the lower half.

Some quantitative estimates can be made to put bounds on the mixing that occurred during the CASP field program. We note first that during CASP, the salinity was increasing at all mooring sites. This is indicated in Figure 38 where we show the averaged salinity for the depth range 0-65 m. This temporal increase of salinity could be caused by the combination of upwelling and vertical mixing. Averaged salinities were calculated using the data from individual current meters as representative halfway between each instrument; for the shallowest instrument, the distance was from the surface to halfway to the next deepest meter. The values from the two deepest instruments were used to interpolate a 65 meter reading, the shallowest depth of the deepest salinity sensor on the moorings of Figure 38. In addition, there was an alongshore gradient, with salinity increasing from east to west (e.g., compare mooring 10 with mooring 6 in Figure 38). The longest period with overlapping records was 83 days (Sta. 6, 2, 7 and 10). This period produced a correlation of 0.81 for salinity versus alongshore distance, and a least squares fit linear gradient of -0.00097 km^{-1}. This gradient could be caused by a tendency of the Nova Scotia current to move offshore as it flows southwestward along the coast or, alternatively, by a salt flux into this layer. Upper bounds for these changes were calculated assuming the temporal increase and the alongshore gradient were caused by vertical mixing and upwelling.

First, consider the salinity increase over the CASP observation period for the area defined by mooring 2 and the 110 m depth of mooring 3, the deepest salinity sensor at this site. We assume that this increase is caused by water from 110 m being upwelled and mixed into the water above. Begin with an average salinity, S_o; at time intervals of Δt, remove a portion of the water column,

Δz, at the current average salinity, S_i, and replace it with water of salinity S_{btmi}, as measured by the Sta. 3, 110 m sensor. Over the entire mooring period we have:

$$110 * S_o - S_i * \Delta z - S_{i+1} * \Delta z - \ldots - S_{i+n} * \Delta z + S_{btmi} * \Delta z + \ldots + S_{btmi+n} * \Delta z = 110 * S_f,$$

where S_f is the salinity at the end of the mooring period. The sum of the S_i and S_{btmi} equals $n*S_{ave}$ and $S_{btm(ave)}$, the average salinities in the area defined by Sta. 2 and 3 and by the Sta. 3, 110 m sensor. Substituting we get:

$$110 * S_o + n * \Delta z\{S_{btm(ave)} - S_{ave}\} = 110 * S_f$$
$$n * \Delta z = 110 * \{S_f - S_o\} / \{S_{btm(ave)} - S_{ave}\}$$

where $S_o = 31.754$, $S_f = 32.437$, $S_{ave} = 32.095$, and $S_{btm(ave)} = 33.639$. This gives a value of 48.7 m for $n^* \Delta z$, corresponding to an average upwelling velocity of $4.4*10^{-6}$ m s^{-1} over the mooring period of 127.79 d. The distance from Sta.2 to Sta. 3 is 16.1 km, thus the upwelled area required to increase the salinity over the mooring period is $16100*48.7 = 7.8*10^5$ m^2. This represents about 5% of the Ekman flux ($15*10^6$ m^2).

In addition to increasing with time, the salinity increases along the coast from east to west, i.e. in the same direction as the Nova Scotia Current. A salt flux is needed to maintain this alongshore salinity gradient. We consider a wedge whose cross-sectional area is defined as above but that stretches along the coast from Sta. 10, on the eastern end of the CASP mooring array to Sta. 6 on the western end. The current meter data from Sta. 2 and 3 provide the best estimate of the transport. Over the mooring period the average transport was 400,000 m^3 s^{-1}. We have made two estimates of the alongshore salinity gradient: -0.00097 /km, using the data from Sta. 10, 7, 2 and 6; –0.0023 /km, using the data from moorings 7 and 6. The first estimate covers the full length of the array; the second is approximately centered around Sta. 2 and 3 where the transport is estimated. Together they give a range of the vertical transport necessary to support the alongshore gradient. The alongshore gradient estimates are made for the upper 65 m since only mooring 3 had a salinity sensor at 110 m. However, we shall assume that the gradients apply for the depth range of 0-110 m. The salt balance yields:

$$U_{in} * S_{in} + w * L * B * S_{btm} = U_{out} * S_{out}$$

Where U_{in} (U_{out}) and S_{in} (S_{out}) are the inflow (outflow) on the eastern (western) end of the wedge, and the inflowing (outgoing) salinity; w is the upwelling velocity, L is the length of the coast over which the gradient applies, and B is the width of the coastal segment. Now $U_{out}=U_{in}+wLB$, $S_{out}=S_{ave}+\Delta S/2$, and $S_{in}= S_{ave}-\Delta S/2$, where S_{ave} is the average salinity in the wedge defined by Sta. 2 and 3 as above and ΔS is the salinity difference over the length of coastline considered. Substituting these expressions in the above gives:

$$w = U_{in}*\Delta S/L*B*\{S_{btm}-S_{ave}-\Delta S/2\}.$$

We shall make all estimates for an alongshore distance of 39 km, the separation between Sta. 6 and 7 since the transport is calculated from the observations at Sta. 2 and 3, which are roughly centered between 6 and 7.

For $\partial S/\partial x$ = -0.00097 /km, U_{in} = 400,000 m^3/s, L = 39 km, ΔS = 0.038, B = 16.1 km, S_{btm} = 33.639 (average at Sta. 3, 110 m), S_{ave} = 32.095 (average defined by Sta. 2 and 3 data), then:

w = $1.6*10^{-5}$ m/s or 1.38 m/d and represents an area of $2.8*10^6$ m^2 ($1.6*10^{-5}$ m/s*127.79 d*86,400 s/d*16,100 m). Note also that this would mean an increase of alongshore transport of 10,000 m^3/s from Sta. 7 to Sta. 6, a small fraction of the overall 400,000 m^3/s.

For $\partial S/\partial x$ = -0.0023 /km, U_{in} = 400,000 m^3/s, L = 39 km, ΔS = 0.089, B = 16.1 km, S_{btm} = 33.817 (average at Sta. 3, 110 m, contemporaneous with the observations at Sta. 6 and 7, note that one salinity sensor at Sta. 6 had only a 91 d record), S_{ave} = 32.211 (average defined by Sta. 2 and 3 data), then:

w = $3.6*10^{-5}$ m/s or 3.1 m/d and represents an area of $6.45*10^6$ m^2 ($3.6*10^{-5}$ m/s*127.79 d*86,400 s/d*16,100 m, note that we have applied the gradient to the entire CASP period in

order to compare it to the Ekman flux over the same time). The increase of alongshore transport is about 23,000 m^3/s.

The first estimate corresponds to about 19% of the Ekman flux, the second to about 43%. Adding the 5% of the Ekman flux required to account for the increasing salinity over time for the section defined by Sta. 2 and 3 to the flux needed to maintain the 2 estimates of alongshore gradient, we have from 24 to 48% of the Ekman flux is required to account for the temporal and spatial changes of salinity. These calculations give crude estimates of the fluxes needed to account for the hydrographic changes and indicate that the wind forcing has sufficient strength to contribute significantly to the observed variations.

The CASP data set indicates that wind forcing can contribute substantially to mixing, upwelling and stratification in the nearshore zone of the Scotian Shelf. Nutrient distributions, light fields and primary production would also be affected by these processes. However, the relationship between wind forcing and ocean response in this area is complex and cannot satisfactorily be explained by simple models. The CASP observations of temperature, salinity and current are coarse with vertical separations of 10s of meters. The accuracy of the salinity data in particular is poor (see Lively, 1988 for a discussion of the problems encountered calibrating the conductivity cells). This compromises estimates of mixing parameters and their relationship to external forcing. The combination of the SeaHorse T/S profiler and the ADCP current observations should allow for a substantial improvement of the vertical mixing studies and the effect on nutrient fluxes and primary production.

4.2 Ocean Turbulence on a Sloping Side of Emerald Basin

Ocean microstructure measurements were made with the profiler EPSONDE (Oakey, 1988) from October 11-16, 1990 on a sloping side of Emerald Basin on the Scotian Shelf (solid square, Figure 1). This field program combined EPSONDE data with ADCP and thermistor chain data to study eddy fluxes of momentum and buoyancy in the bottom boundary layer (van Haren et al.,

1994). The focus of the van Haren et al. study was on the lower 30 m of the water column in a water depth of 178 m.

Given the proximity of these ocean turbulence observations to the present study at Station 2 (Halifax Line), it was decided to reprocess the EPSONDE data to provide a background data set for planned microstructure measurements at Station 2. The reprocessing did not involve any re-editing of the original data, but focused on the microstructure measurements made throughout the whole water column. The design of EPSONDE does not allow estimates of turbulence parameters within 5-8 m of the ocean surface. An example of the results from one EPSONDE station (Figure 39) indicate that the ocean mixed layer extends to a depth of approximately 30 m, typical for the Scotian Shelf during this time of year. The panels displaying the rates of dissipation of turbulent kinetic energy (ε) and thermal variance (χ) show that, at a given depth, these quantities can change by several orders of magnitude in the time it takes to do a few profiles (typically 5 min/profile). Below the mixed layer, the mean profile of ε is relatively constant at ~10^{-8} W kg^{-1} except at 80 m depth where one short event increases this by an order of magnitude. In contrast, χ steadily decreases in value from the surface to the bottom, aside from the event at 80 m as well. The eddy diffusivities for mass (K_ρ) and heat (K_T) are largest in the ocean mixed layer (OML) and drop to a minimum (10^{-5}) at the base of the OML. Below the pycnocline the diffusivities gradually increase with depth reaching 10^{-3} at 160 m. The mean profile plots for the remainder of the stations in this field program are documented in Appendix A.

Using wind data collected at Shearwater during this experiment, a time series of wind stress has been computed and is shown in the upper left panel of Figure 40. The wind stress is only greater than 0.05 Pa during two short time periods, one at the start of the data record and one on October 15th. On the remaining panels on the left-hand side of the figure, time series of ε have been plotted for the upper part of the water column using 5-m depth bins. It is evident from these plots that the variability of ε decreases as depth increases, as does the mean value. There does not appear to be a strong correlation between wind stress and the magnitude of ε even in the uppermost bin. However, the range of wind stress values is small for this period and may not provide an adequate test of this relationship. In the upper right panel, the dissipation integrated

from the surface to the base of the mixed layer, ε_I, is plotted as a function of the cube of the wind speed. The dashed line from a study of mixed layer dissipation on the Scotian Shelf (Oakey and Elliott, 1982) indicates that approximately 1% of the wind energy at 10 m is dissipated in the ocean mixed layer. The results from this study are clustered around the low end of the data set obtained by Oakey and Elliott (1982) and, therefore, do not provide enough range for a conclusive comparison.

5. SUMMARY

Short-term physical, chemical and biological variability on the Scotian Shelf has been studied using a combination of in-hand data sets and current field programs. This analysis has demonstrated that there is significant variability on the timescale of days to weeks. However, the data sets do not provide enough information to show the impact of this variability on primary production.

A Fall 2000 deployment of the SeaHorse provided bi-hourly profiles of CTD and chlorophyll at one location over a three-week period. This was complemented with an upward-looking ADCP mounted at mid-depth on a second mooring. Results from this deployment indicate a subsurface chlorophyll maximum below the pycnocline during the first part of the time series. An event occurred in mid-October during which the temperature, salinity and density iso-surfaces rose approximately 25 m in the water column. During the peak of this event, the SeaHorse fluorometer indicates that a small bloom begins as nutrients are brought into the upper part of the water column. However, while there is a five-fold increase in integrated nutrients measured *in situ* during this period, the *in situ* integrated chlorophyll displayed no corresponding increase. SeaWiFS ocean color satellite images prove to be valuable in providing a spatial context for chlorophyll concentrations, however, the lack of temporal resolution due to poor quality individual images means that this data set provides limited information for short-term chlorophyll variability. Combining estimates of buoyancy frequency from CTD data with shear calculated from the ADCP provided estimates of gradient Richardson number, *Ri*, in 2 m bins. A

significant portion of the *Ri* values were less than one, indicating conditions favorable to mixing throughout most the water column but especially in the ocean mixed layer. A trend of decreasing Richardson number in the ocean mixed layer with increasing surface wind stress has been demonstrated.

The Canadian Atlantic Storms Program 1985-86 (CASP) provided a low-resolution array of ocean currents and hydrographic properties over a 4-month winter period on the Scotian Shelf. This data set recorded the seasonal cooling in the surface layer as well as an increasing salinity near the surface. Several events categorized by upward movement of warm, salty water were captured in this record. These events lasted from a few days to approximately 10 days. A strong coherence in hydrographic variability is evident at all the CASP mooring sites. The most likely cause of this variability is wind-driven upwelling. Low resolution estimates of *Ri* indicated a tendency for lower values at higher total and alongshore stress. The CASP data set has proved useful because it provides a set of observations similar to the ones that have been collected in the present observation program and indicates that wind forcing can contribute substantially to mixing, upwelling and stratification.

Direct measurements of dissipation of turbulent kinetic energy in an area close to Station 2 were studied using an existing data set from 1990. Unfortunately, the range of wind speeds encountered during this experiment was small and made it difficult to determine if any relationship exists between surface wind stress and turbulent mixing rates.

ACKNOWLEDGMENTS

This project was funded through the DFO Strategic Science Fund. The authors would like to thank Victor Soukhovtsev, Erin Carruthers and Cathy Porter for their assistance in the data analysis.

REFERENCES

Anderson, C. and P. Smith 1989. Oceanographic observations on the Scotian Shelf during CASP. *Atmos.-Ocean*, **27**, 130-156.

Donohue, S. 2000. A numerical model of an upwellingevent off the coast of Nova Scotia. M.Sc. thesis, Royal Military College of Canada, Kingston, Canada, 254 pp.

Fowler, G. A., J. M. Hamilton, B. D. Beanlands, D. J. Belliveau and A. R. Furlong, 1997: A wave powered profiler for long term monitoring. *Oceans '97 MTS/IEEE Conference Proc.*, 6-9 October, Halifax, 225-228.

Hachey, H. B., 1937. Ekman's theory applied to water replacement on the Scotian Shelf. *Proc. N. S. Inst. Sci.*, **19**, 264-276.

Hamilton, J. M., G. Fowler and B. Beanlands, 1999: Long-term monitoring with a moored wave-powered profiler. *Sea Technology*, **40**, 68-69.

Lively, R. 1988. Current meter, meteorological, sea level and hydrographic observations for the CASP experiment off the coast of Nova Scotia, November 1985 to April 1986. Can. Tech. Rep. Hydrogr. Ocean Sci. **100**, 428 pp.

Oakey, N.S., 1988: EPSONDE: An instrument to measure turbulence in the deep ocean. *IEEE J. Oceanic Eng.*, **13**, 124-128.

Oakey, N. S., and J. A. Elliott, 1982. Dissipation within the surface mixed layer. *J. Phys. Oceanogr.*, **12**, 171-185.

Petrie, B. 1975. M2 surface and internal tides on the Scotian shelf and slope. *J. Mar. Res.*, **33**, 303-323.

Petrie, B. 1983. Current response at the shelf break to transient wind forcing. *J. Geophys. Res.*, **88**, 9567-9578.

Petrie, B. and P. Yeats 2000. Annual and interannual variability of nutrients and their estimated fluxes in the Scotian Shelf-Gulf of Maine region. *Can. J. Fish. Aquat. Sci.*, **57**, 2536-2546.

Petrie, B., B. Topliss, and D. Wright 1987. Coastal upwelling and eddy development off Nova Scotia. *J. Geophys. Res.*, **29**, 12,979-12,991.

Sandstrom, H. 1980. On wind induced sea level changes on the Scotian Shelf. *J. Geophys. Res.*, **85**, 461-468.

Schwing, F. 1989. Subtidal response of the Scotian Shelf bottom pressure field to meteorological forcing. *Atmos.-Ocean*, **27**, 157-180.

Smith, P. C. 1989. Inertial oscillations near the coast of Nova Scotia during CASP. *Atmos.-Ocean*, **27**, 181-209.

Smith, P. C., and F. B. Schwing, 1991. Mean circulation and variability on the eastern Canadian continental shelf. *Cont. Shelf Res.*, **11**, 977-1012.

Therriault, J.-C., B. Petrie, P. Pepin, J. Gagnon, D. Gregory, J. Helbig, A. Herman, D. Lefaivre, M. Mitchell, B. Pelchat, J. Runge, and D. Sameoto. 1998. Proposal for a northwest Atlantic zonal monitoring program. Can. Tech. Rep. Hydrogr. Ocean Sci. **194**: vii+57p.

Turner, J. S. 1973. Buoyancy Effects in Fluids. Cambridge University Press. London, 367 pp.

Umoh, J. 1992. Seasonal and interannual variability of sea temperature and surface heat fluxes in the Northwest Atlantic. Ph. D. thesis, Dalhousie University, Halifax, N.S., Canada. 237 pp.

Umoh, J. and K. Thompson 1994. Surface heat flux, horizontal advection, and the seasonal evolution of water temperature on the Scotian Shelf. *J. Geophys. Res.*, **99**, 20,403-20,416.

Van Haren, H., N. Oakey, and C. Garrett 1994. Measurements of internal wave band eddy fluxes above a sloping bottom. *J. Mar. Res.*, **52**, 909-946.

TABLES

Table 1: Correlations\slopes between alongshore wind stress and currents at CASP Station 3. Correlations are in lower left half, slopes in upper right.

	Stress	U(16 m)	U(50 m)	U(70 m)	U(110 m)
Stress	1				
U(16 m)	0.16	1	0.86	0.71	0.38
U(50 m)	0.06	0.88	1	0.81	0.47
U(70 m)	0.17	0.81	0.91	1	0.51
U(110 m)	0.17	0.51	0.61	0.71	1

FIGURES

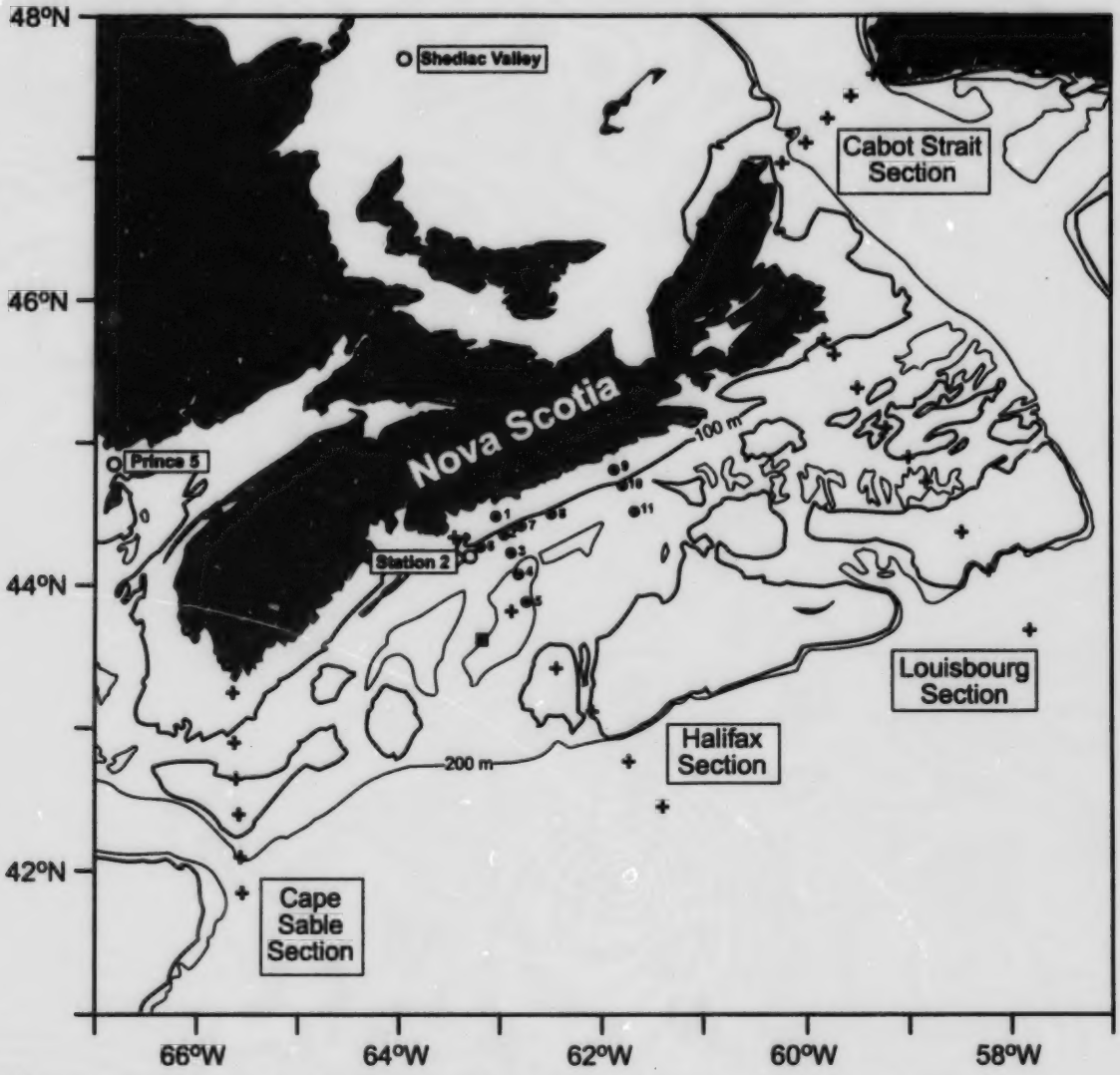

Figure 1: Map of Scotian Shelf showing the fixed stations (open circles) and monitoring sections (plus signs) which are part of the AZMP. Station 2 on the Halifax Section is the site of SeaHorse and ADCP moorings deployed in the Fall 2000. The 100 and 200 m isobaths are drawn as thick and thin solid lines, respectively. Canadian Atlantic Storms Program (CASP) mooring locations are marked with solid circles. The location of the 1990 microstructure measurements are indicated by the solid square.

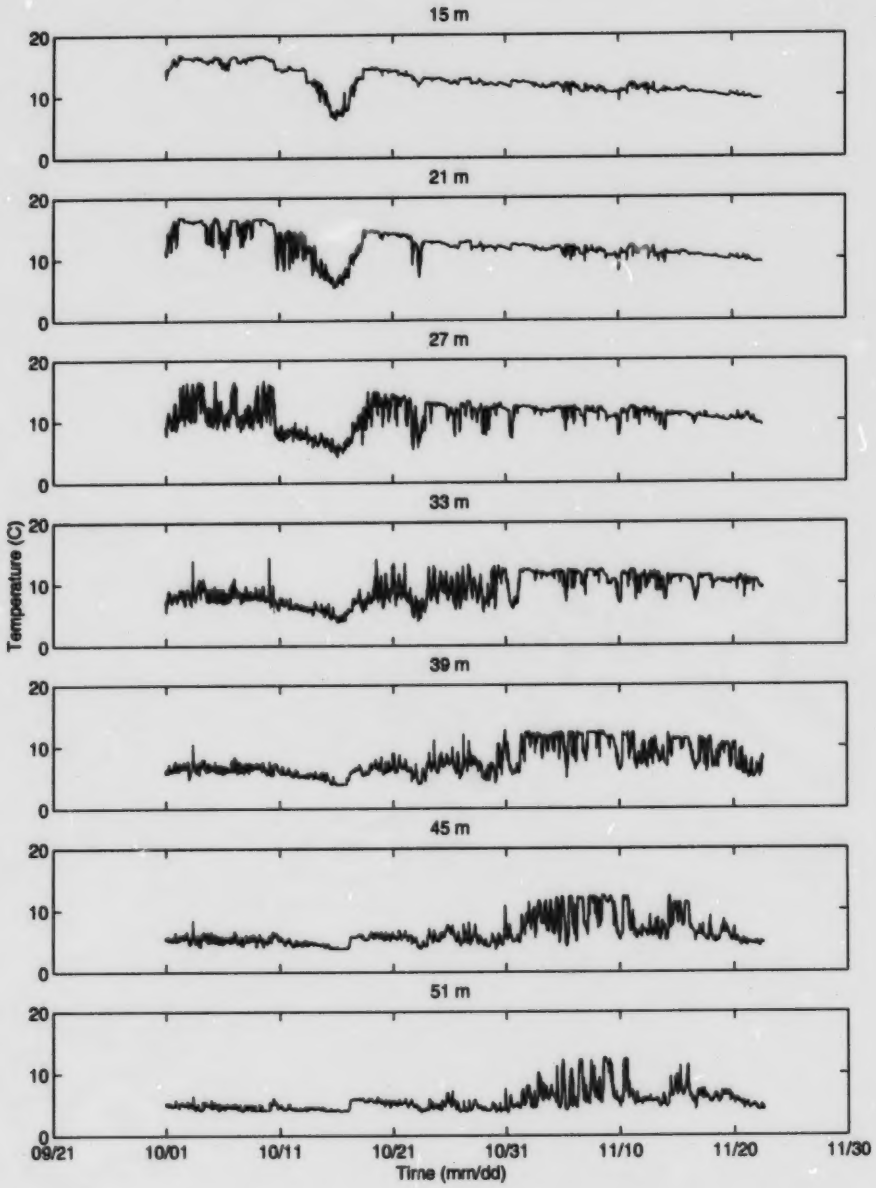

Figure 3: Time series of water temperatures measured with Minilog recorders at fixed depths spaced 6 m apart on the mooring wire.

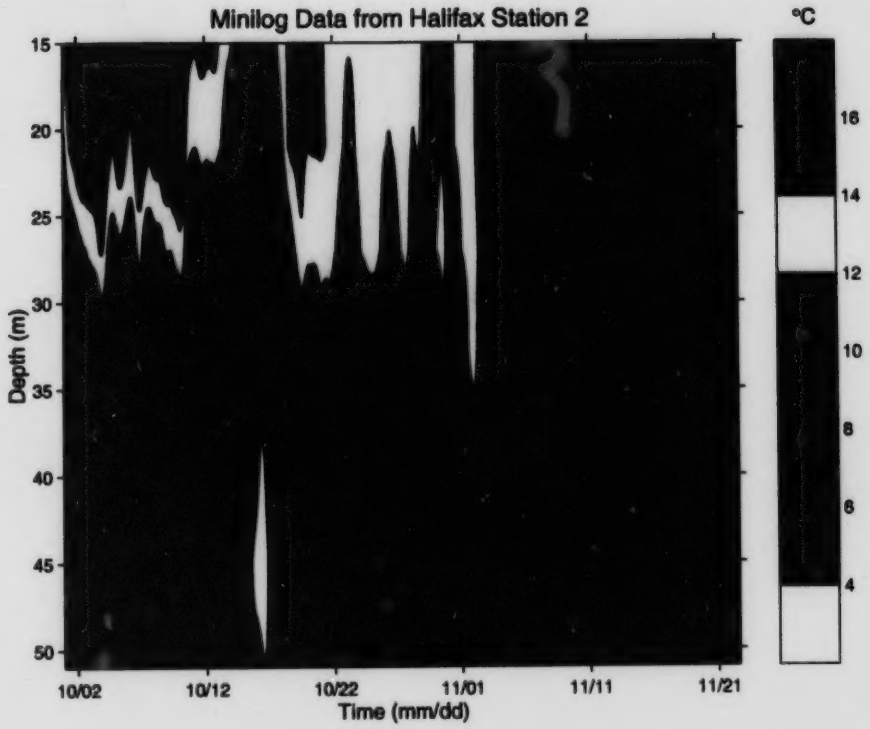

Figure 4: Contour plot of the seven temperature time series recorded with Vemco Minilogs. The Minilogs were spaced 6 m apart starting at 15 m depth and ending at 51 m.

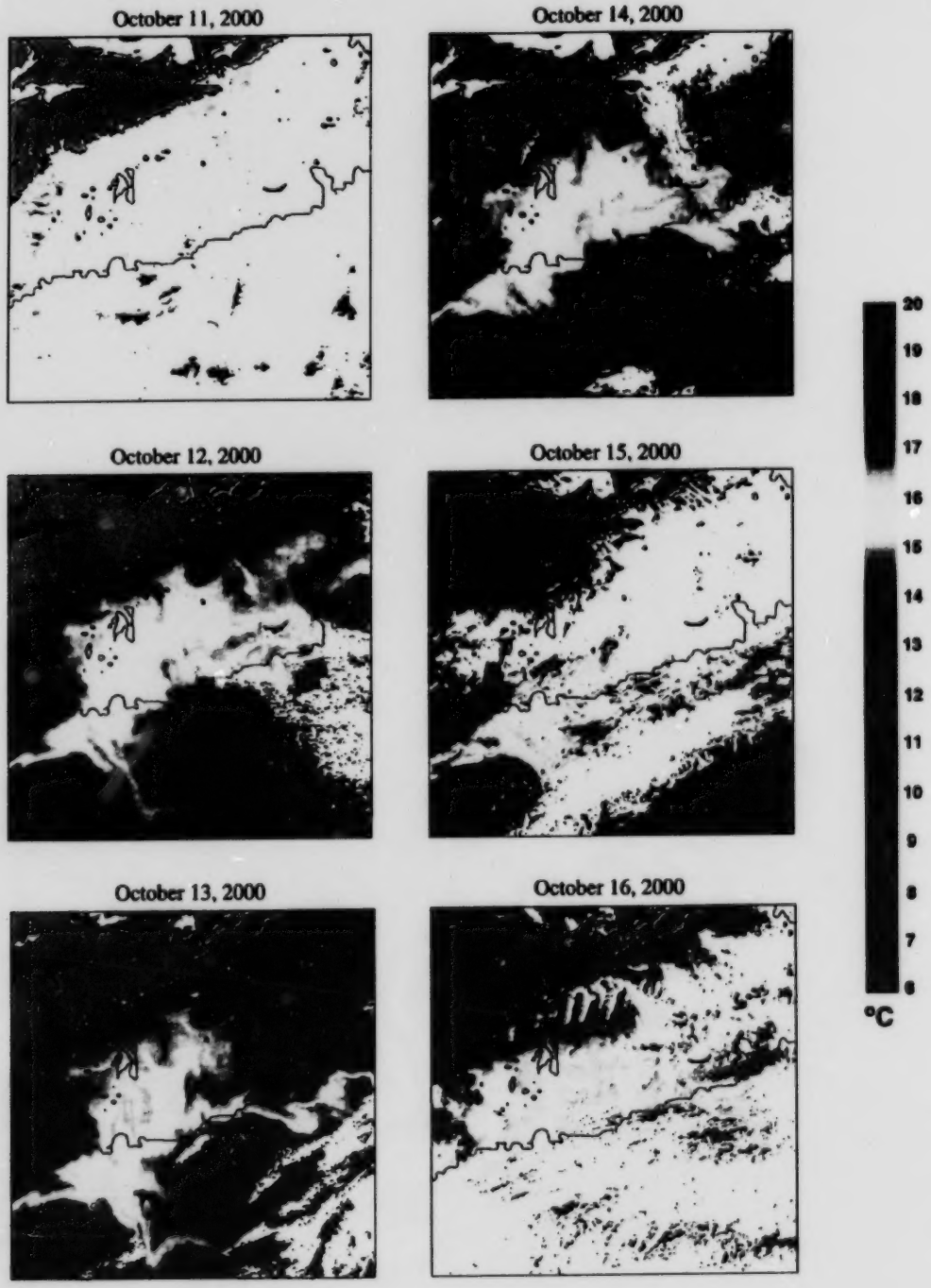

Figure 5: NOAA AVHRR sea surface temperature for the period surrounding the cooling event captured by the Minilog temperature recorders.

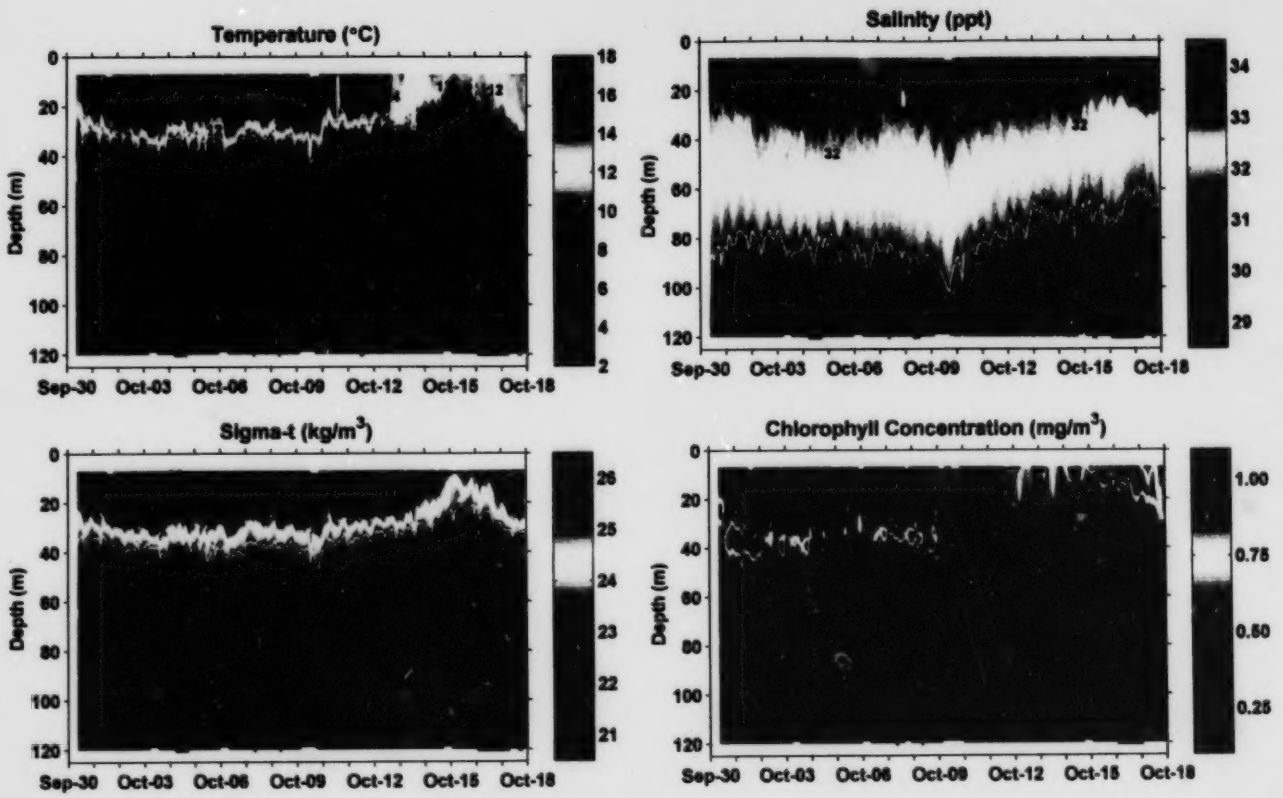

Figure 6: Temperature, salinity, density (sigma-t) and chlorophyll at Sta. 2, September 30 – October 18, 2000.

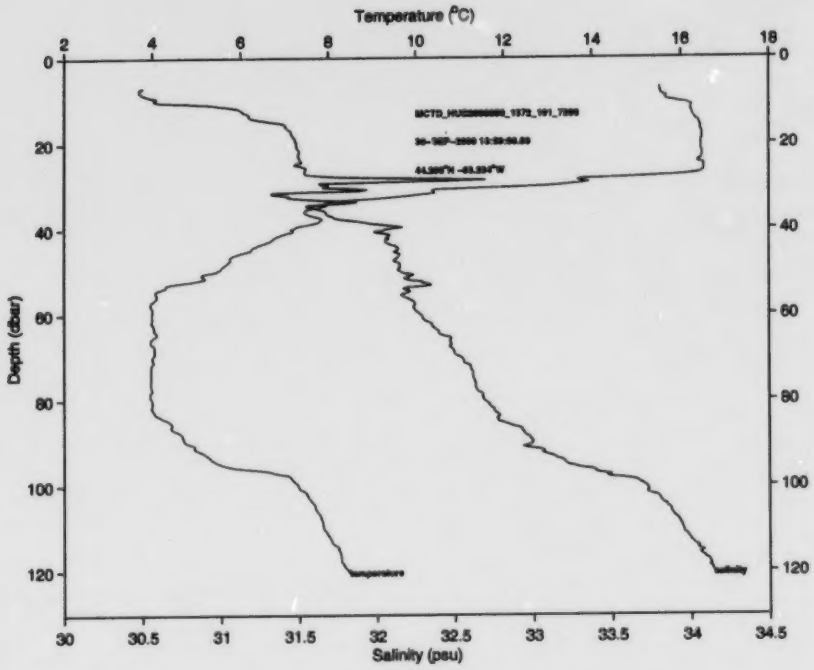

Figure 7: Typical Station 2 (Halifax Section) temperature and salinity profile from the Sea-Bird model 19 CTD. The "spikes" in salinity are caused by different response functions of the temperature and conductivity sensors.

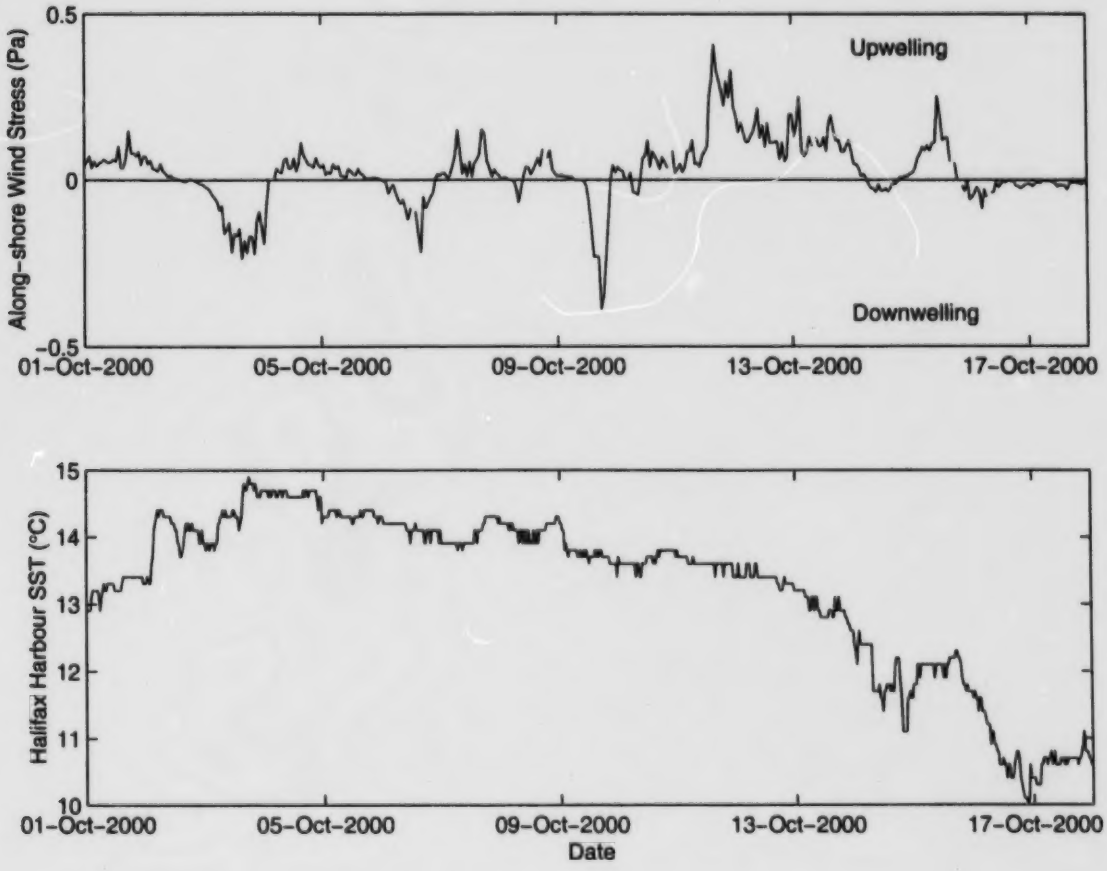

Figure 8: (Upper panel) Along-shore (60°T) wind stress calculated using Sable Island wind data. Positive (negative) stress is upwelling (downwelling) favorable. (Lower panel) Halifax harbour sea surface temperature from Minilog recorder.

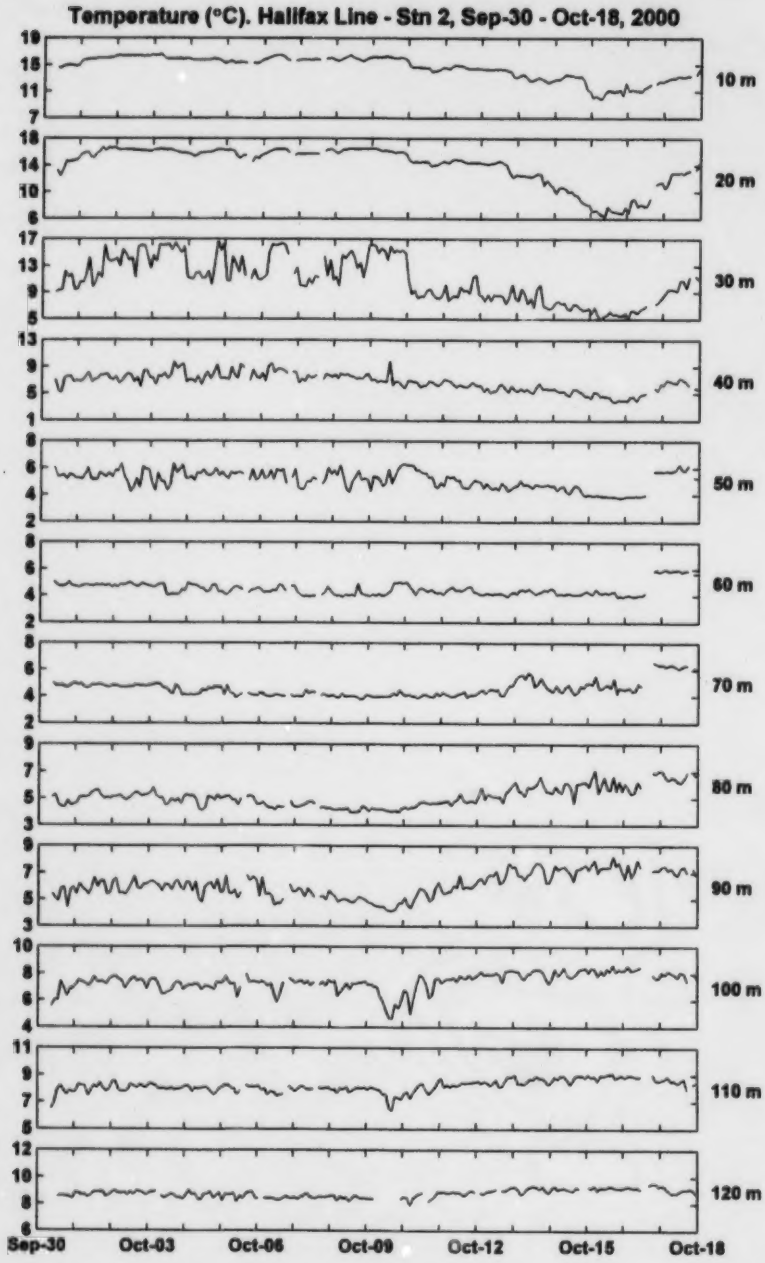

Figure 9a: Temperature time series from selected depths at Sta. 2. Gaps indicate that the SeaHorse failed to rise to the top of the mooring during a sampling cycle.

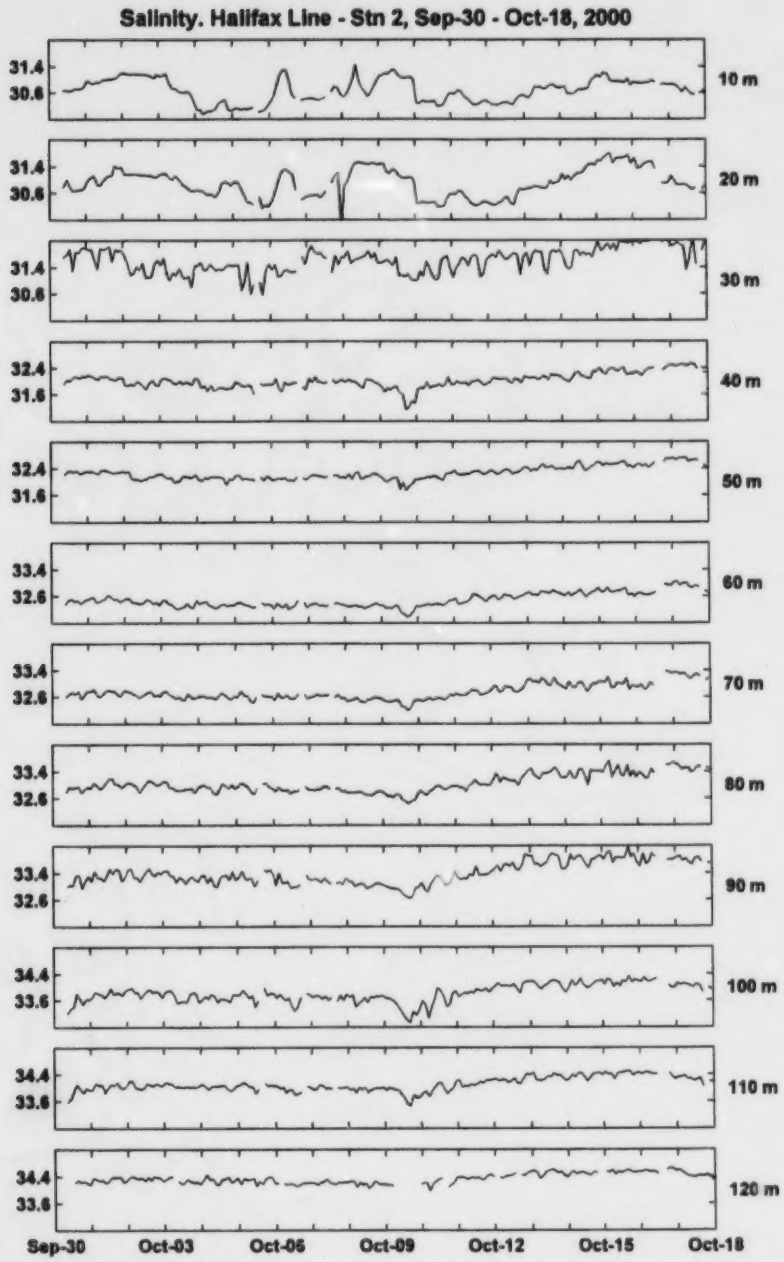

Figure 9b: Salinity time series from selected depths at Sta. 2. Gaps indicate that the SeaHorse failed to rise to the top of the mooring during a sampling cycle.

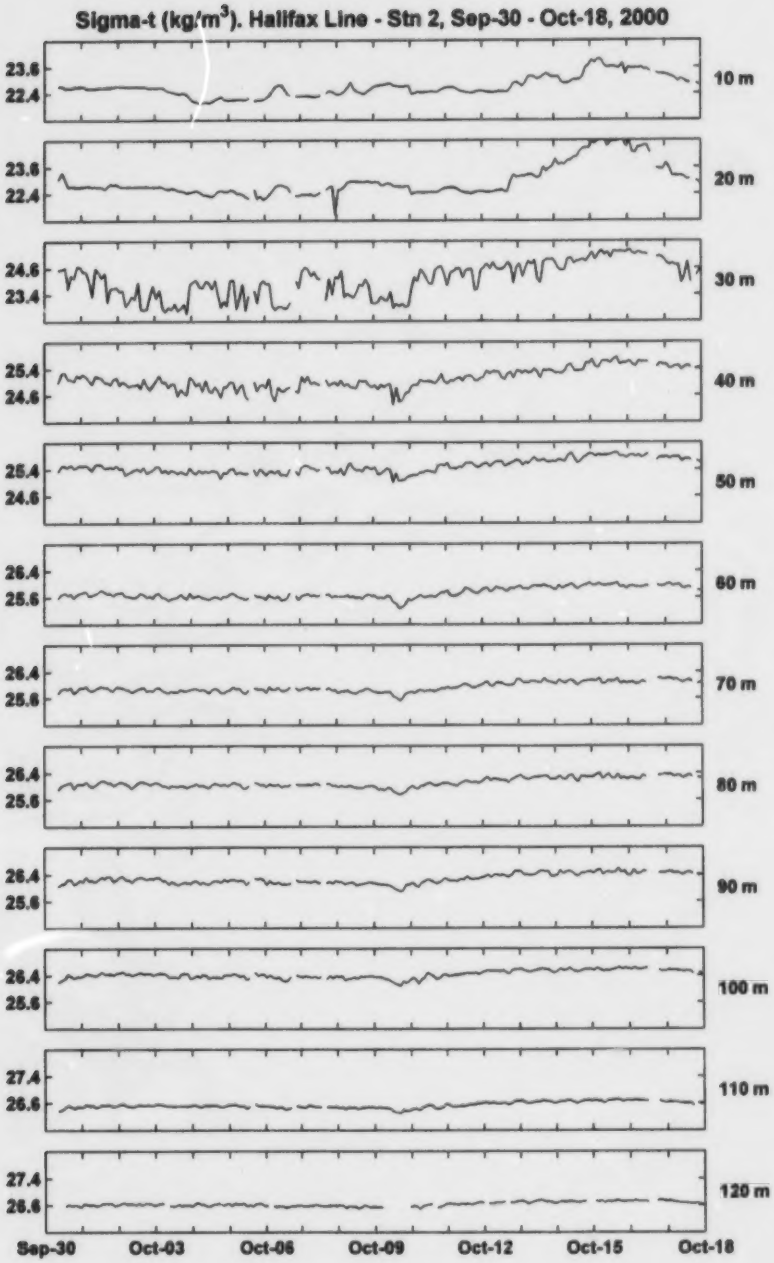

Figure 9c: Density time series from selected depths at Sta. 2. Gaps indicate that the SeaHorse failed to rise to the top of the mooring during a sampling cycle.

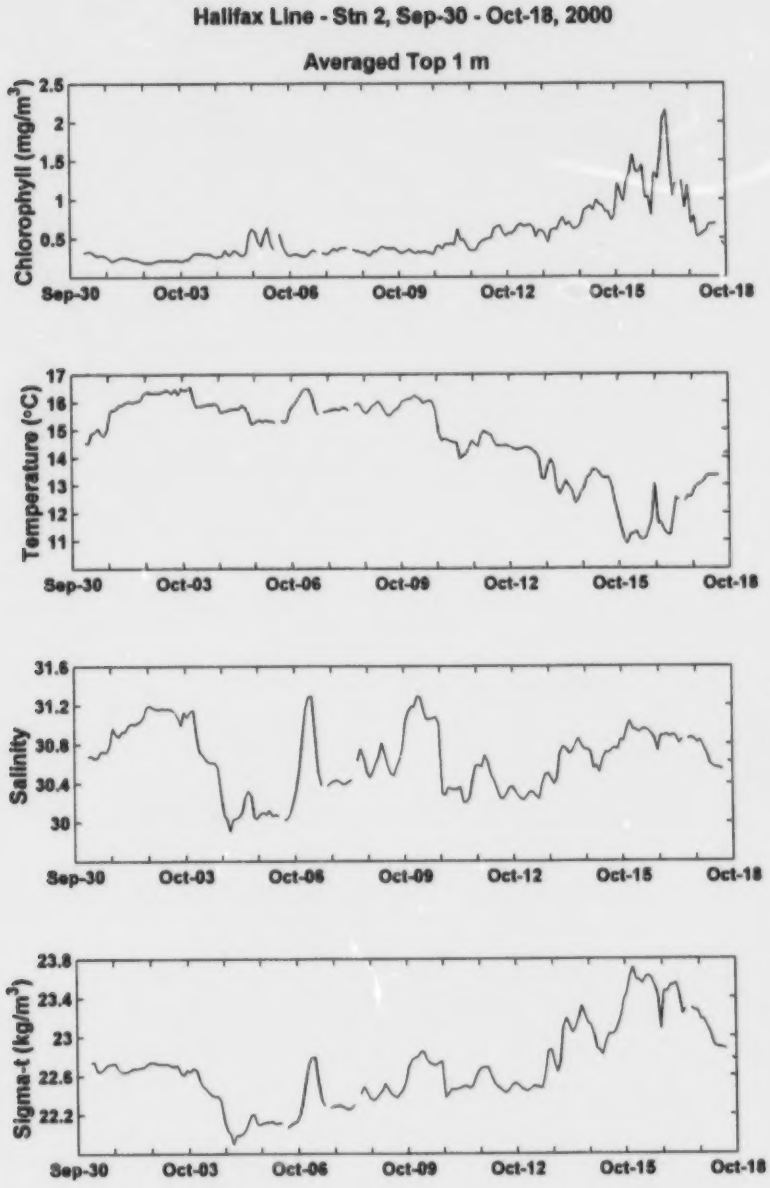

Figure 10: Average top 1 m chlorophyll, temperature, salinity and density from the SeaHorse profiles. In nearly all cases, the top 1 m corresponds to the 7-8 m interval below the sea surface.

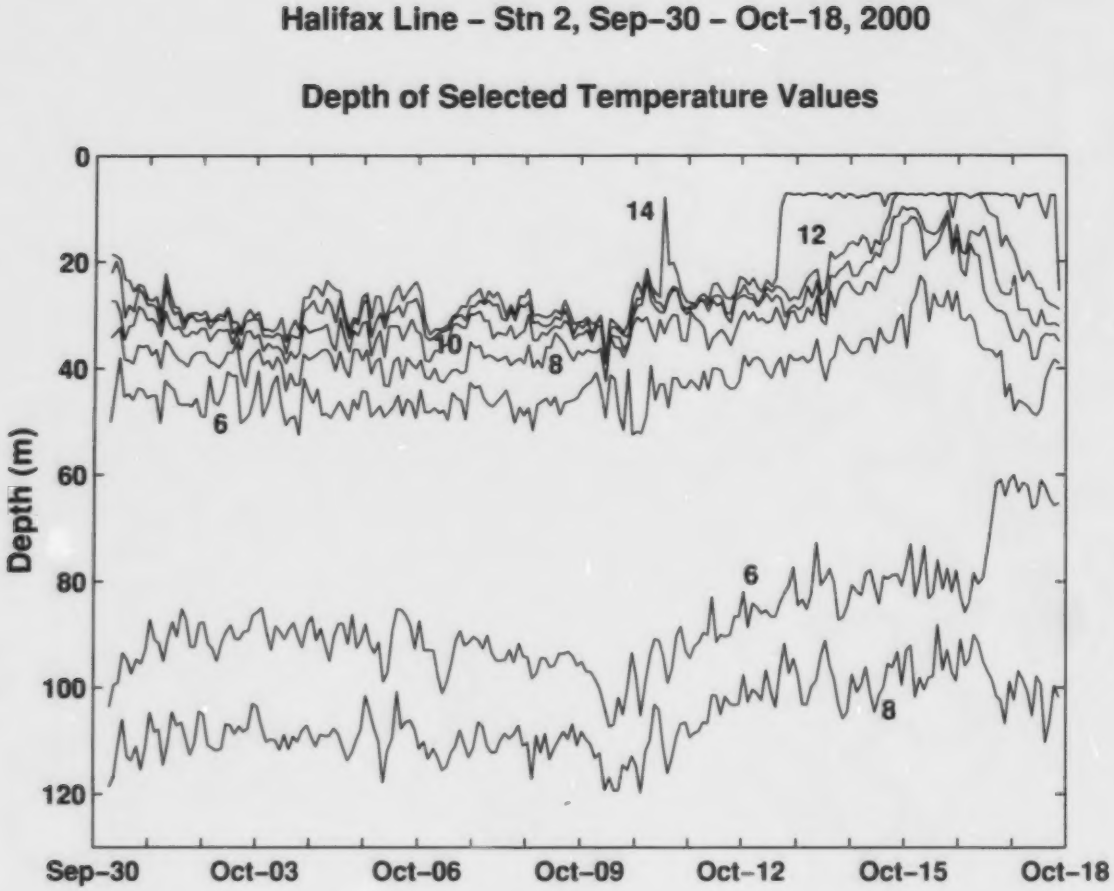

Figure 11a: Depth of selected temperature surfaces.

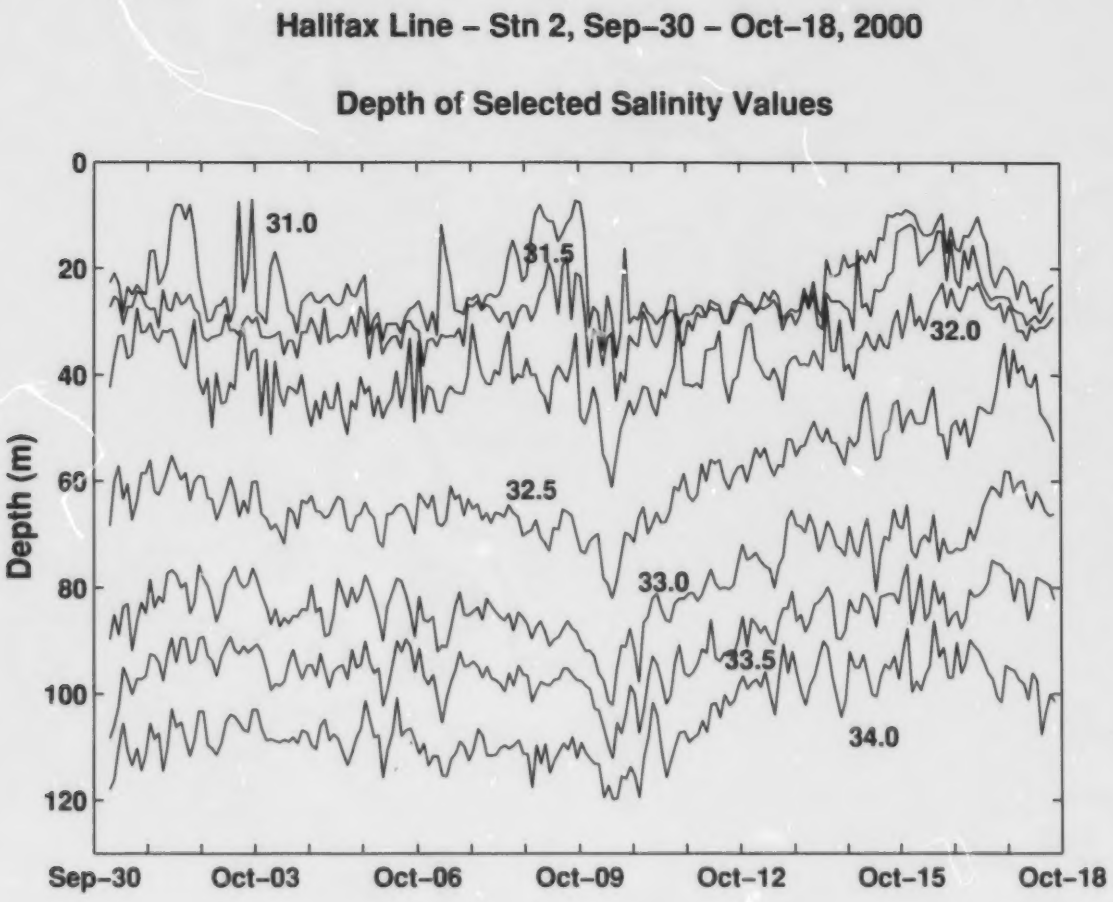

Figure 11b: Depth of selected salinity surfaces.

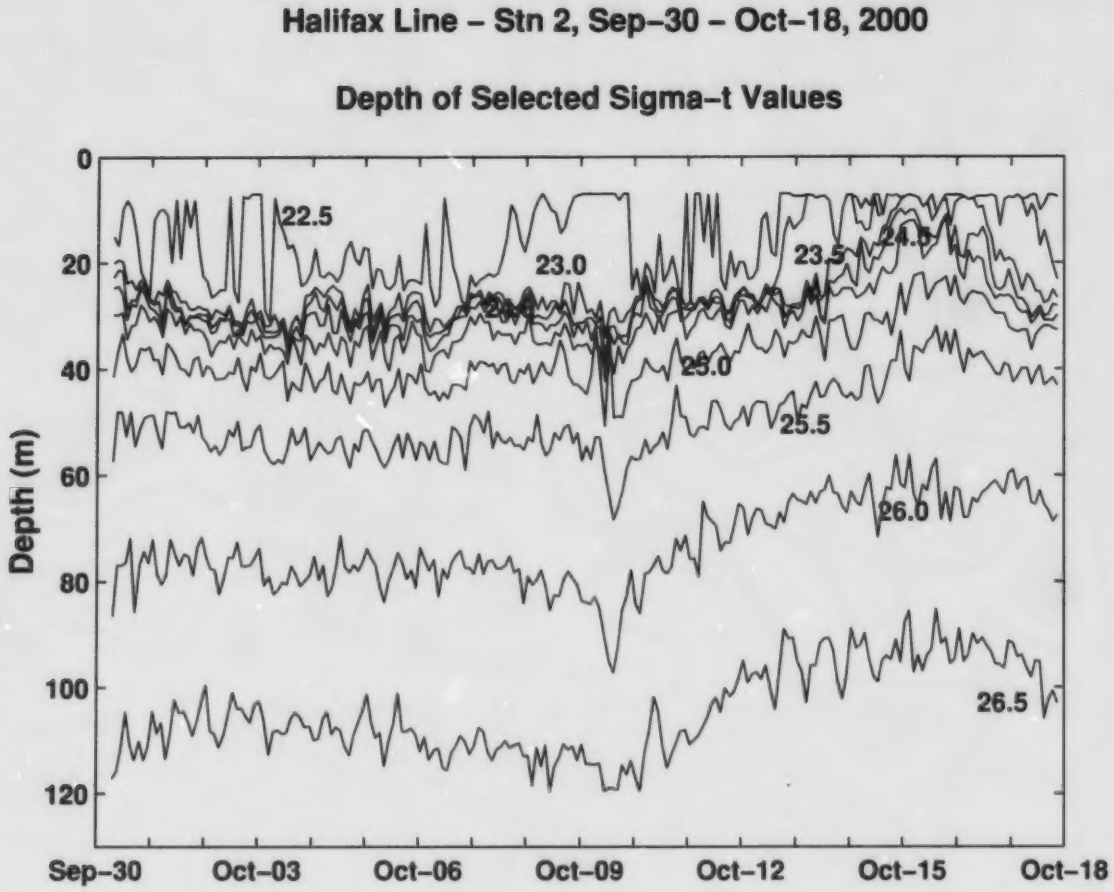

Figure 11c: Depth of selected density surfaces.

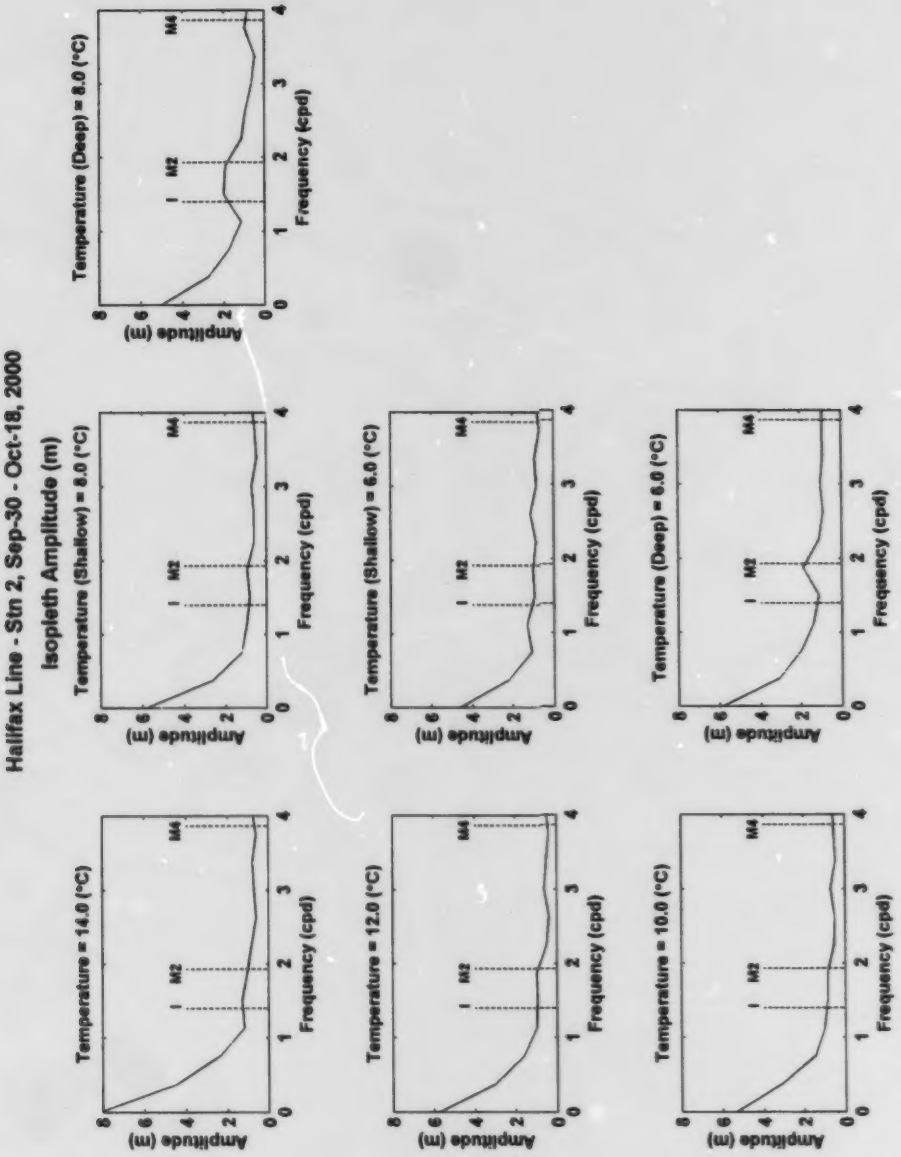

Figure 12a: Spectra of vertical amplitude for selected temperature isopleths. Note that the amplitude corresponds to that associated with the harmonic component at each frequency.

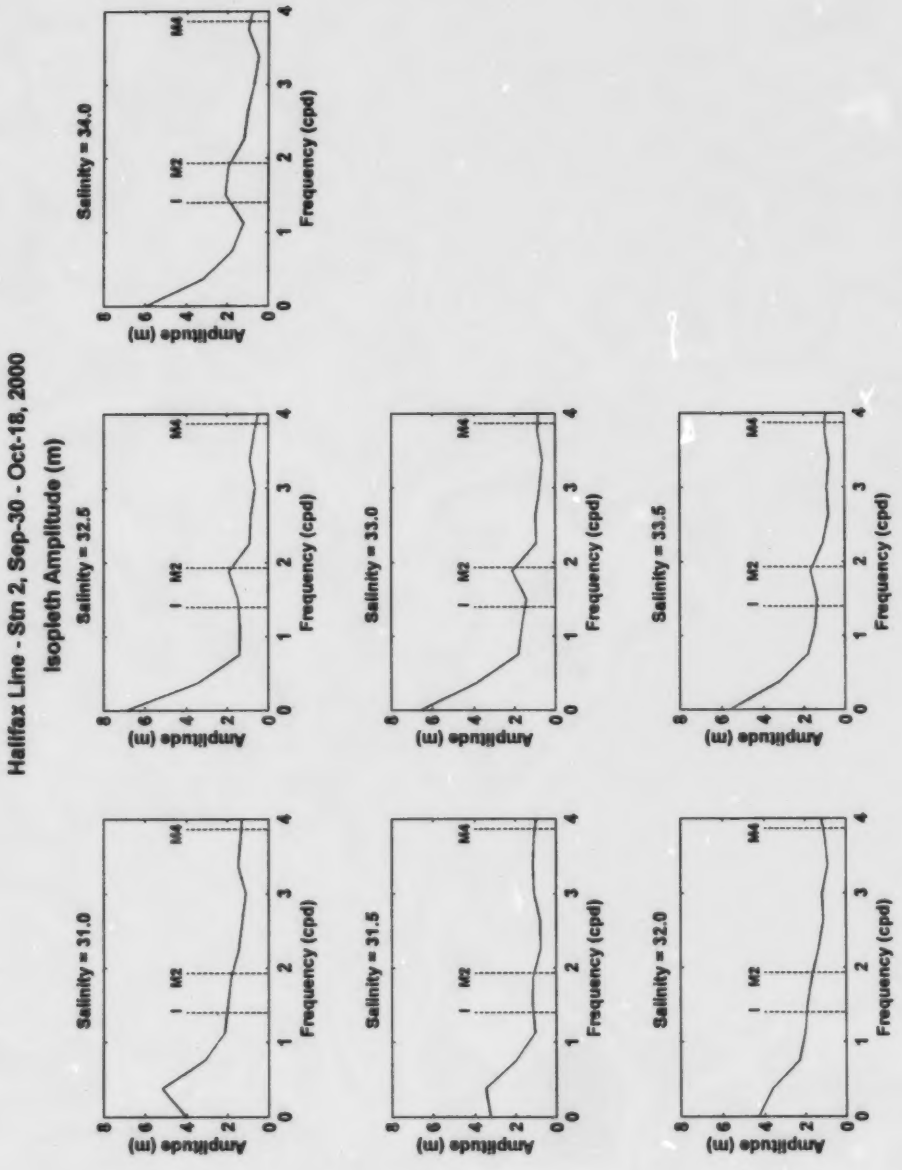

Figure 12b: Spectra of vertical amplitude for selected salinity isopleths. Note that the amplitude corresponds to that associated with the harmonic component at each frequency.

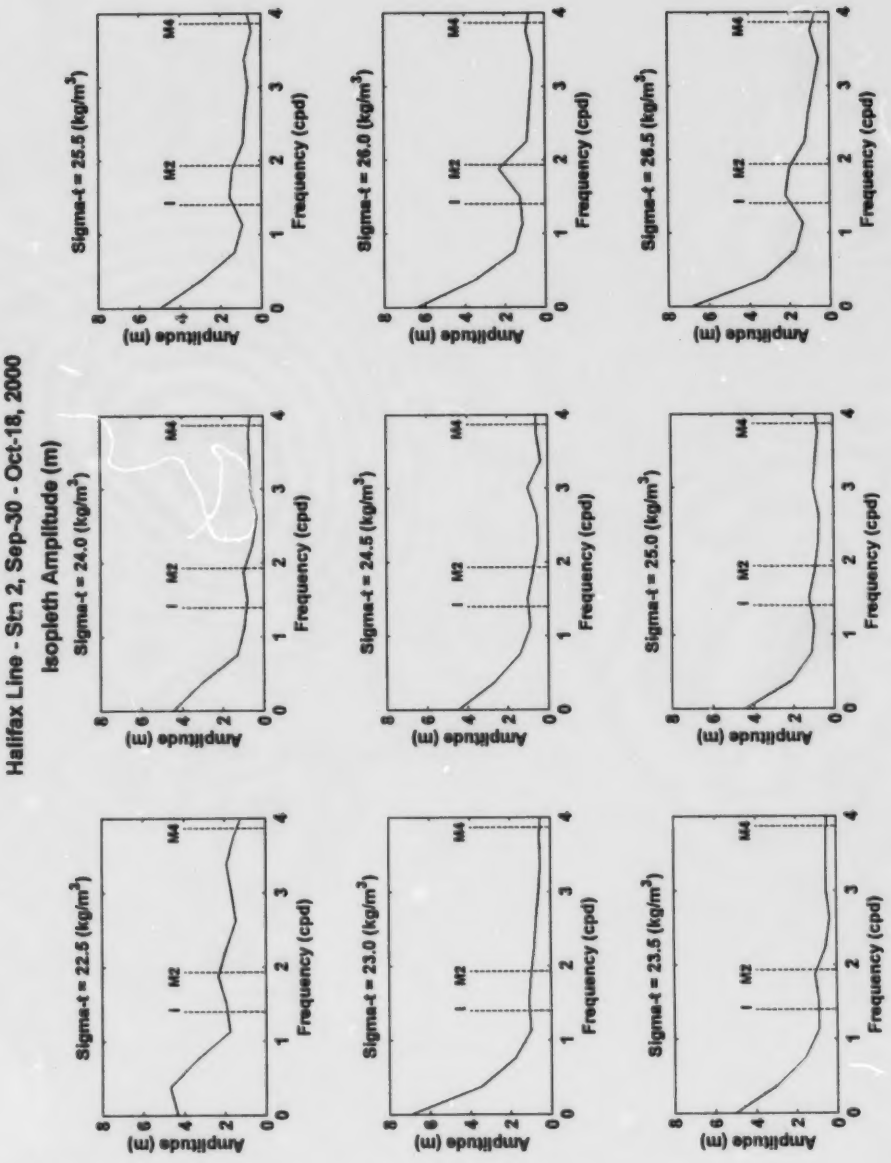

Figure 12c: Spectra of vertical amplitude for selected density isopleths. Note that the amplitude corresponds to that associated with the harmonic component at each frequency.

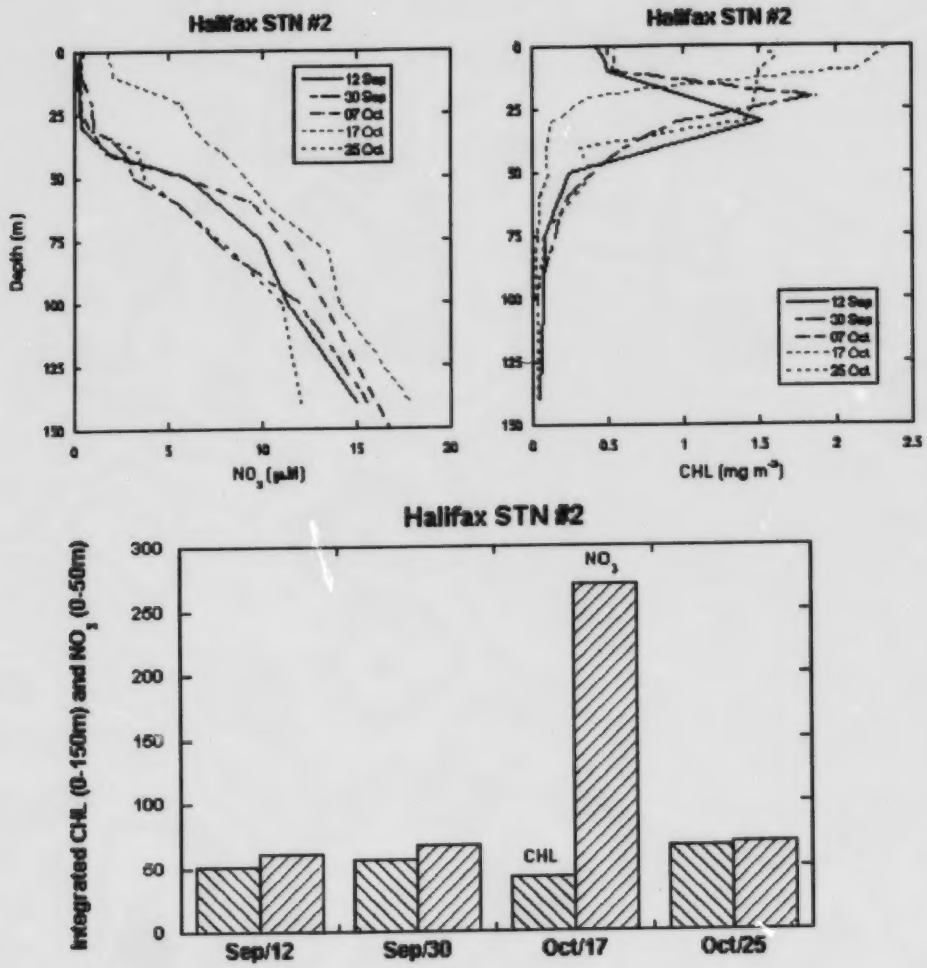

Figure 13: Top panels: vertical profiles of nitrate and chlorophyll concentrations taken during AZMP cruises to Halifax Line – Station 2. Five dates were selected to bracket the Seahorse deployment of 30 September - 18 October. Bottom panel: column integrals of nitrate and chlorophyll concentrations for same stations. Note: there were no chlorophyll samples for the 7 October station occupation.

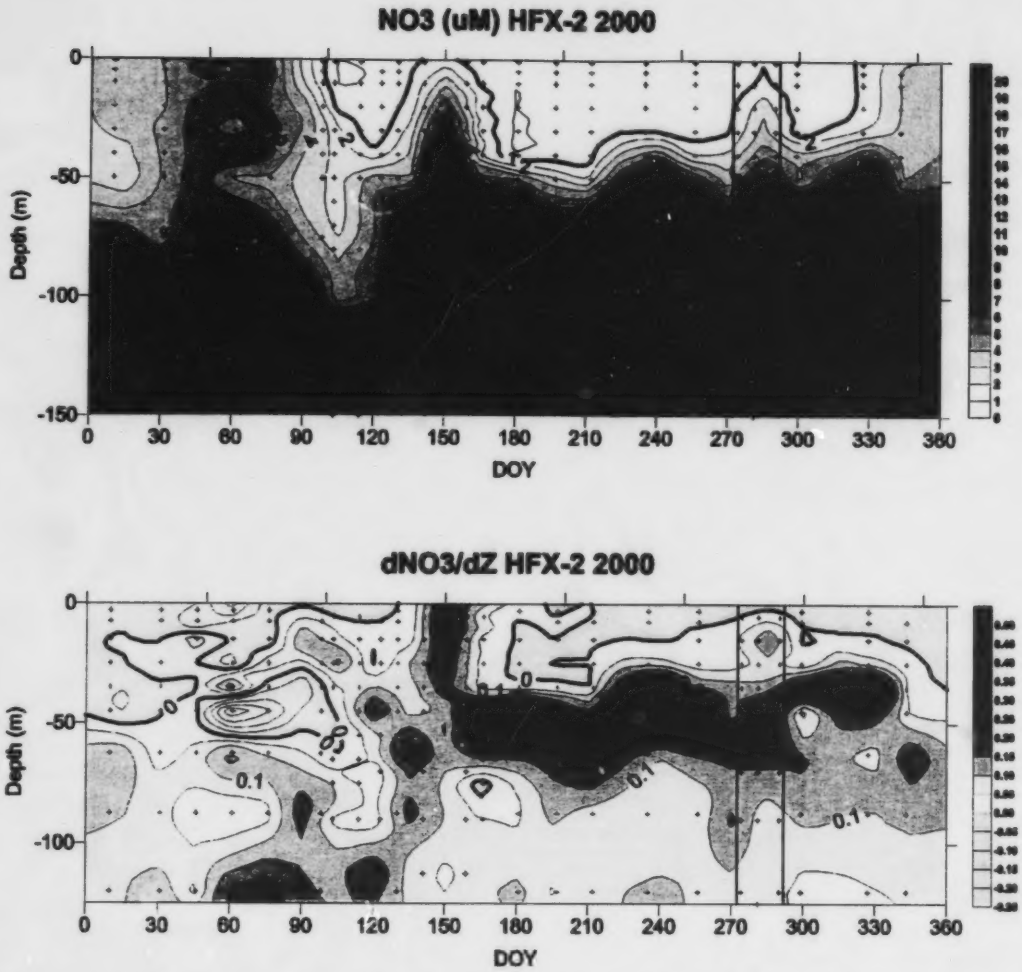

Figure 14: Contour plots of nitrate concentrations (upper panel) concentration gradients (lower panel) at Halifax Line – Station during 2000. Vertical lines in both figures between days 270 and 300 represent the Seahorse deployment period.

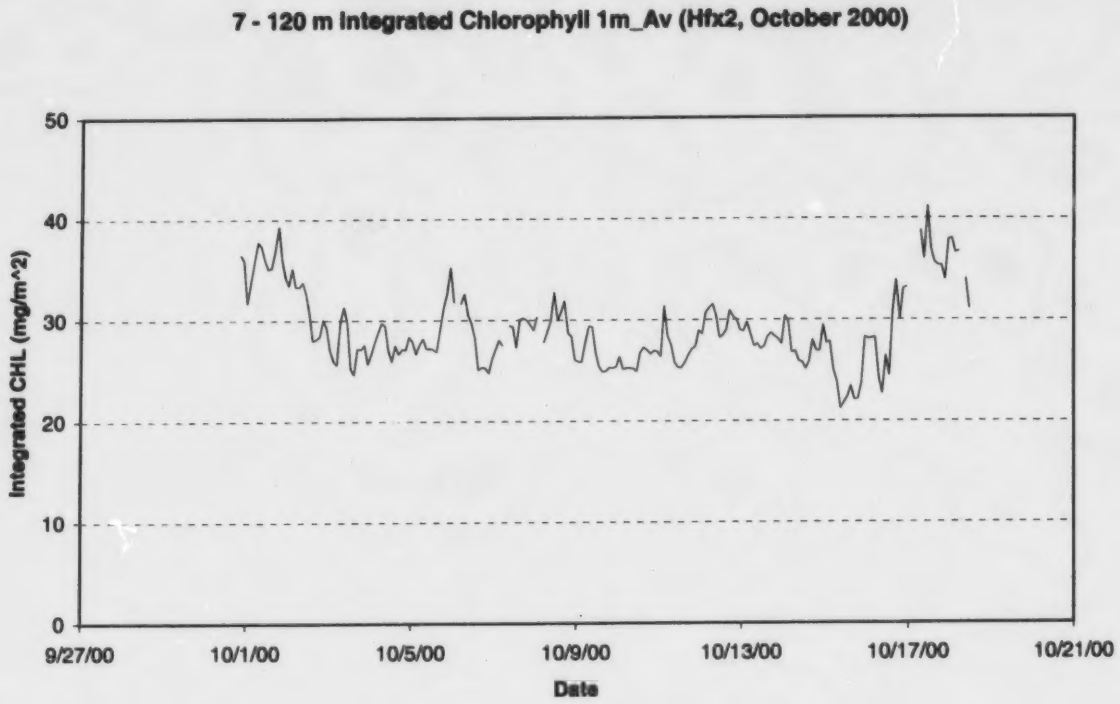

Figure 15: Integrated chlorophyll from 7-120 m depth as measured by the WetLabs fluorometer on the SeaHorse.

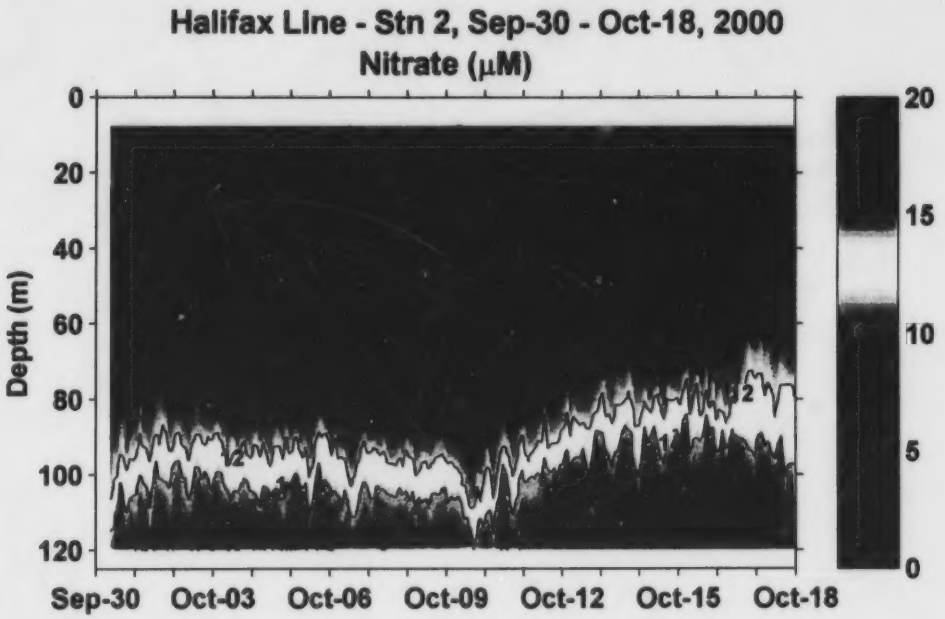

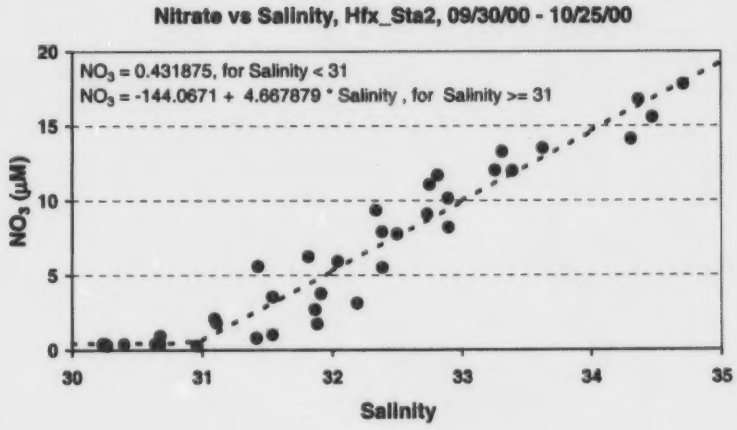

Figure 16a: Nitrate field created from the SeaHorse salinity data using the relationships derived from ship-based CTD and nutrient profiles from September 30, October 7, 17 and 25.

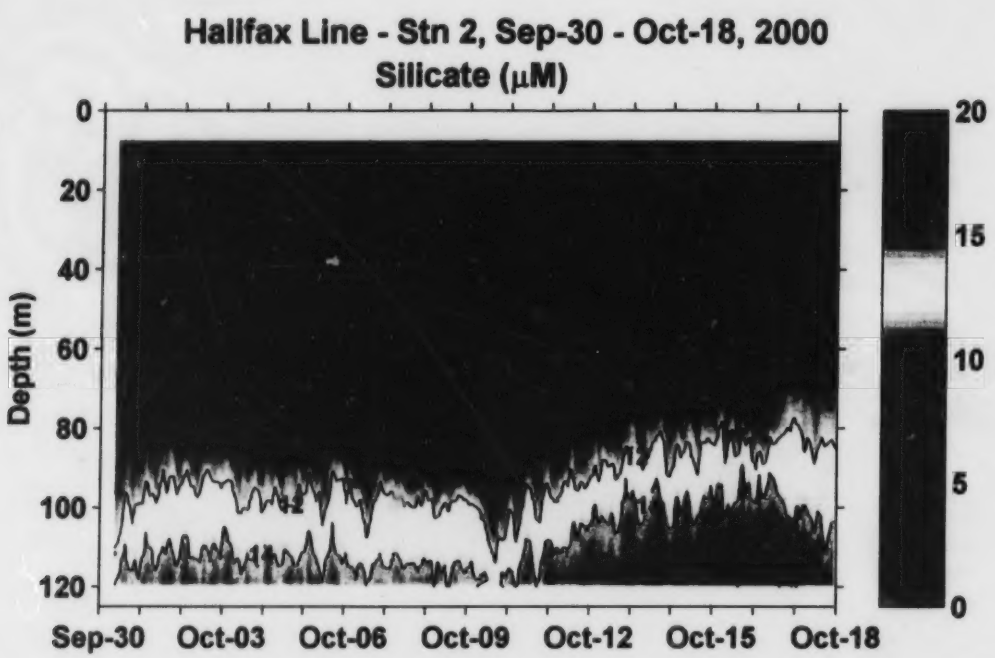

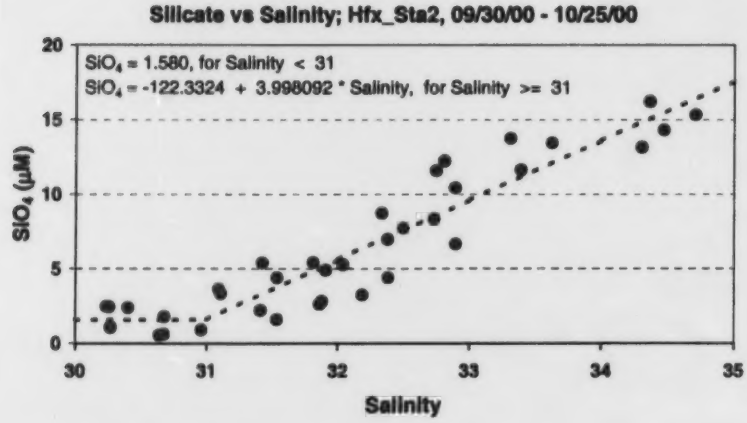

Figure 16b: Silicate field created from the SeaHorse salinity data using the relationships derived from ship-based CTD and nutrient profiles from September 30, October 7, 17 and 25.

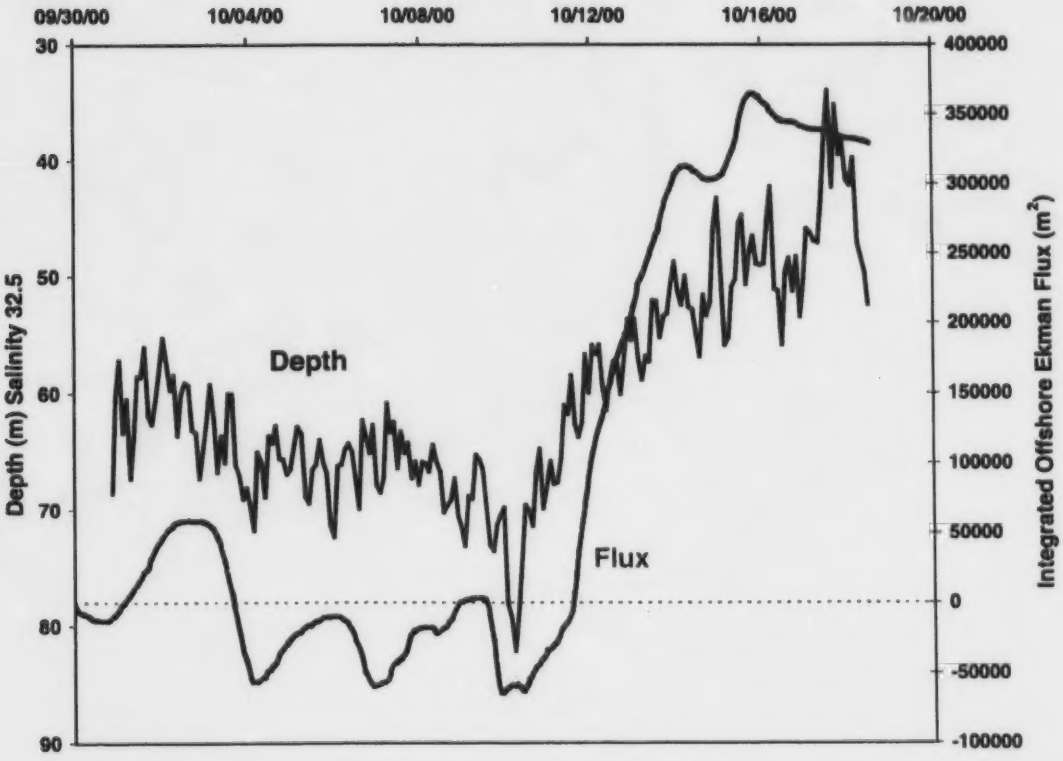

Figure 17: Time series of the depth of the 32.5 isohaline and the integrated offshore Ekman flux.

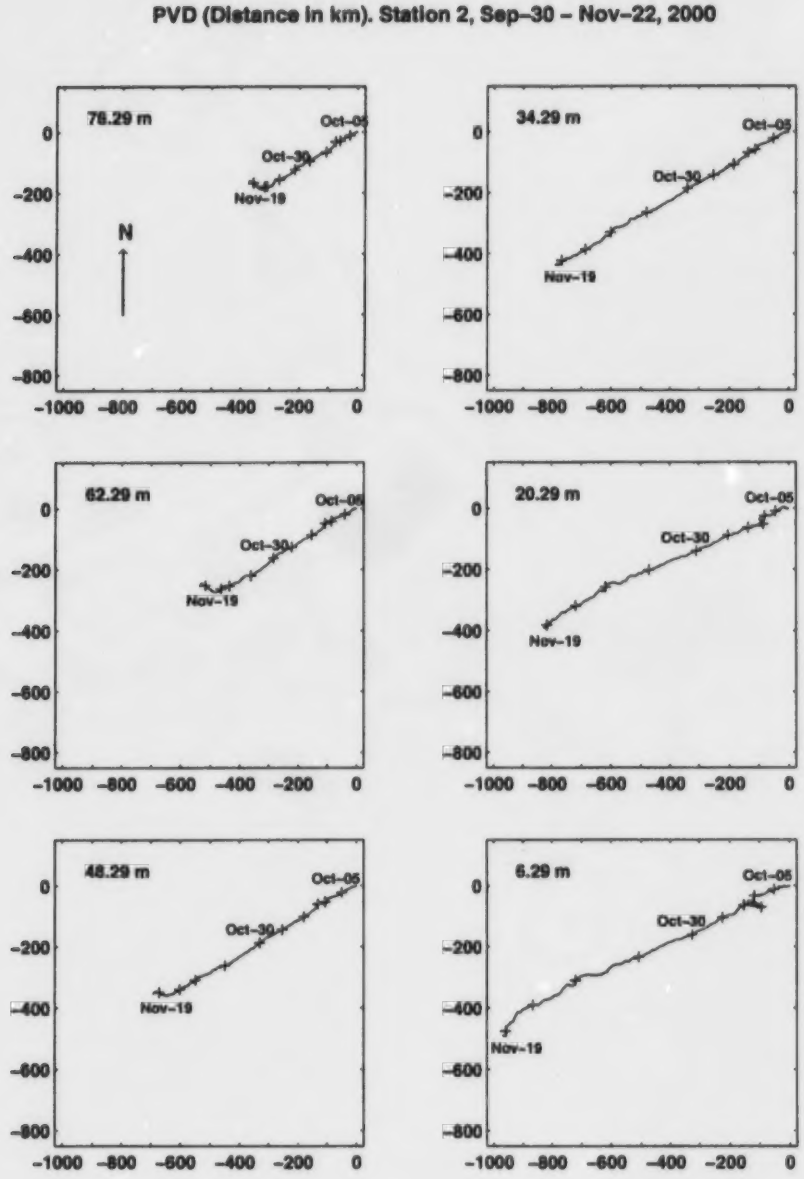

Figure 18: Progressive vector diagram for selected ADCP bins. Each cross marker denotes five days elapsed time. The depth of the bin is indicated in the upper left of each panel.

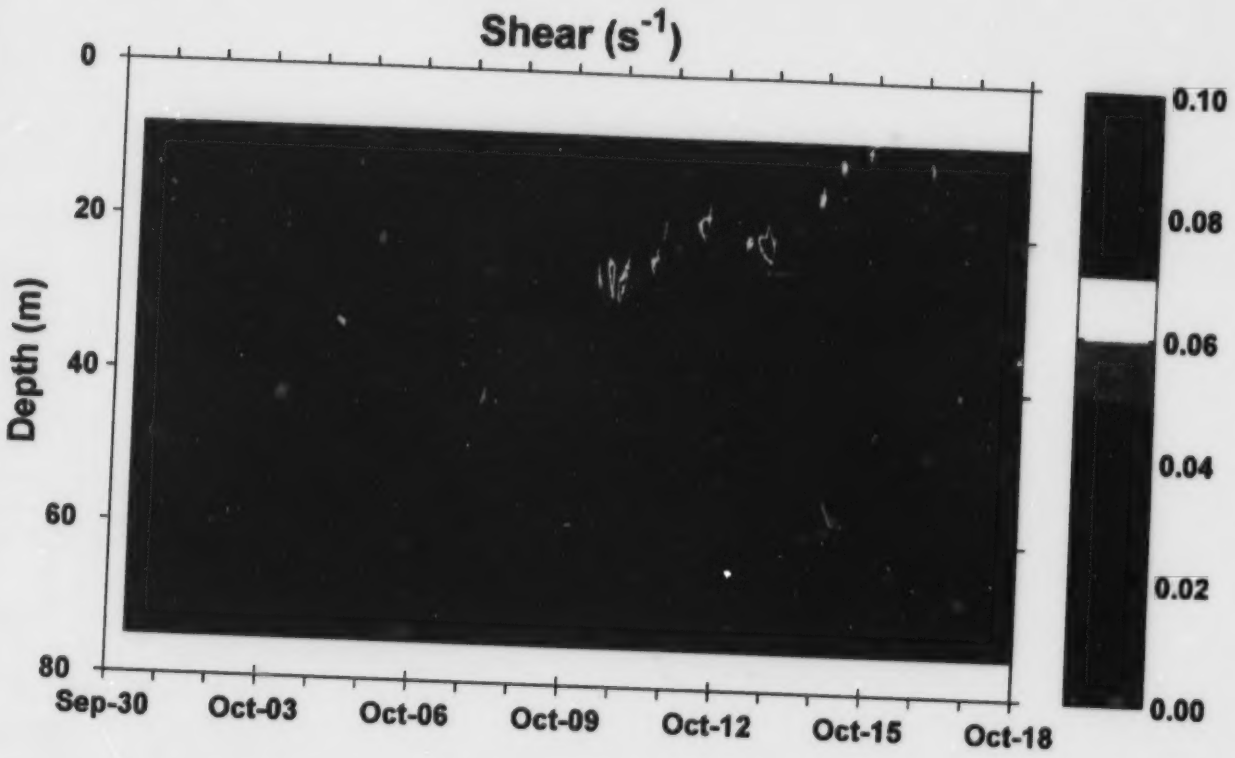

Figure 19: Vertical shear in the water column calculated using RDI ADCP. This includes only ADCP data within 15 minutes of SeaHorse CTD profiles.

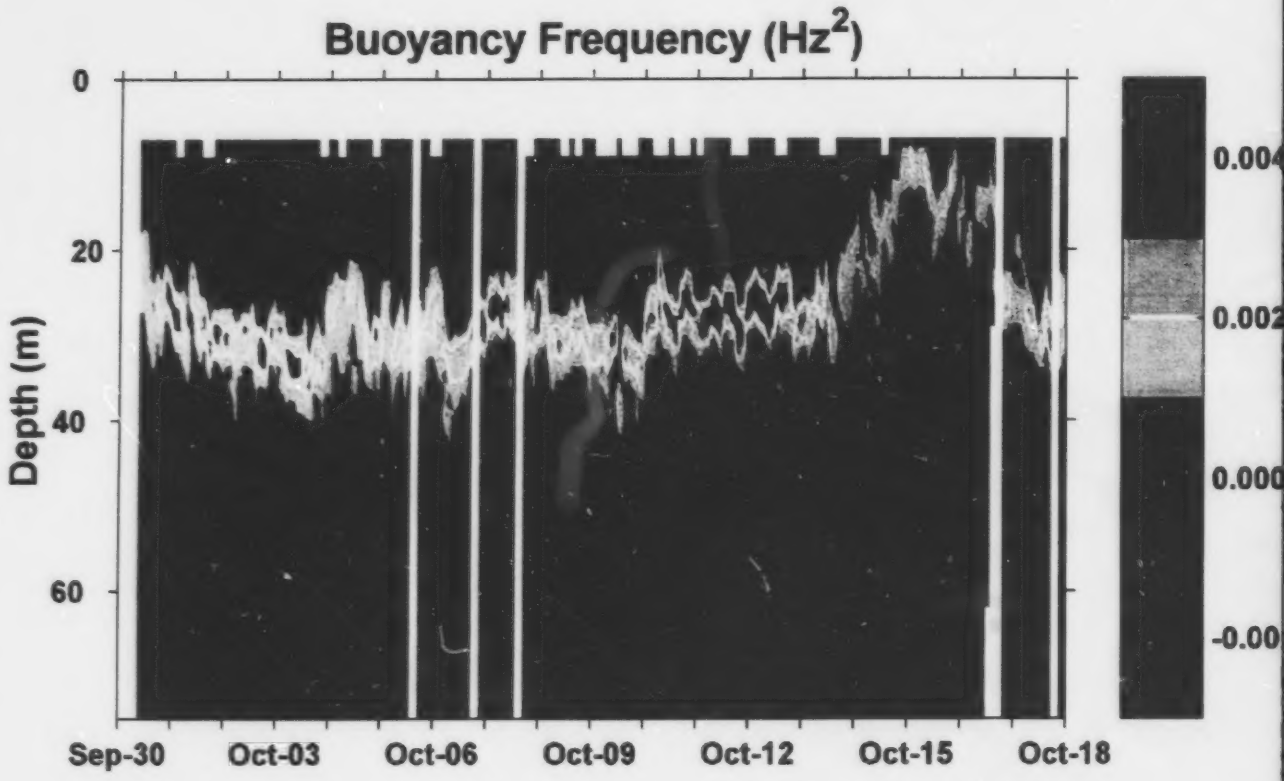

Figure 20: Contour plot of buoyancy frequency calculated from the SeaHorse CTD profiles.

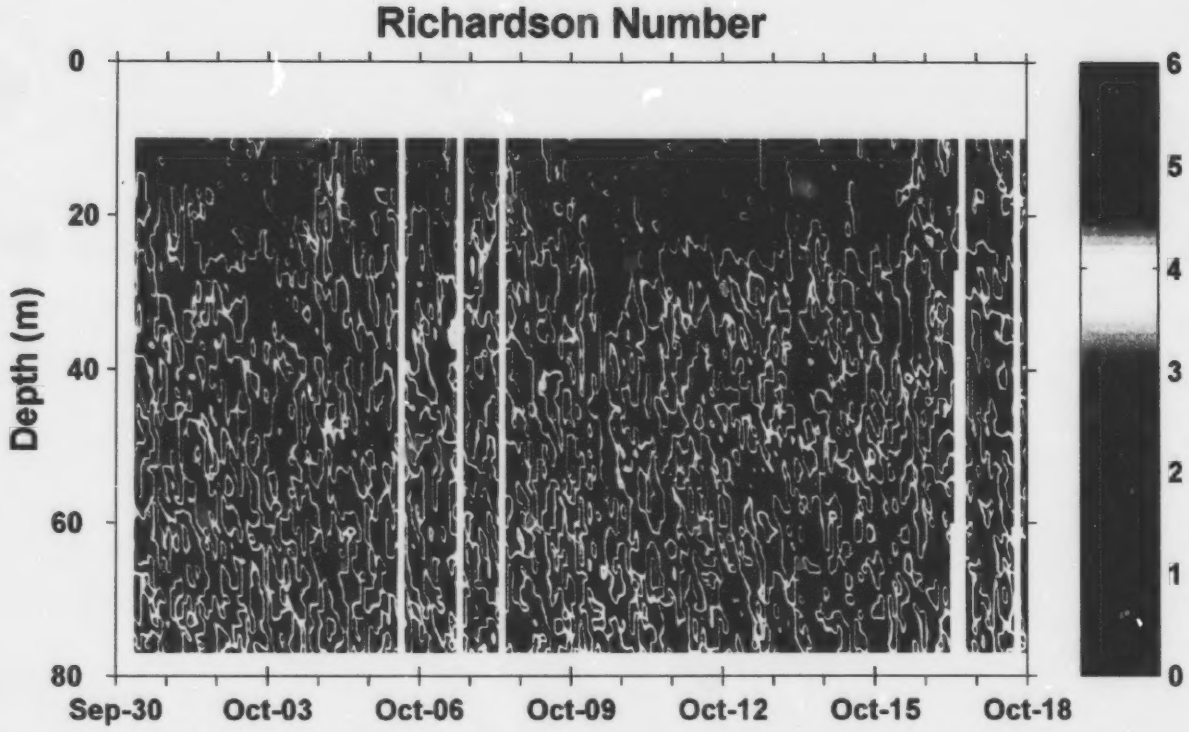

Figure 21: Gradient Richardson number calculated by combining ADCP and CTD data from the two moorings at Station 2.

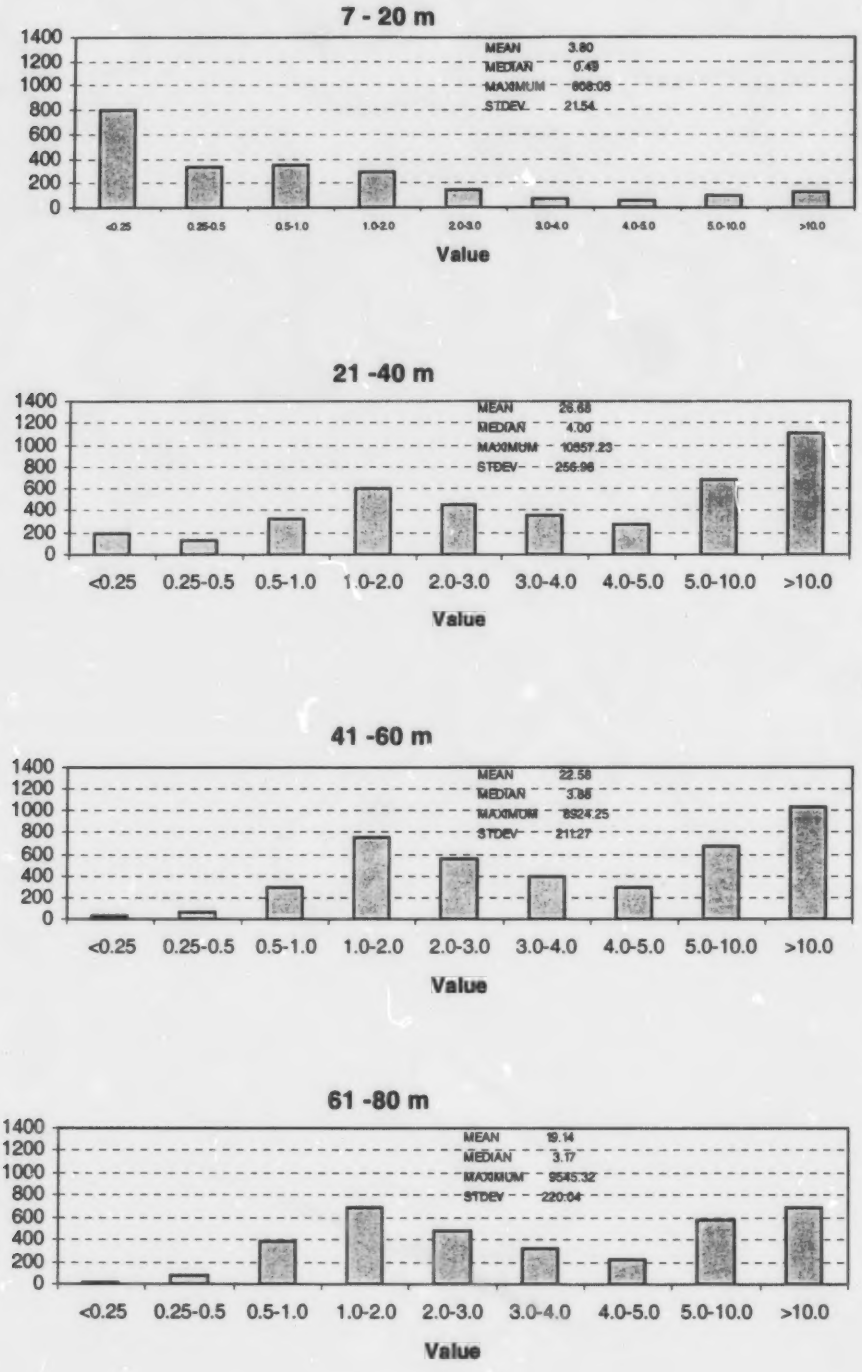

Figure 22: Histograms of Richardson number estimates at four depth intervals for the period 30 Sep – 18 Oct, 2000 at Station 2, Halifax Section. Statistics are included in the legend of each histogram.

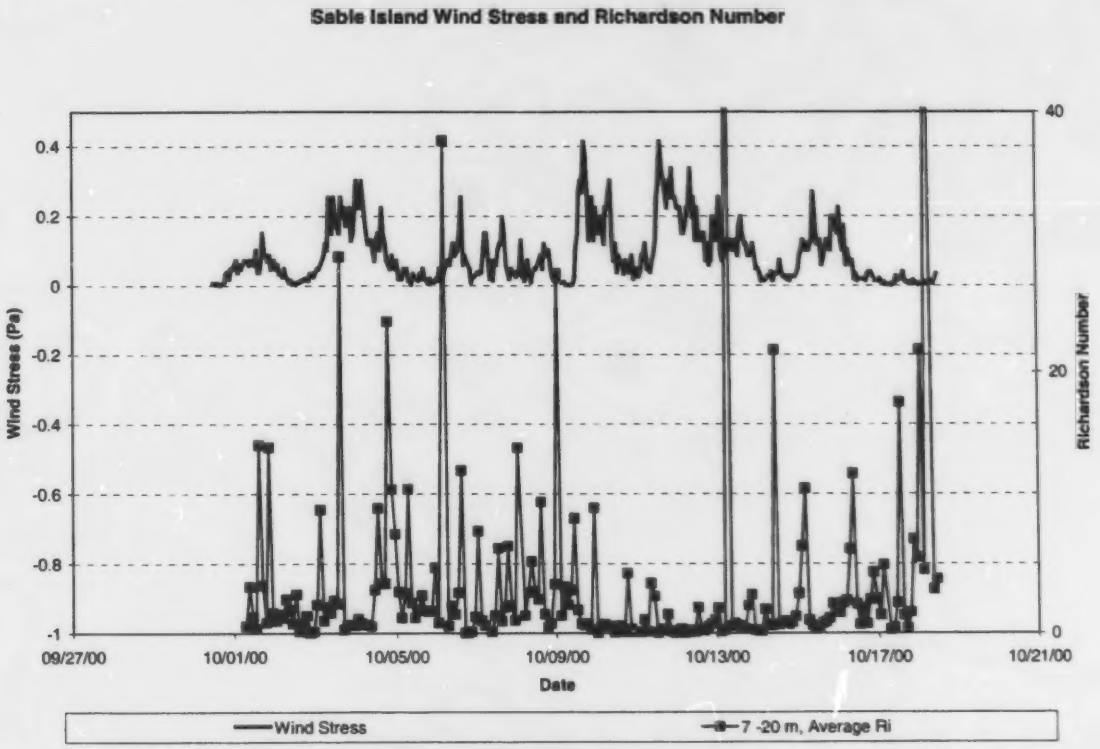

Figure 23: Time series of wind stress from Sable Island and Richardson number at Station 2 derived from SeaHorse CTD and ADCP data. The Richardson number represents an average for the depth range of 7-20 m.

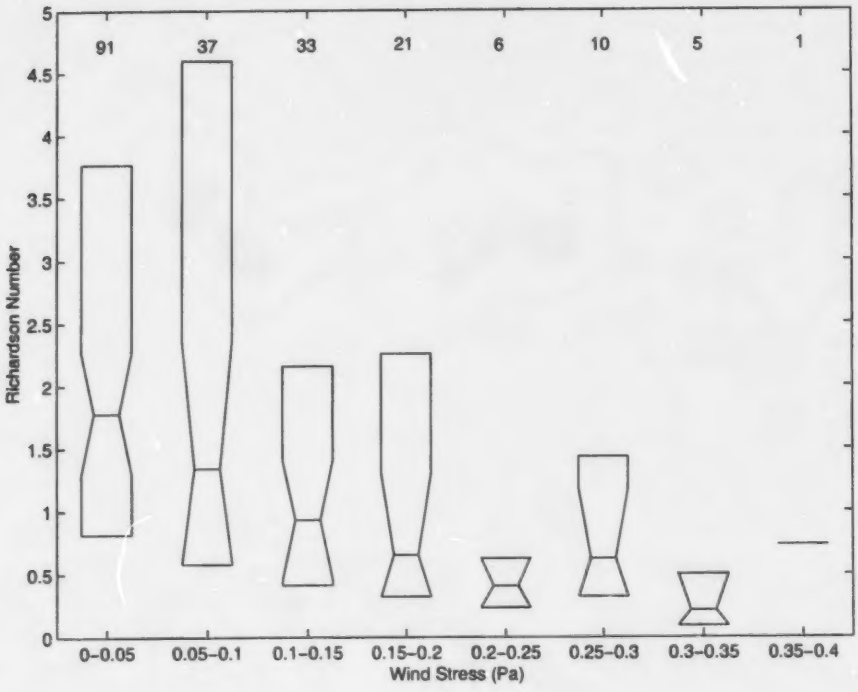

Figure 24: Boxplot of Richardson number for the 7-20 m depth range. The data has been binned in 0.05 Pa intervals of wind stress. The horizontal line in the middle of the box is the median, the top of the box is the 3rd quartile, and the bottom is the 1st quartile. If the notches in the sides of two boxes do not overlap, then the medians are significantly different at the 5% level. The numbers at the top of each column represent the number of observations in each wind stress bin.

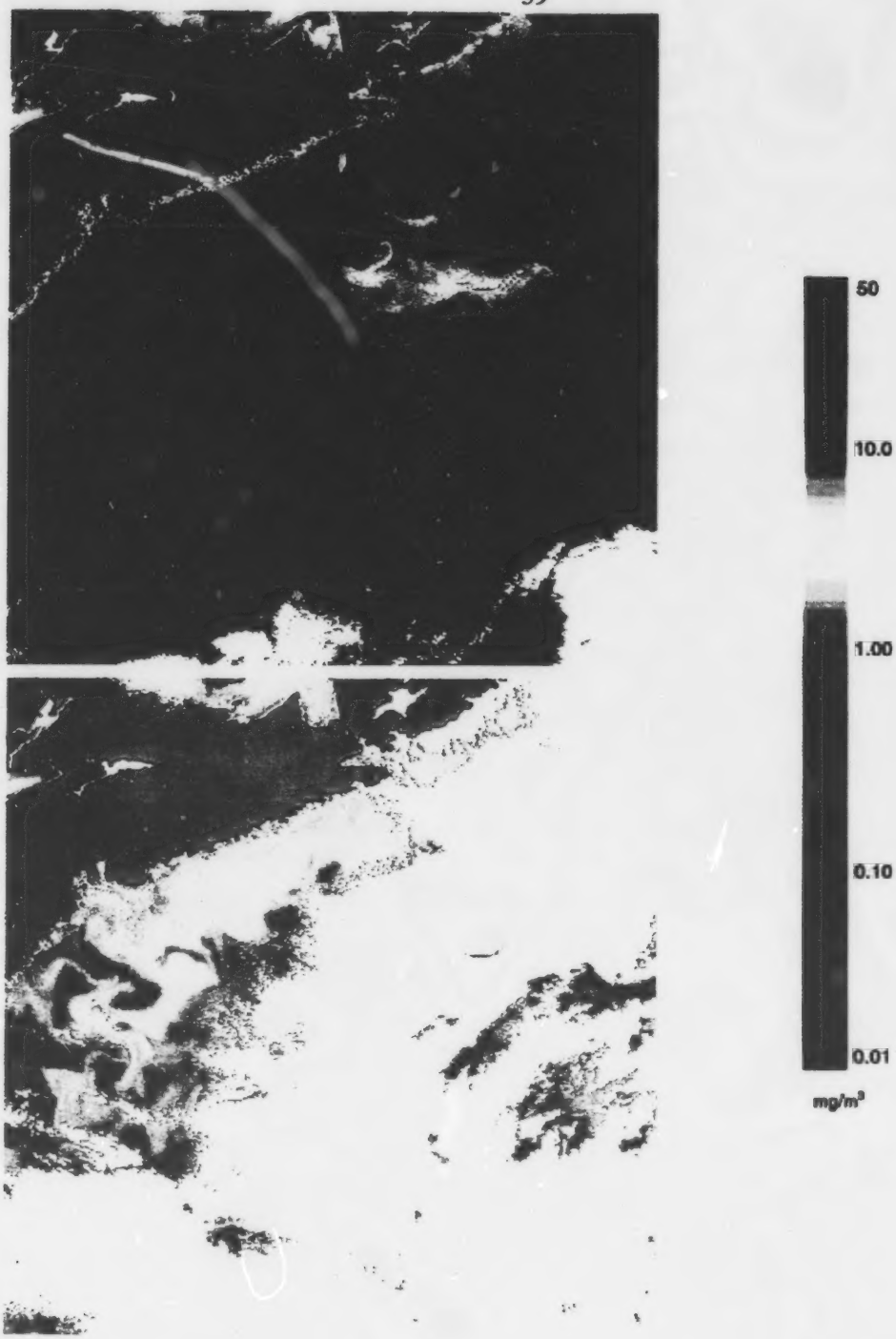

Figure 25: SeaWiFS near-surface chlorophyll images for May 1, 1999 1657 UTC (upper panel) and April 6, 2000 1631 UTC (lower panel).

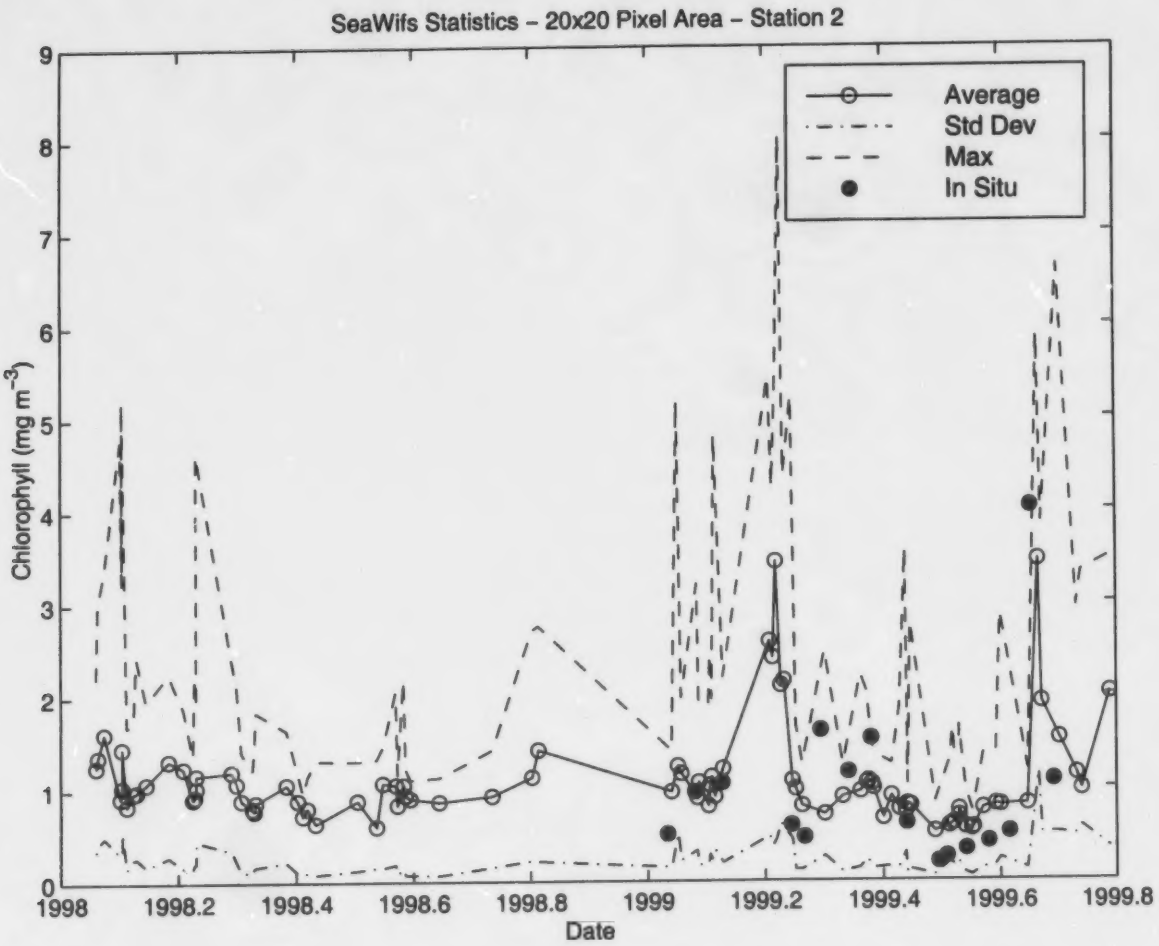

Figure 26: Time series of near-surface chlorophyll average (open circles), standard deviation (dash-dot line) and maximum values (dash line) in a 20 by 20 pixel area centered on Station 2. *In situ* surface chlorophyll measurements at Station 2 are shown as solid circles.

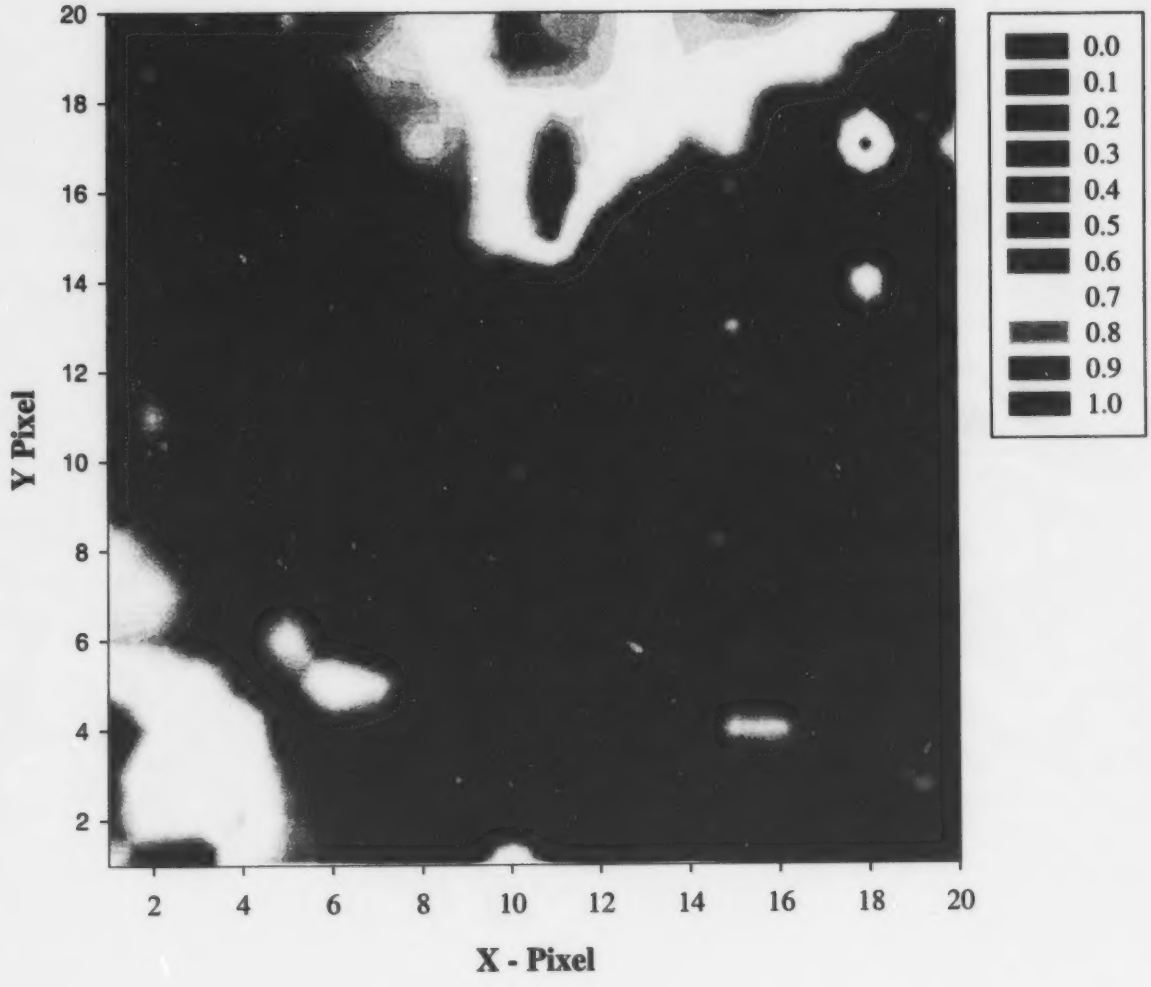

Figure 27: Correlation field from the SeaWiFS images from 1998-1999. The pixel at the centre of the field is at the Station 2 location.

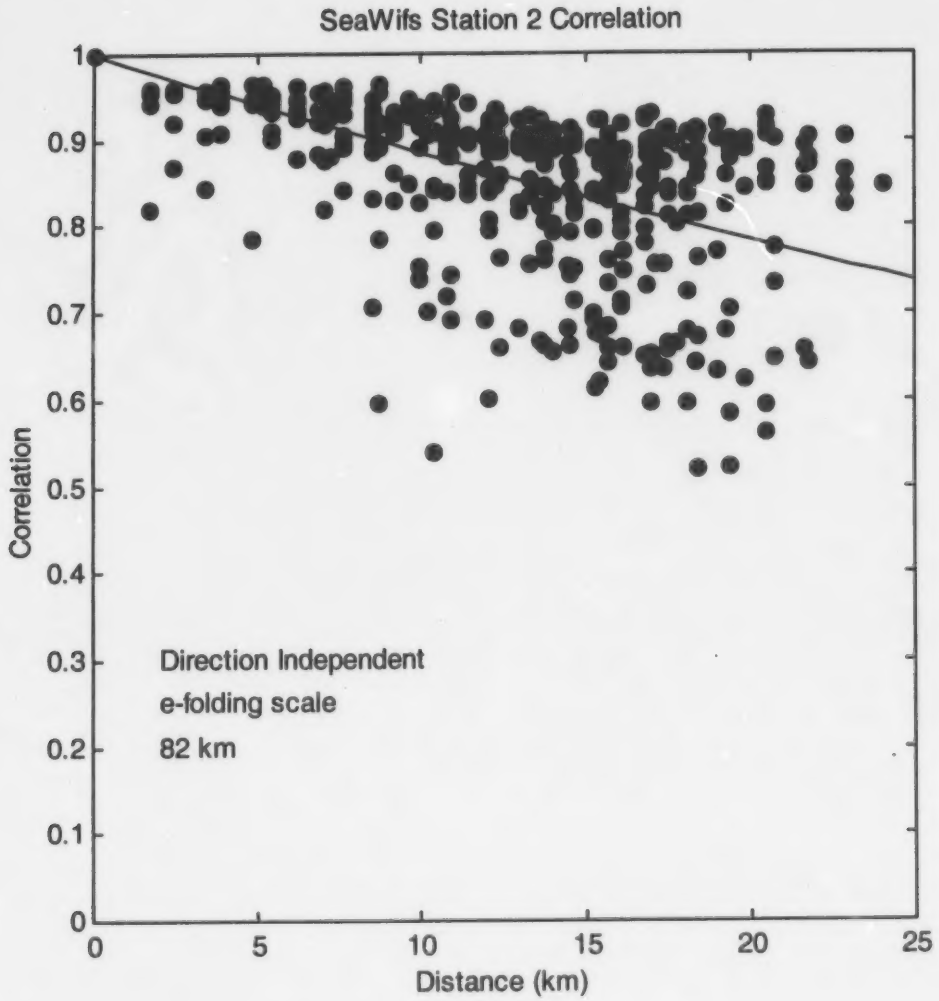

Figure 28: Correlation of near-surface chlorophyll with centre pixel, located at station 2, as a function of separation. The solid line is a least squares fit of $e^{-\lambda r}$, where $1/\lambda$ is the e-folding scale

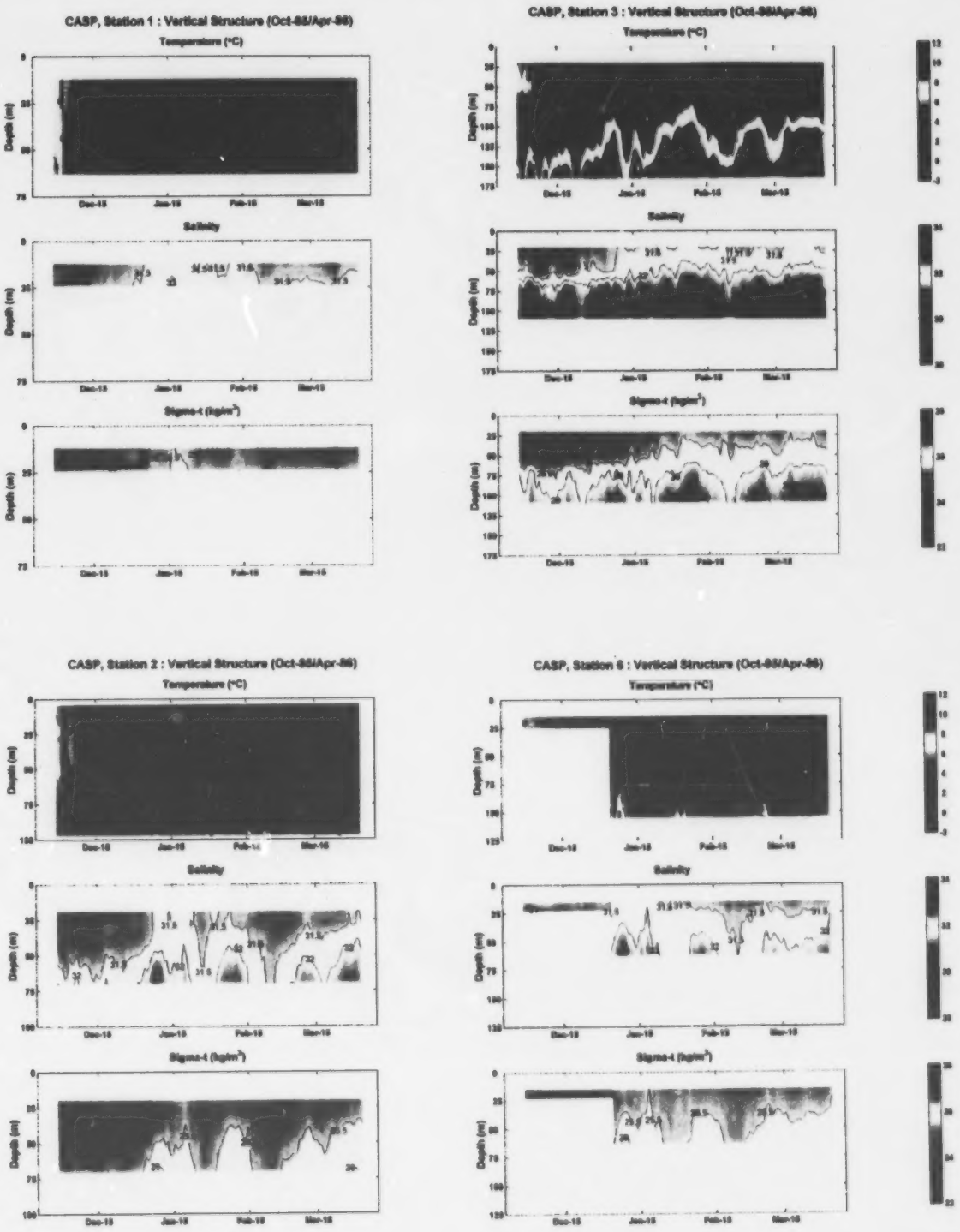

Figure 29: Temperature, salinity and density fields from CASP moorings 1, 2, 3 and 6.

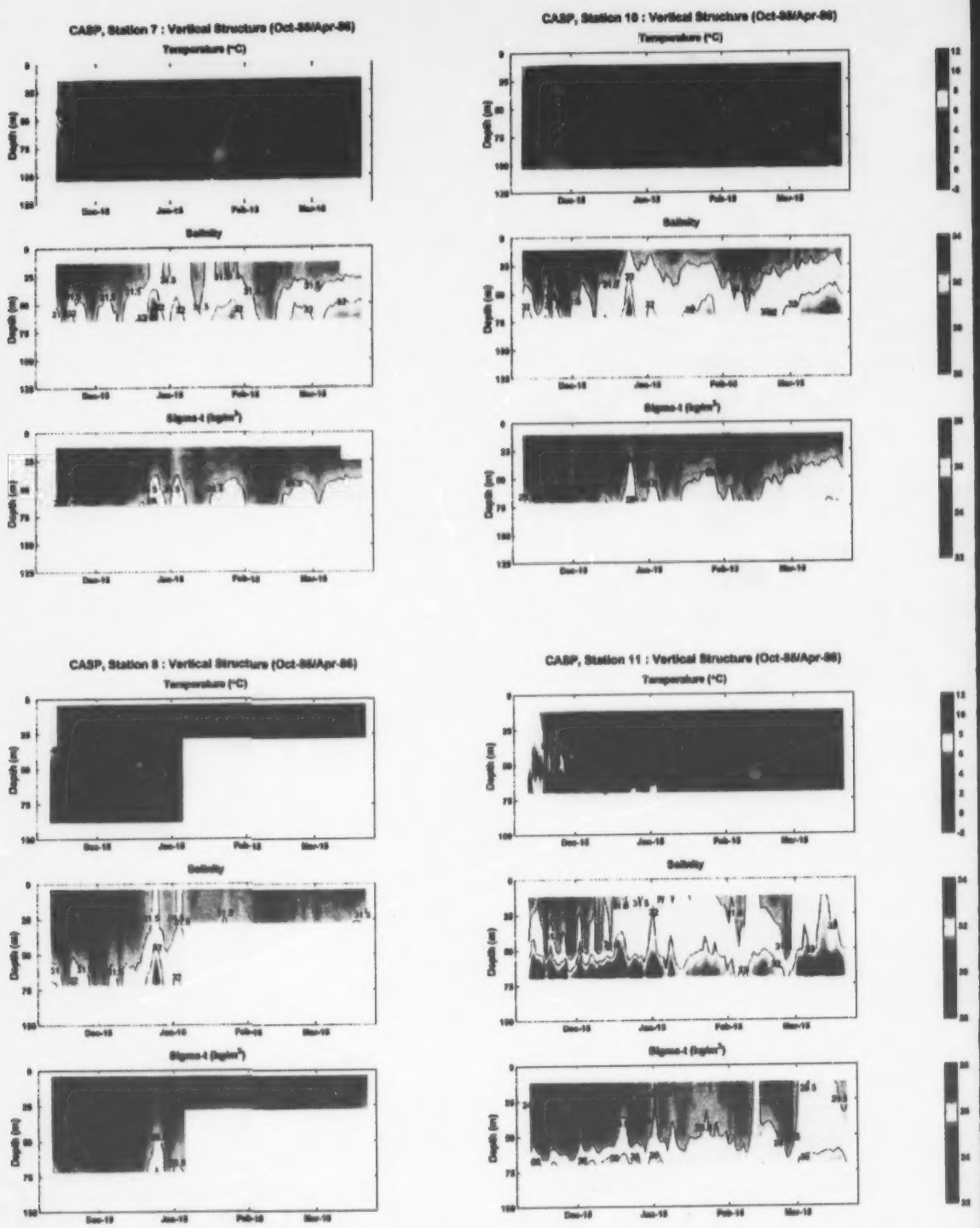

Figure 29 Continued: Temperature, salinity and density from CASP moorings 7, 8, 10 and 11.

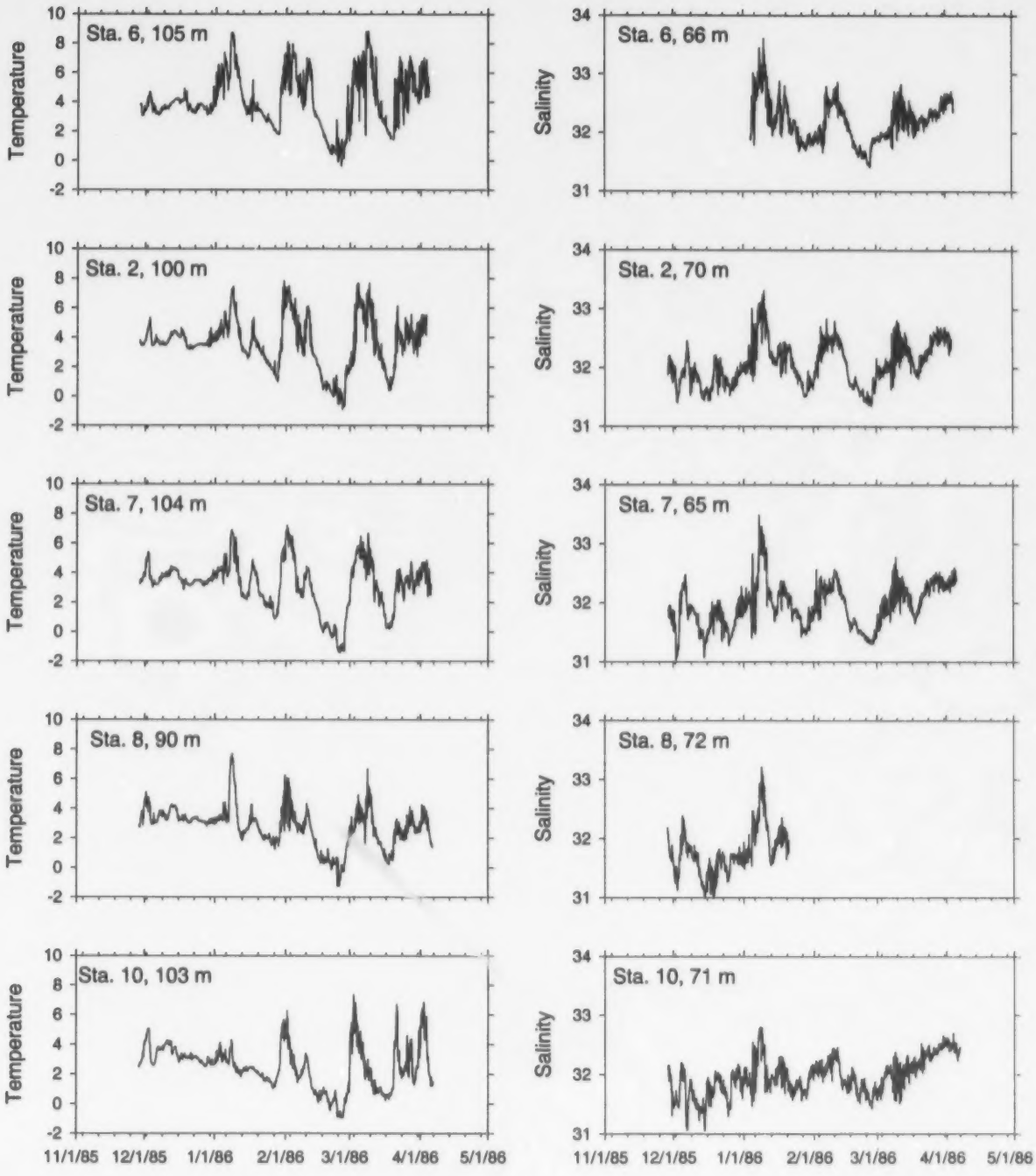

Figure 30: Time series of the deepest temperature and salinity records from instruments along the 100 m isobath.

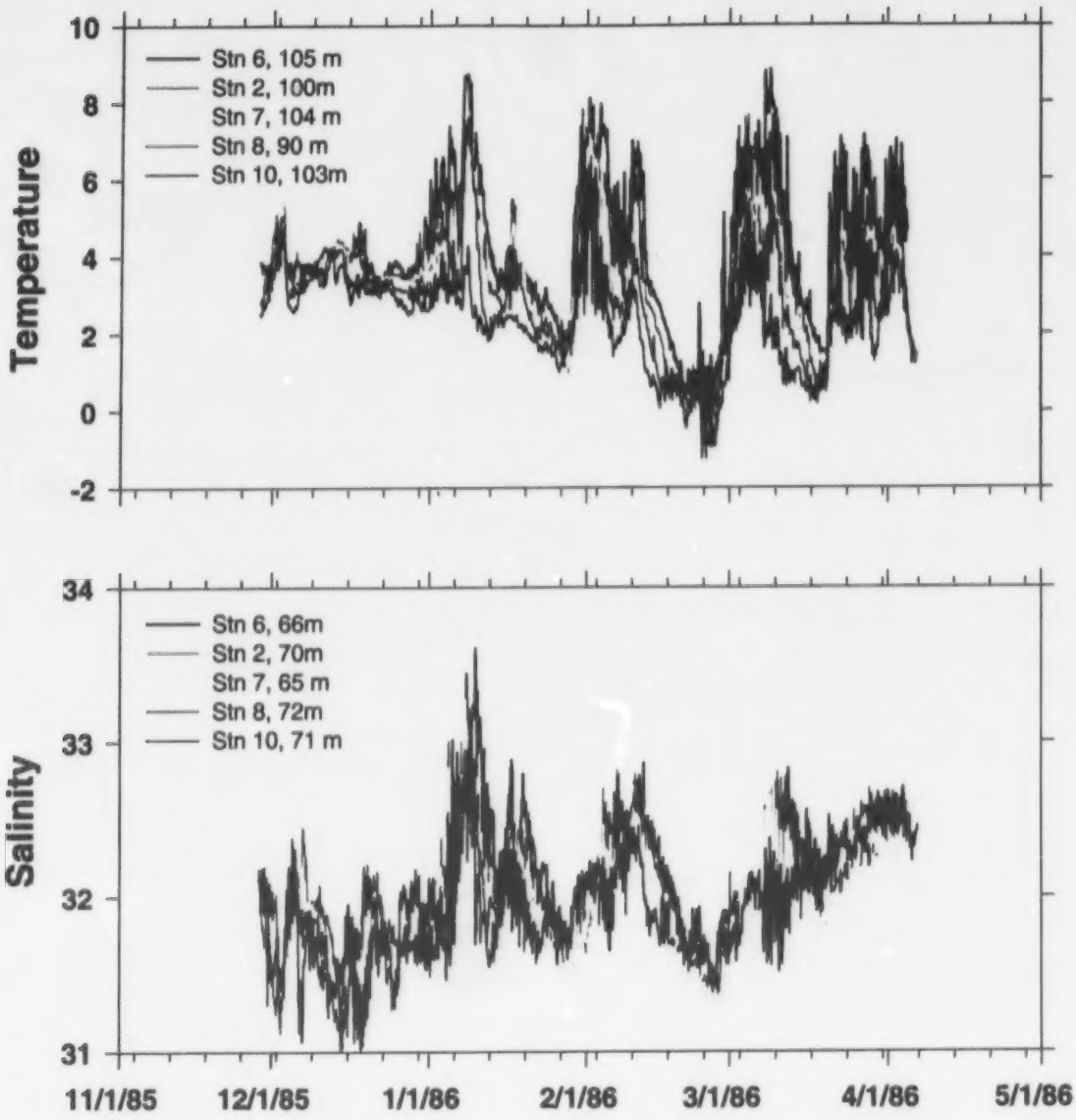

Figure 31: Superimposed time series of the deepest temperature and salinity records from instruments along the 100 m isobath.

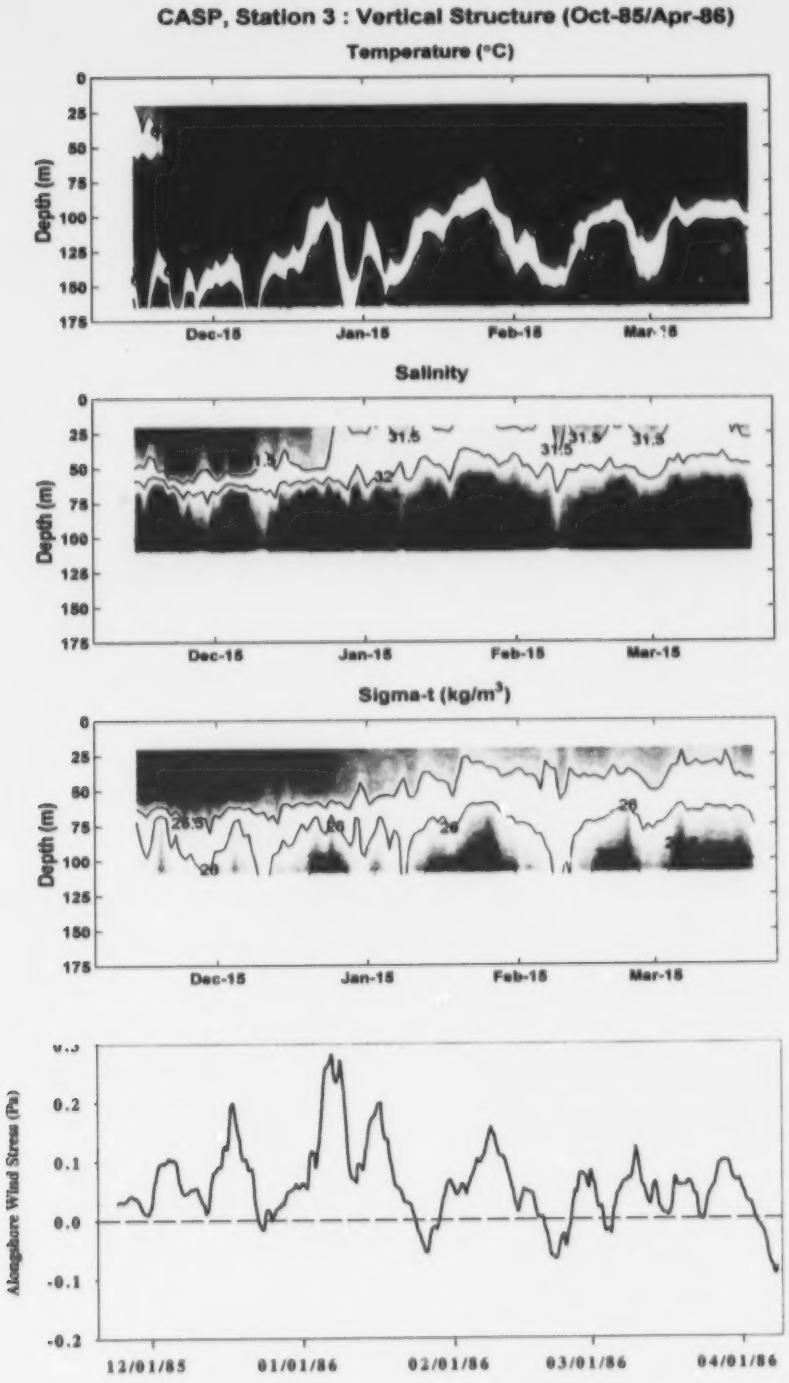

Figure 32: Comparison of the temperature, salinity and density fields from mooring 3 with the alongshore wind stress calculated from Sable Island observations.

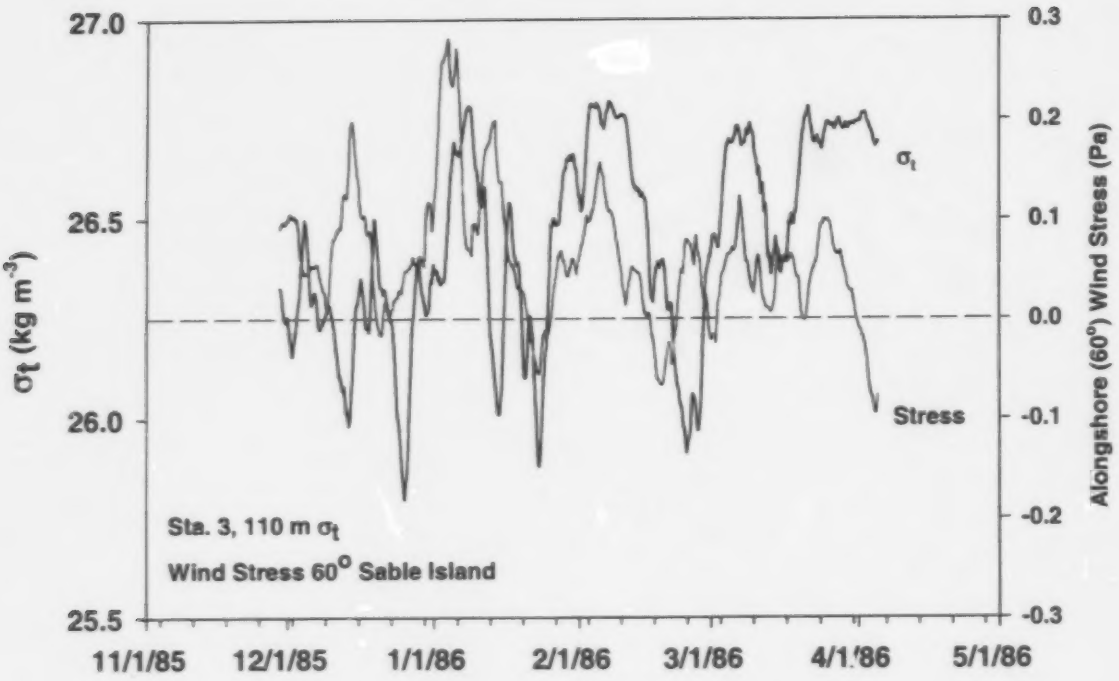

Figure 33: Comparison of density variability at Sta. 3, 110 m with the alongshore wind stress calculated from Sable Island observations. The density (stress) data have been filtered with a 25 h (5 d) running mean filter.

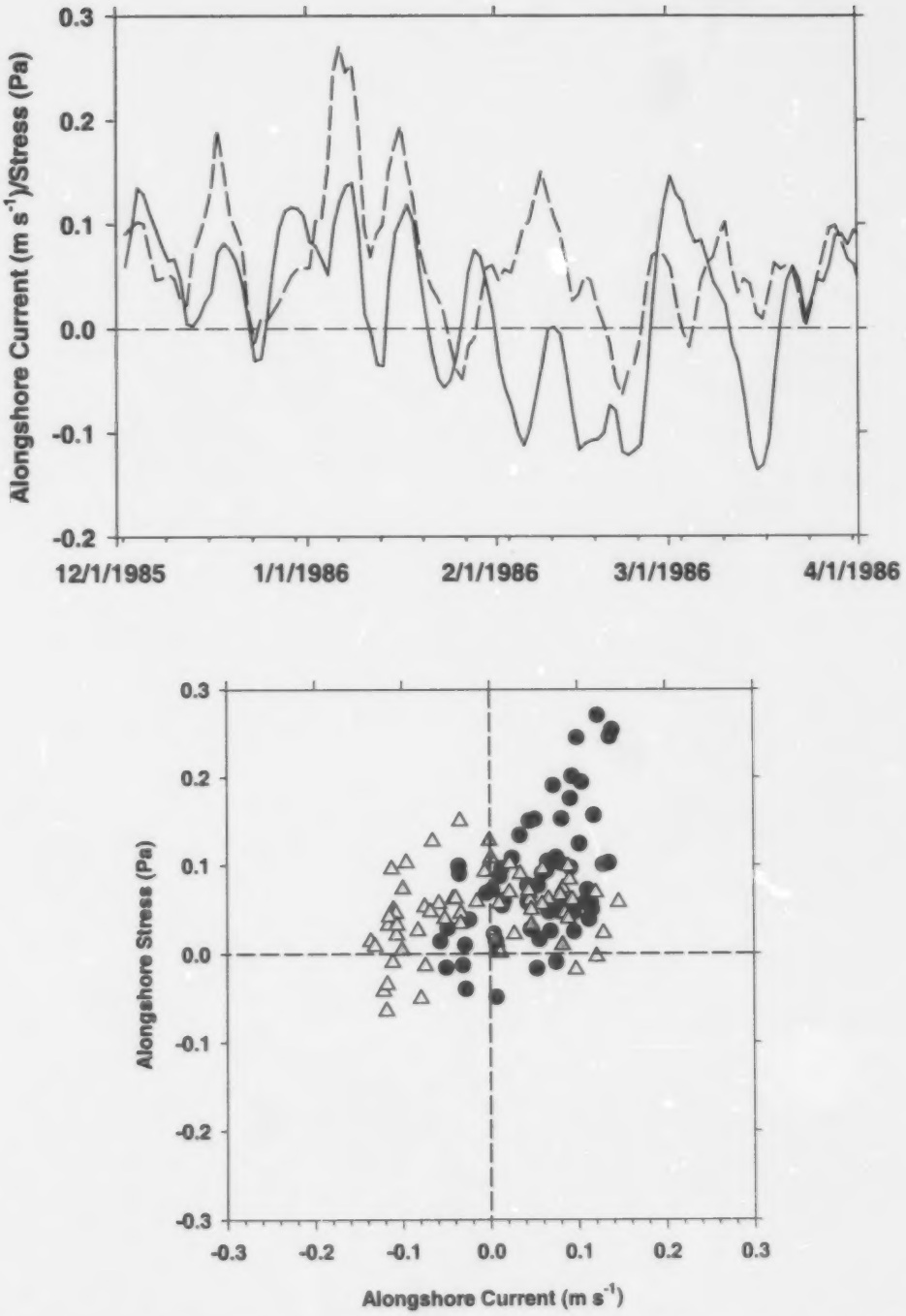

Figure 34: Time series of alongshore current from station 1, 12 m (solid line) and wind stress (broken line, upper panel). Alongshore current versus stress for the first half of the record (solid dots) and second half (triangles). Both data sets have been filtered with a 5 day running mean filter.

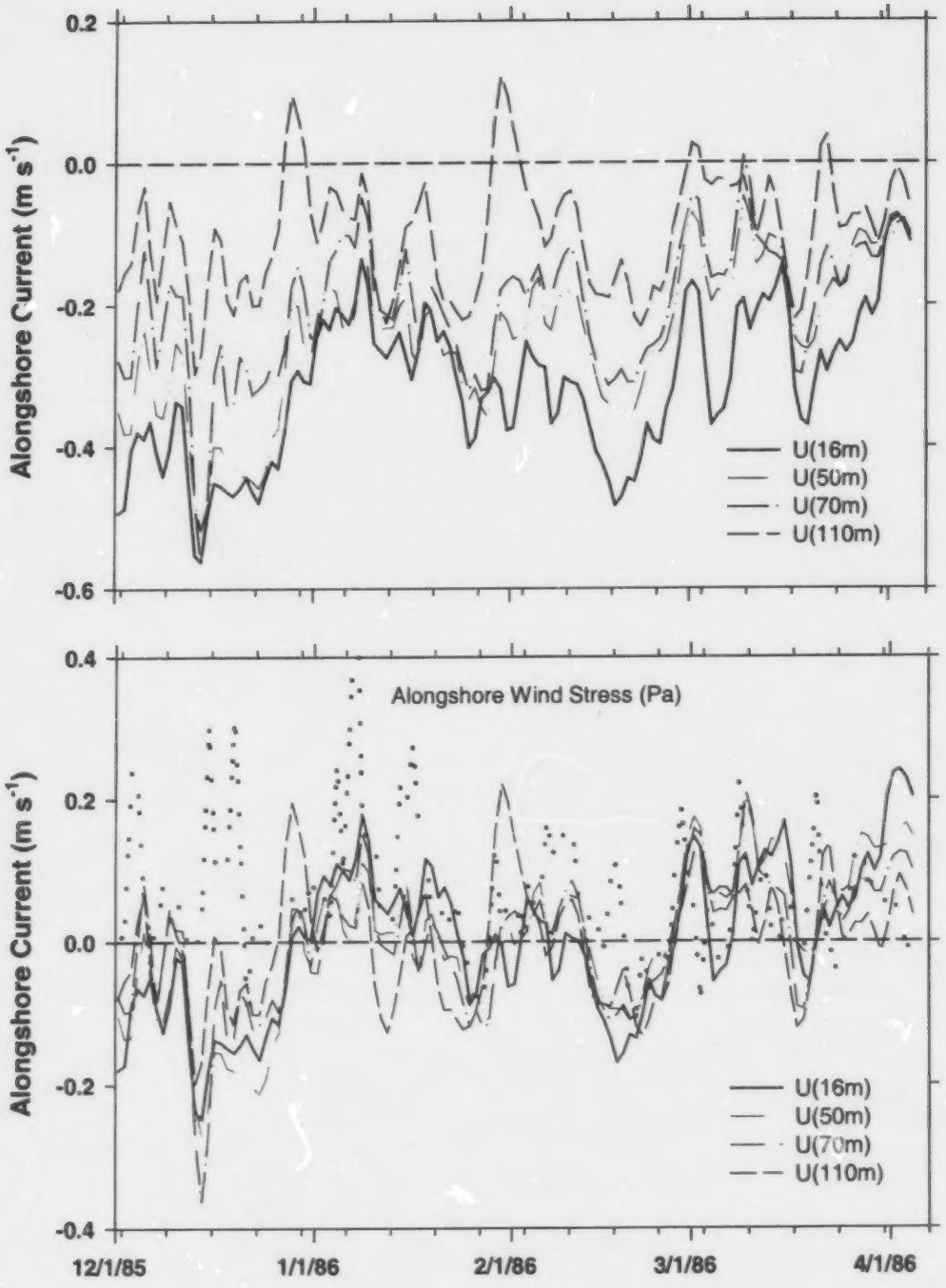

Figure 35: The alongshore currents at Sta. 3, (16, 50, 70 and 110 m, upper panel) and with the mean removed (lower panel). The alongshore wind stress (dotted line) is also plotted in the lower panel. All records had a 25 hour running mean filter applied.

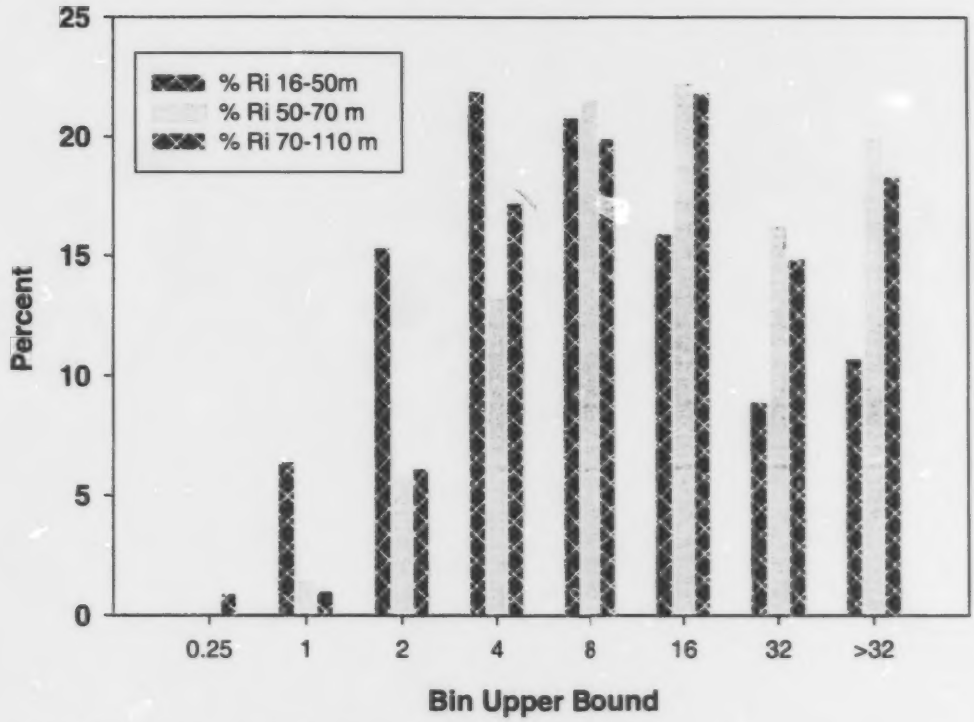

Figure 36: Histogram of Richardson numbers for mooring 3.

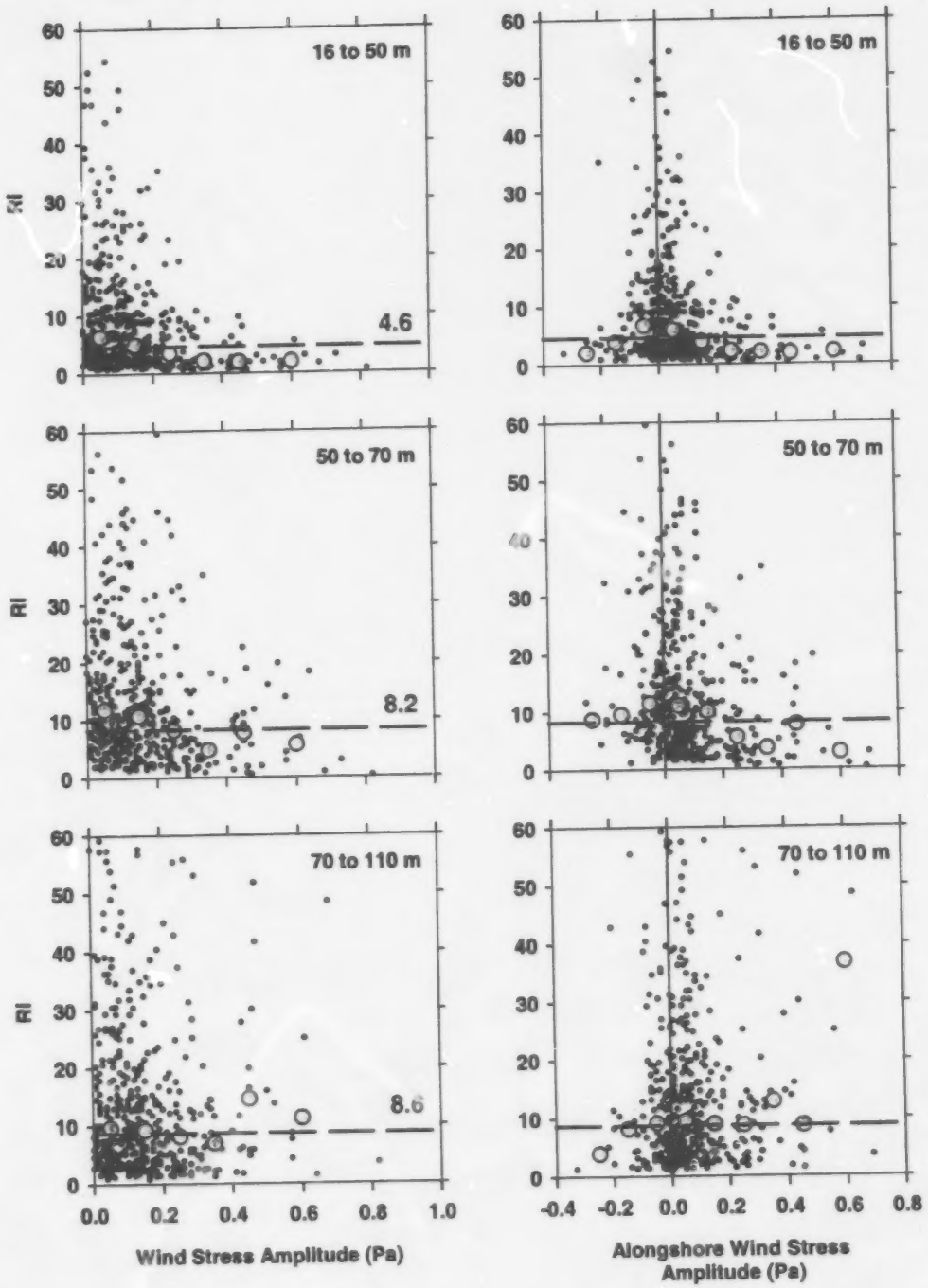

Figure 37: Richarson numbers at mooring 3 are plotted against the total and alongshore stress. Six-hour median values (solid black dots) and median of these values in 0.1 Pa bins (grey dots) are also shown. The broken grey line and the number is the Richardson number calculated from the mean density and current shears.

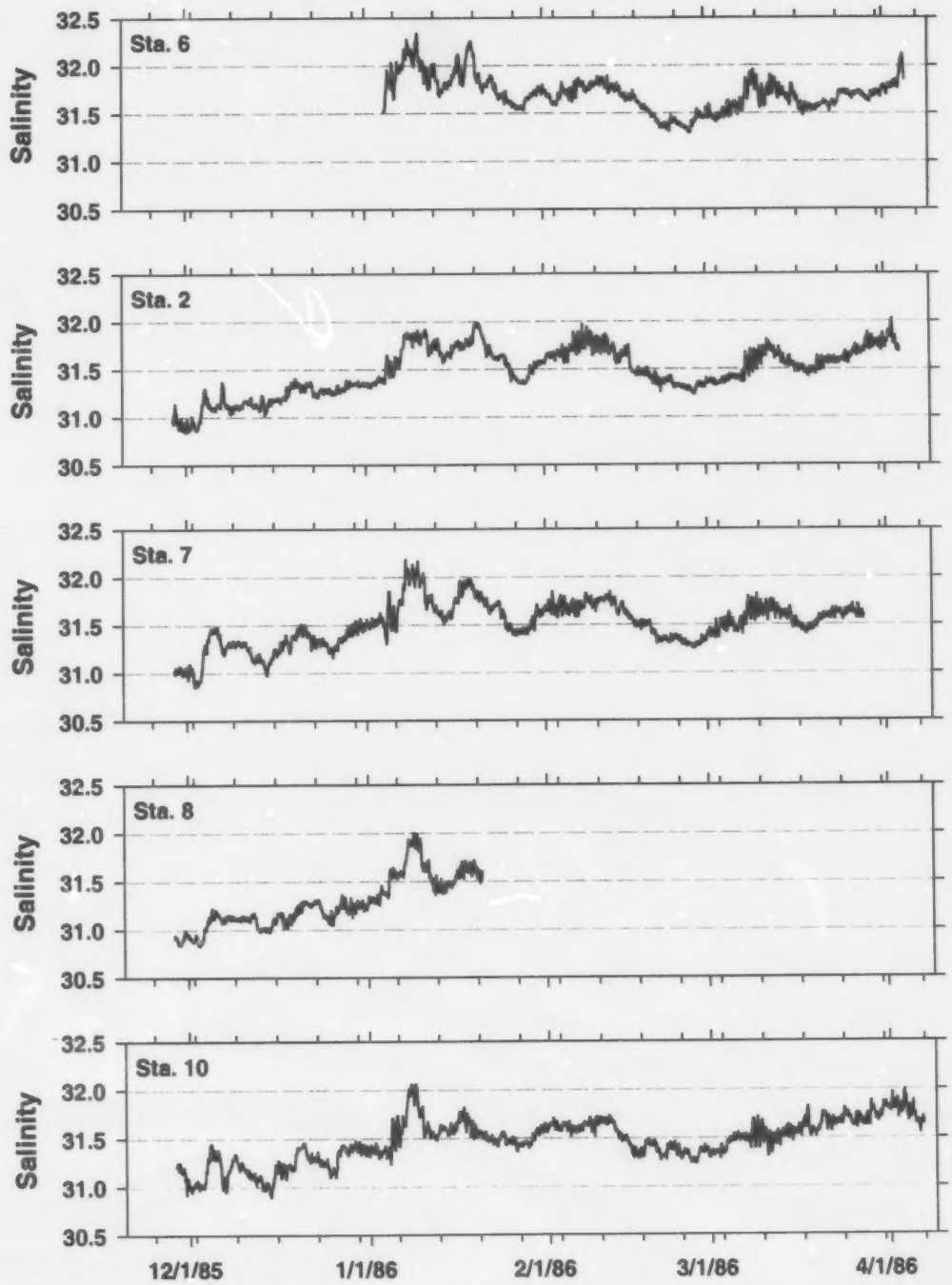

Figure 38: Averaged salinity from 0 to 65 m for Sta. 6, 2, 7, 8 and 10.

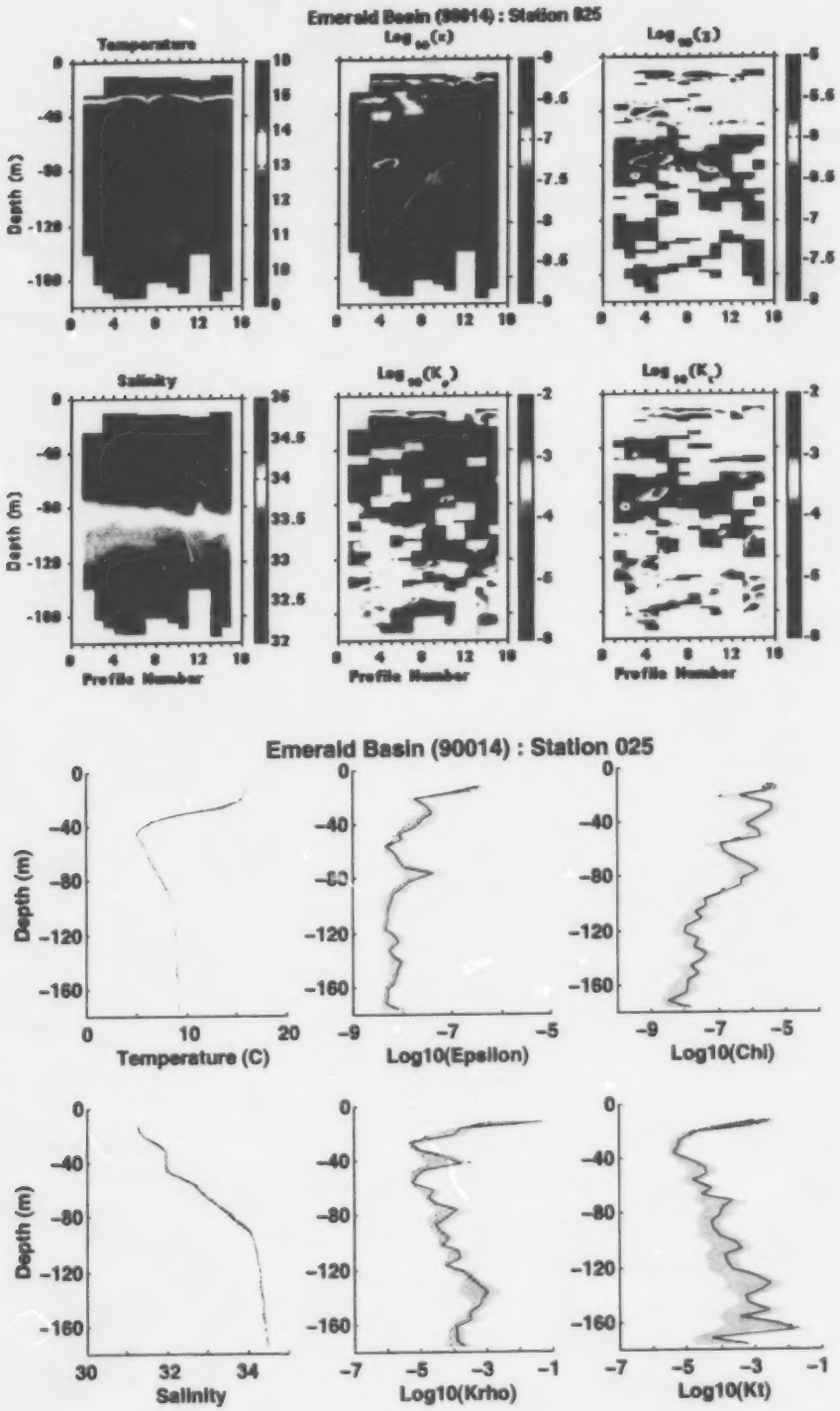

Figure 39: (top) Individual profiles have been stacked side-by-side to provide a contour plot of EPSONDE data. The two left-hand panels are temperature and salinity; the middle panels are dissipation of TKE (ε) and mass diffusivity (K_ρ); the right hand panels are dissipation of thermal variance (χ) and heat diffusivity (K_t). (bottom) bootstrap estimated mean and confidence intervals for the station.

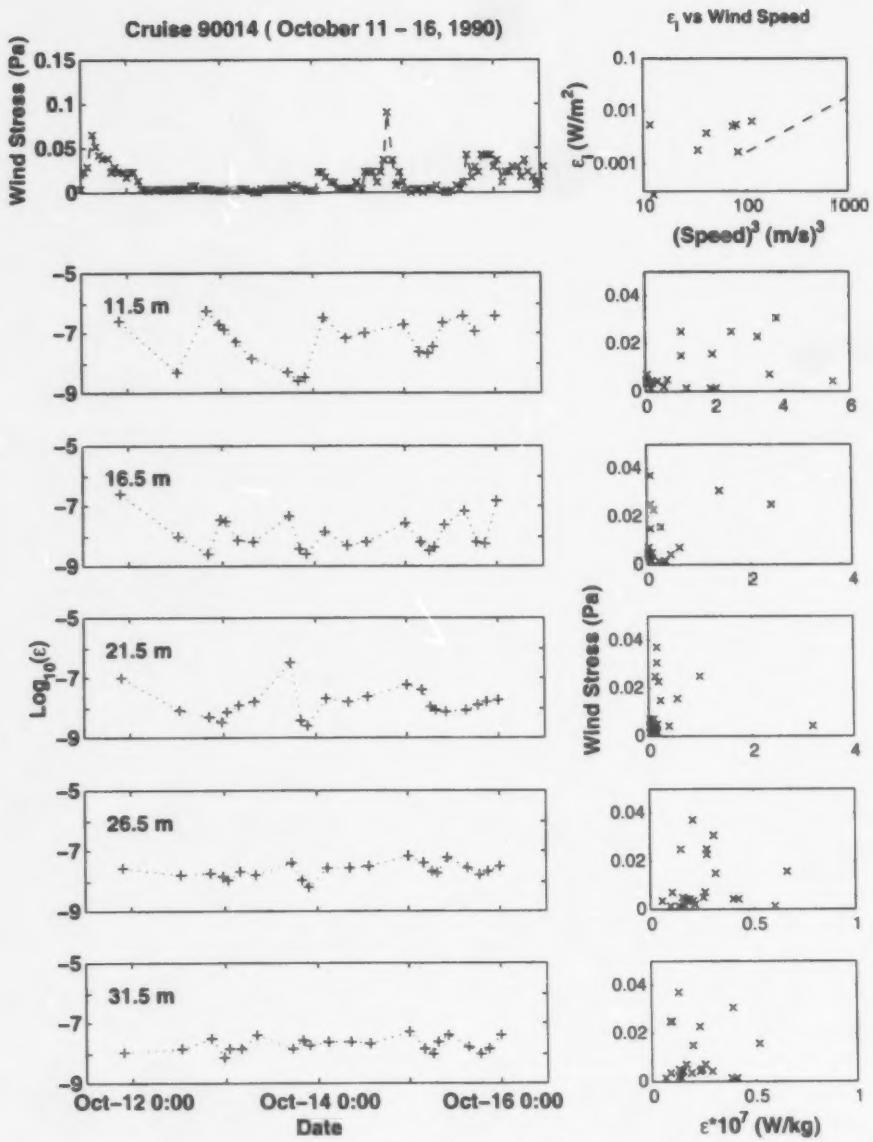

Figure 40: Time series of wind stress calculated using Shearwater winds (top left panel). Time series of ε for 5 m bins in the ocean mixed layer (lower left panels). Depth-integrated dissipation of TKE versus the wind speed cubed (upper right panel, dashed line represents fit of data from Oakey and Elliott, 1982). Scatter plots of wind stress and ε for the various bins (lower right panels).

Appendix A: EPSONDE Station Profiles

This appendix includes station profiles of temperature, salinity, rates of dissipation of turbulent kinetic energy (ε) and thermal variance (χ), and eddy diffusivities of mass (K_ρ) and heat (K_T). The data for all profiles in each station are grouped in 4-m depth bins and a bootstrap statistical technique is used to calculate a mean profile (black line) for the station as well as 95% confidence intervals (gray shaded area).

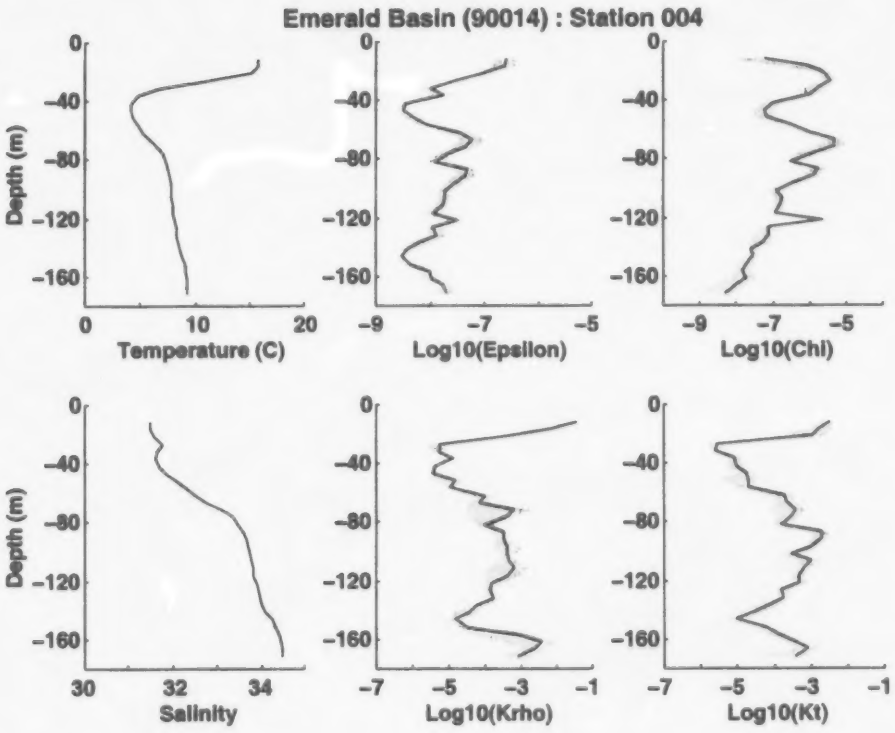

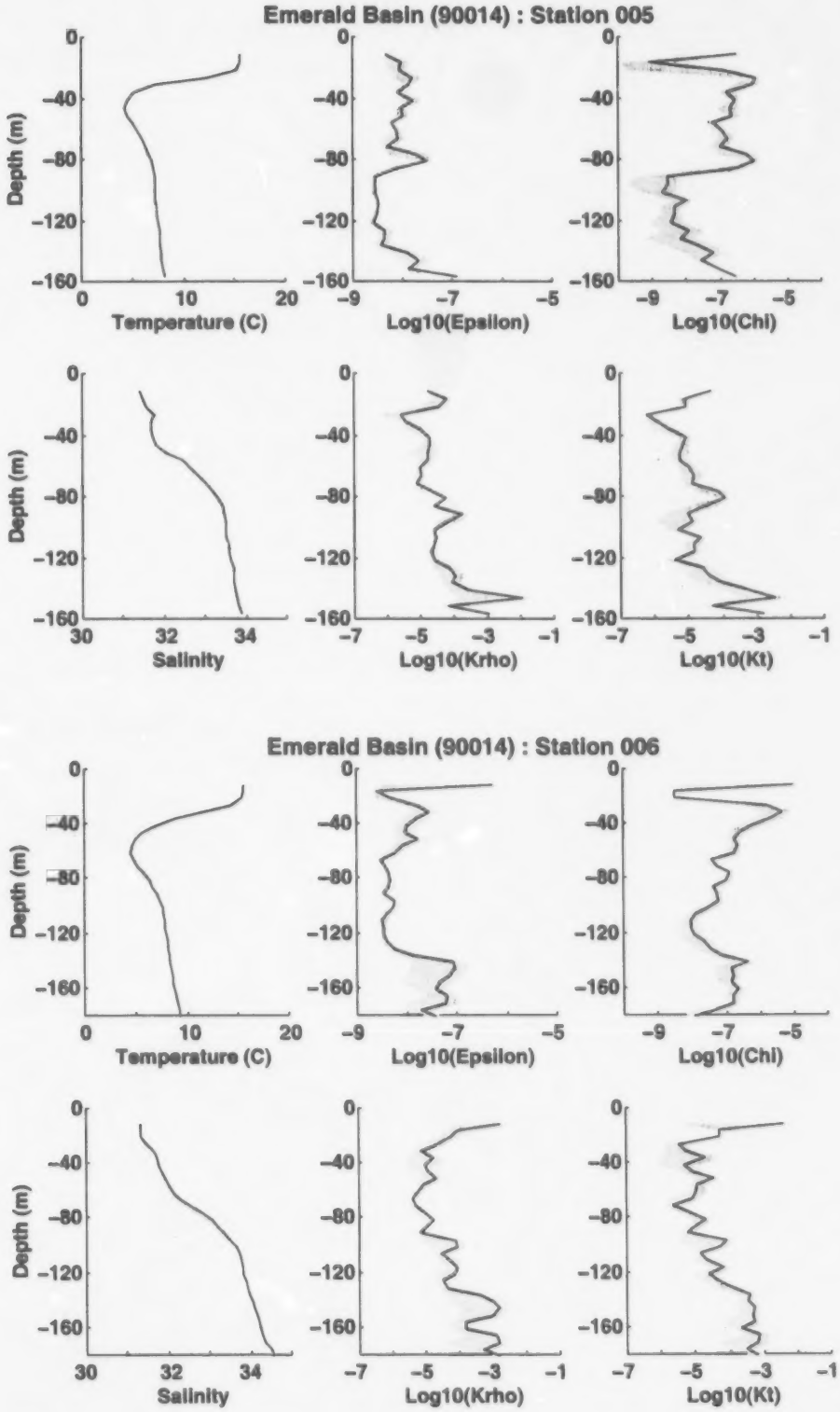
Emerald Basin (90014) : Station 005
Depth (m)
0
-40
-80
-120
-160
Temperature (C)
0
10
20
Log10(Epsilon)
-9
-7
-5
Log10(Chi)
Salinity
30
32
34
Log10(Krho)
-7
-5
-3
-1
Log10(Kt)
Emerald Basin (90014) : Station 006

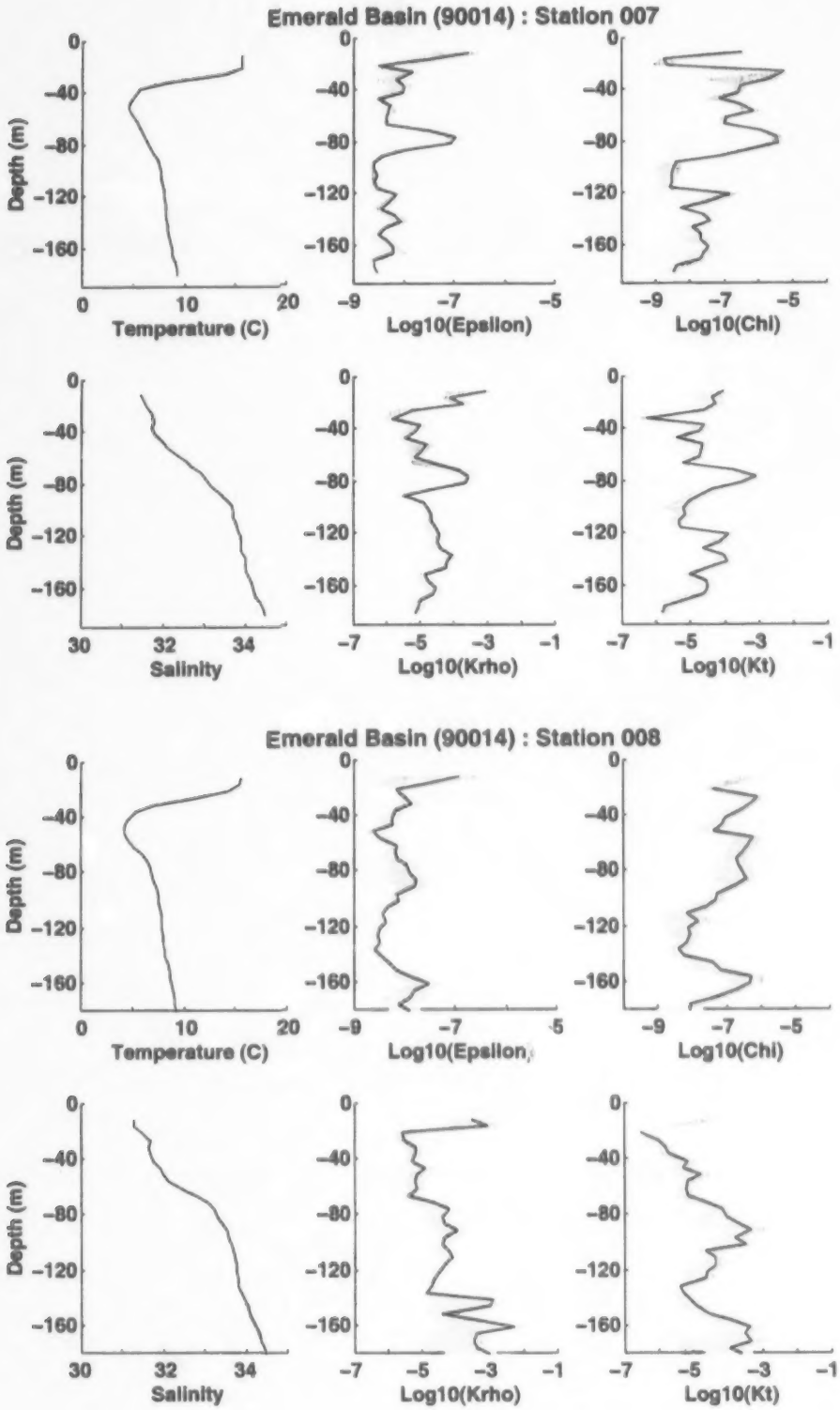
Emerald Basin (90014) : Station 007
Depth (m)
0
-40
-80
-120
-160
0
10
20
Temperature (C)
-9
-7
-5
Log10(Epsilon)
Log10(Chl)
30
32
34
Salinity
-7
-5
-3
-1
Log10(Krho)
Log10(Kt)
Emerald Basin (90014) : Station 008
Temperature (C)
Log10(Epsilon)
Log10(Chl)
Salinity
Log10(Krho)
Log10(Kt)

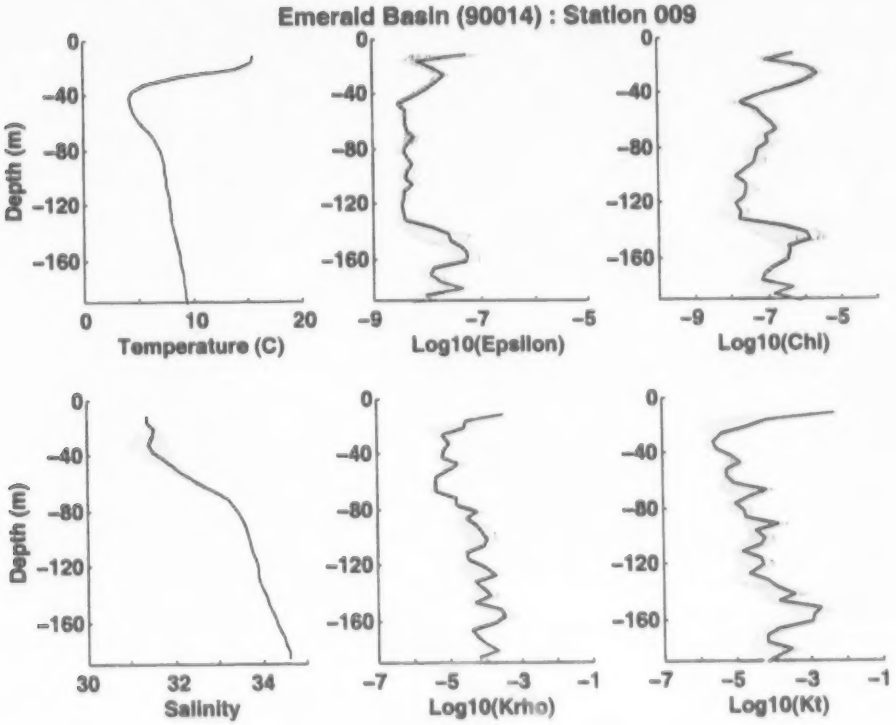
Emerald Basin (90014) : Station 009
Depth (m)
Temperature (C)
Log10(Epsilon)
Log10(Chl)
Salinity
Log10(Krho)
Log10(Kt)

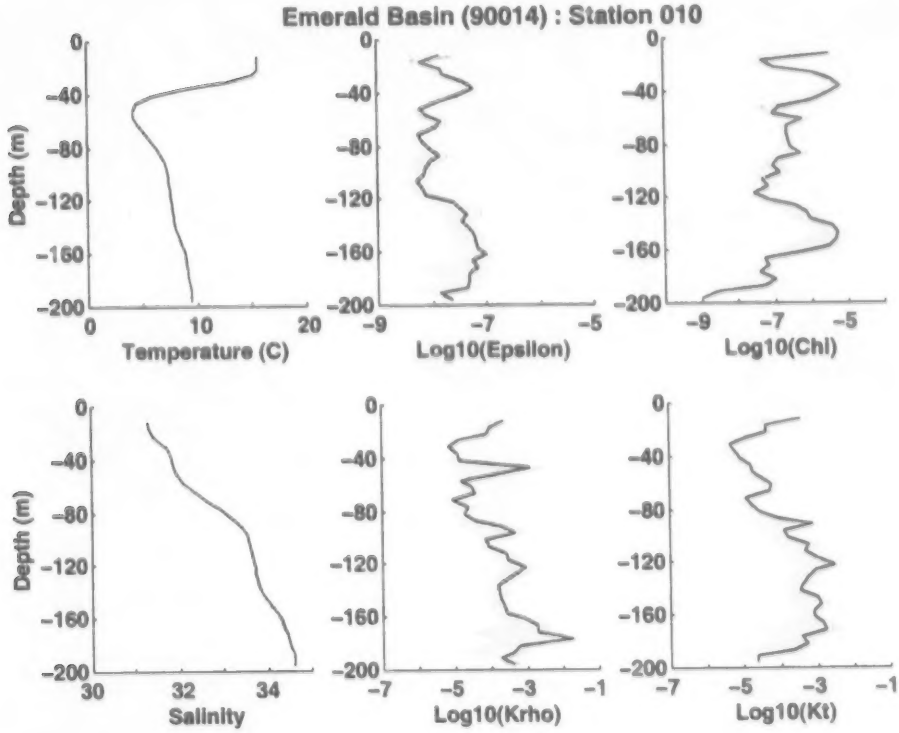
Emerald Basin (90014) : Station 010
Depth (m)
Temperature (C)
Log10(Epsilon)
Log10(Chl)
Salinity
Log10(Krho)
Log10(Kt)

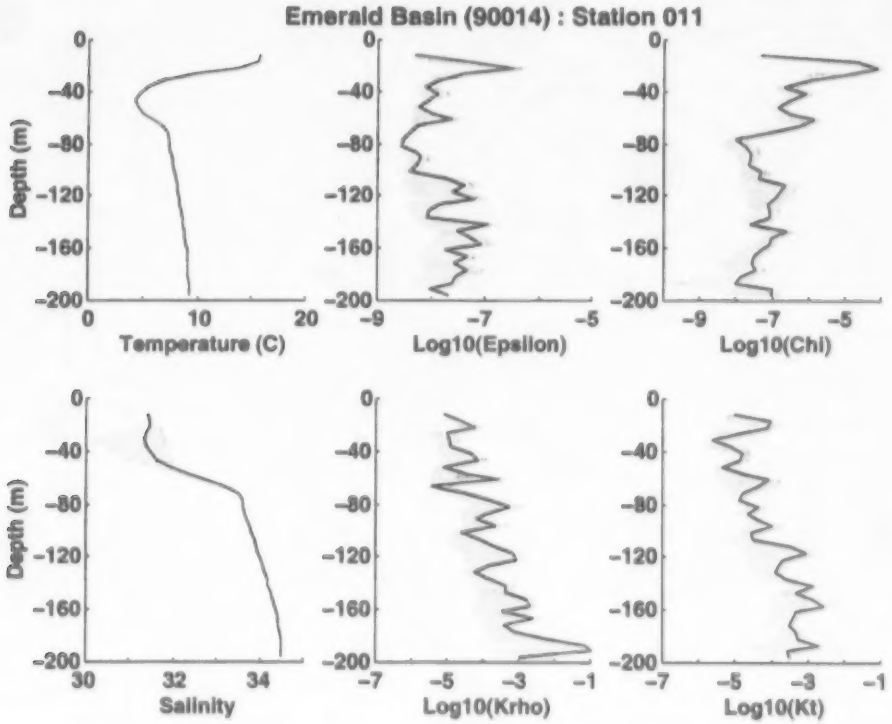
Emerald Basin (90014) : Station 011
Depth (m)
Temperature (C)
Log10(Epsilon)
Log10(Chi)
Salinity
Log10(Krho)
Log10(Kt)

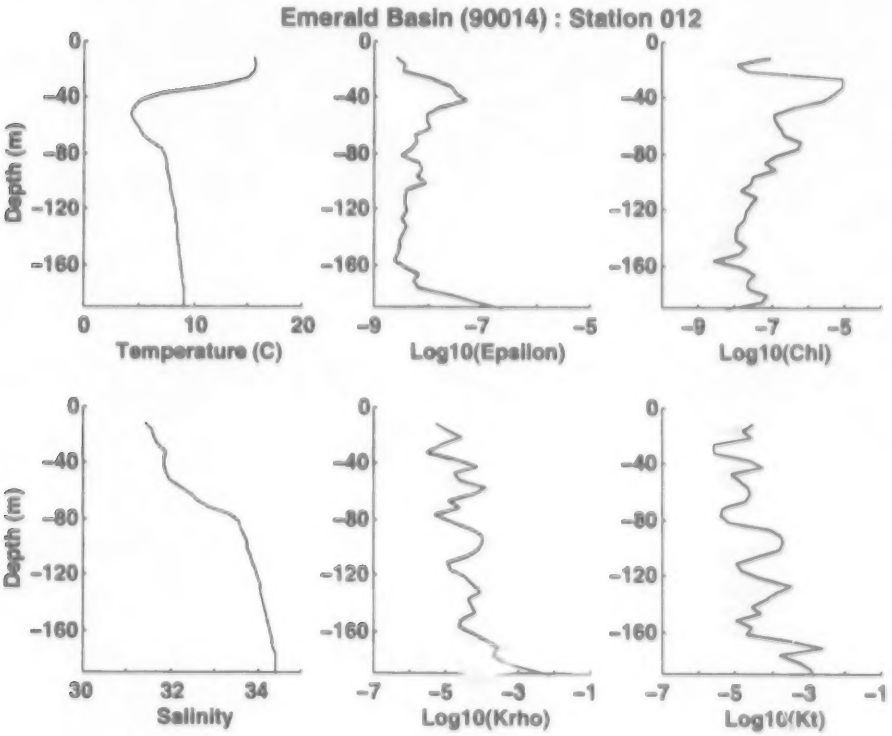
Emerald Basin (90014) : Station 012
Depth (m)
Temperature (C)
Log10(Epsilon)
Log10(Chi)
Salinity
Log10(Krho)
Log10(Kt)

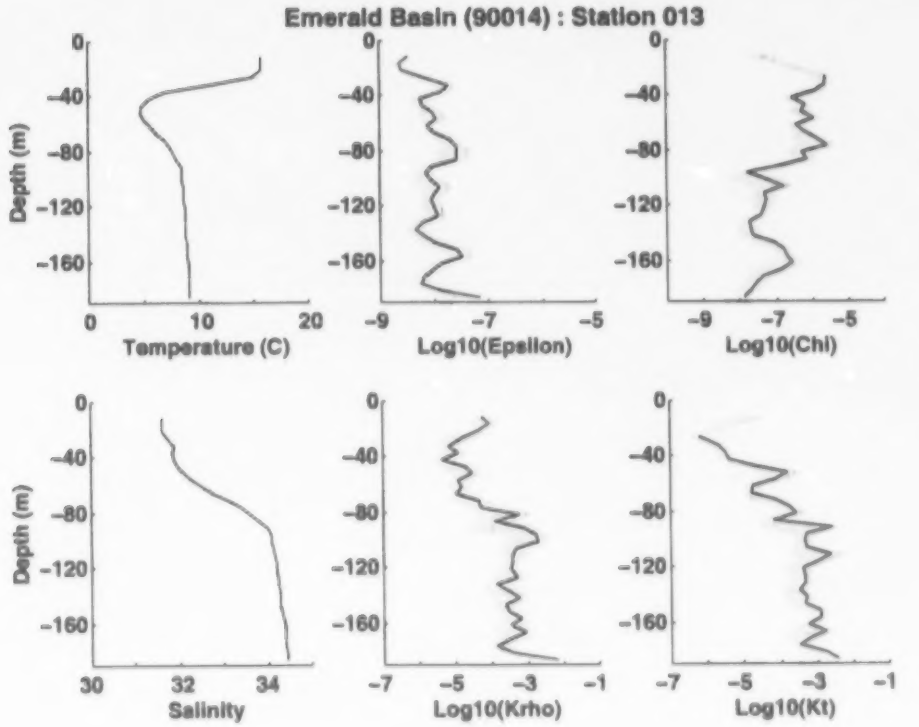
Emerald Basin (90014) : Station 013
Depth (m)
0
-40
-80
-120
-160
0
10
20
Temperature (C)
-9
-7
-5
Log10(Epsilon)
Log10(Chi)
30
32
34
Salinity
-7
-5
-3
-1
Log10(Krho)
Log10(Kt)

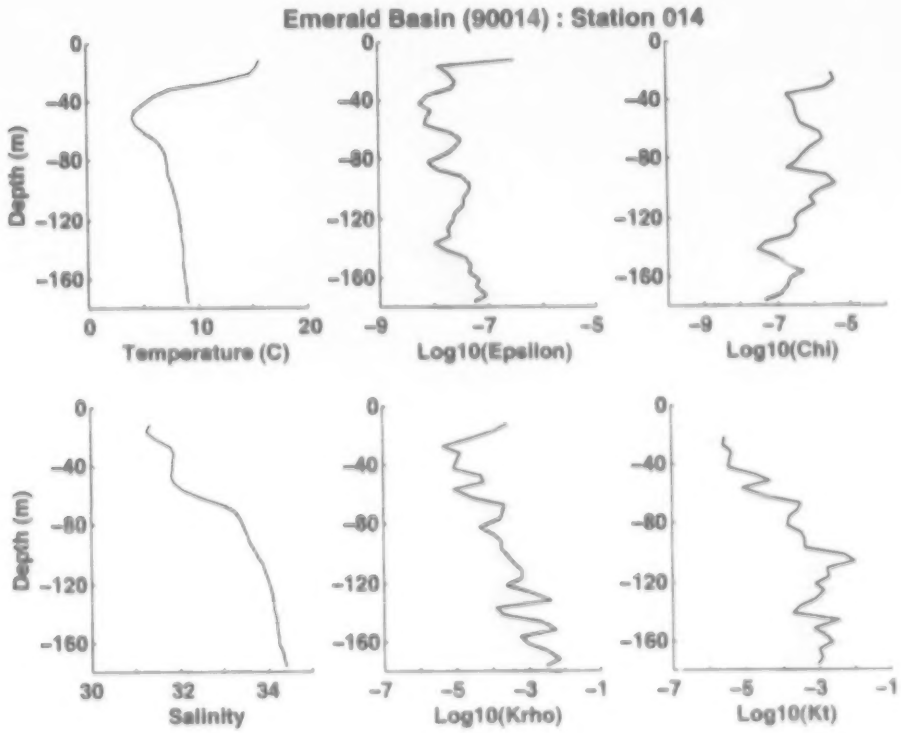
Emerald Basin (90014) : Station 014
Depth (m)
0
-40
-80
-120
-160
0
10
20
Temperature (C)
-9
-7
-5
Log10(Epsilon)
Log10(Chi)
30
32
34
Salinity
-7
-5
-3
-1
Log10(Krho)
Log10(Kt)

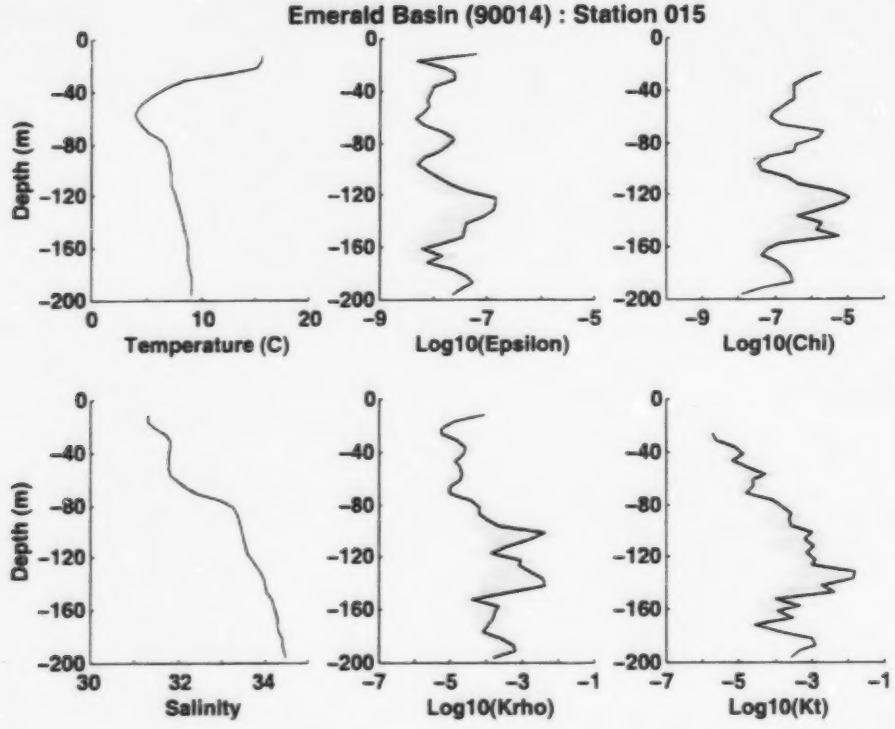
Emerald Basin (90014) : Station 015
Depth (m)
Temperature (C)
Log10(Epsilon)
Log10(Chi)
Salinity
Log10(Krho)
Log10(Kt)

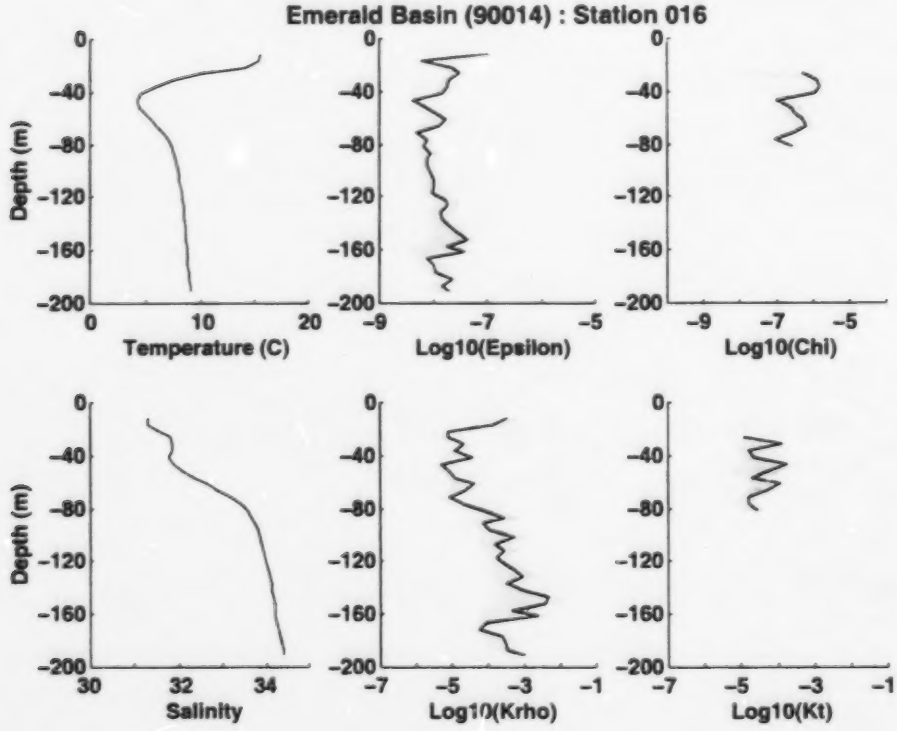
Emerald Basin (90014) : Station 016
Depth (m)
Temperature (C)
Log10(Epsilon)
Log10(Chi)
Salinity
Log10(Krho)
Log10(Kt)

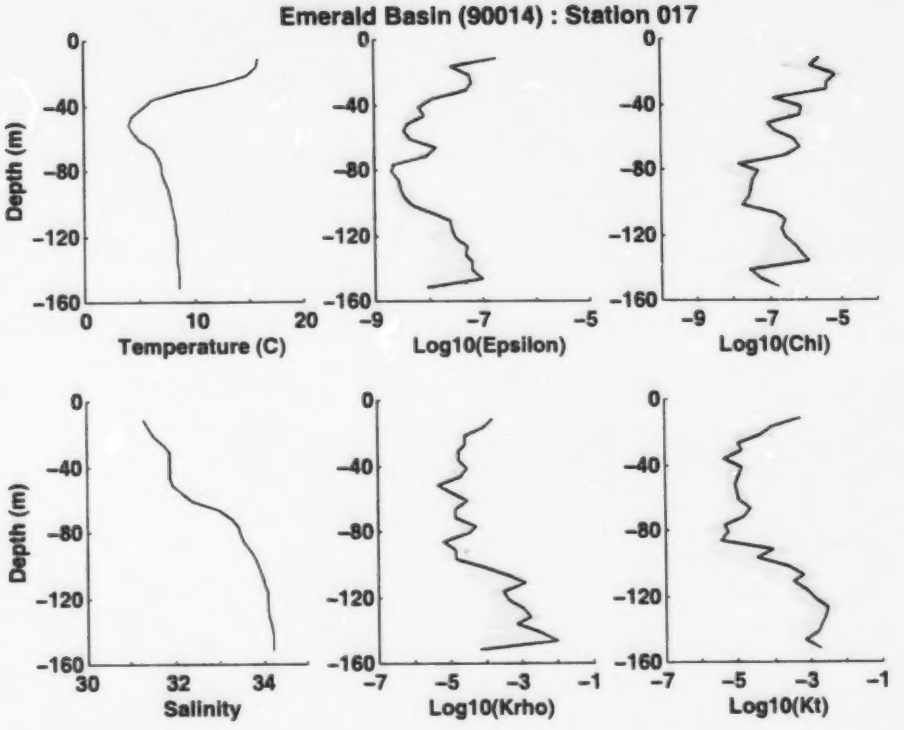
Emerald Basin (90014) : Station 017
Depth (m)
0
-40
-80
-120
-160
0
10
20
Temperature (C)
-9
-7
-5
Log10(Epsilon)
Log10(Chi)
30
32
34
Salinity
-7
-5
-3
-1
Log10(Krho)
Log10(Kt)

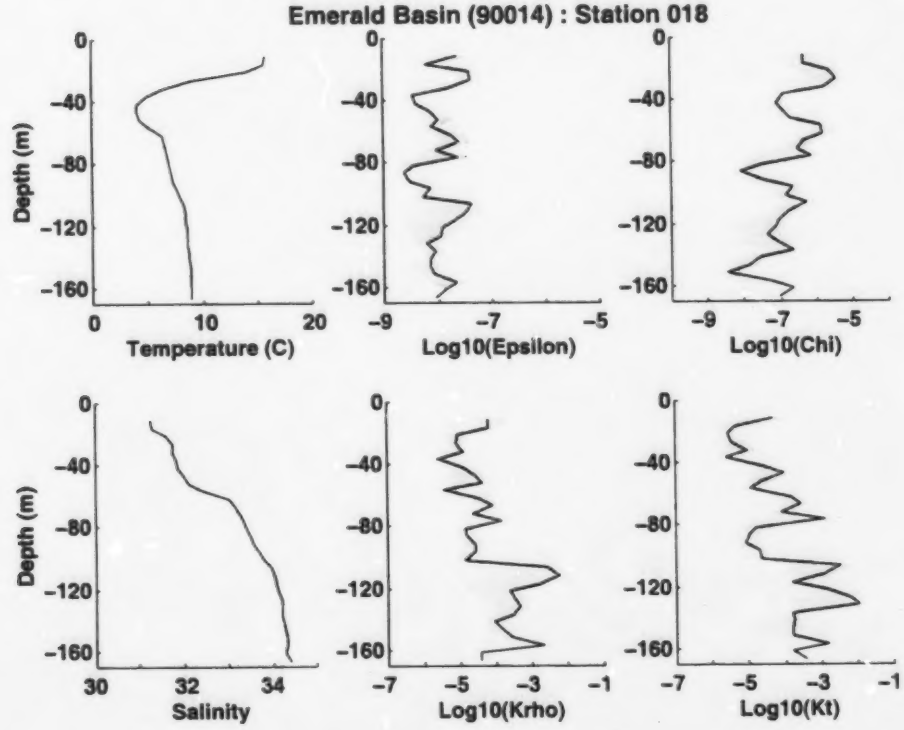
Emerald Basin (90014) : Station 018
Depth (m)
0
-40
-80
-120
-160
0
10
20
Temperature (C)
-9
-7
-5
Log10(Epsilon)
Log10(Chi)
30
32
34
Salinity
-7
-5
-3
-1
Log10(Krho)
Log10(Kt)

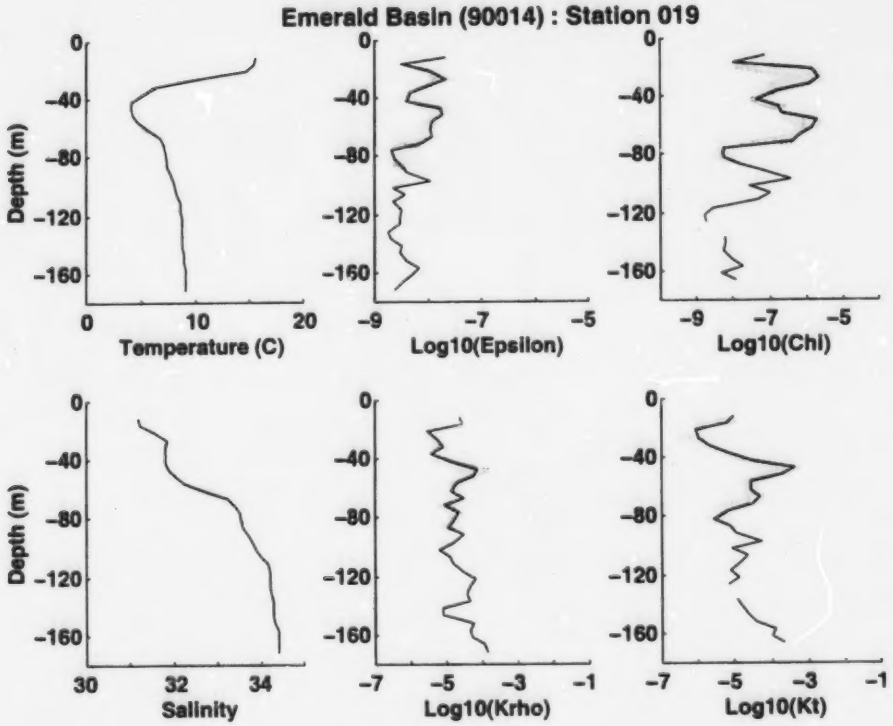
Emerald Basin (90014) : Station 019
Depth (m)
0
-40
-80
-120
-160
0
10
20
Temperature (C)
-9
-7
-5
Log10(Epsilon)
Log10(Chl)
30
32
34
Salinity
-7
-5
-3
-1
Log10(Krho)
Log10(Kt)

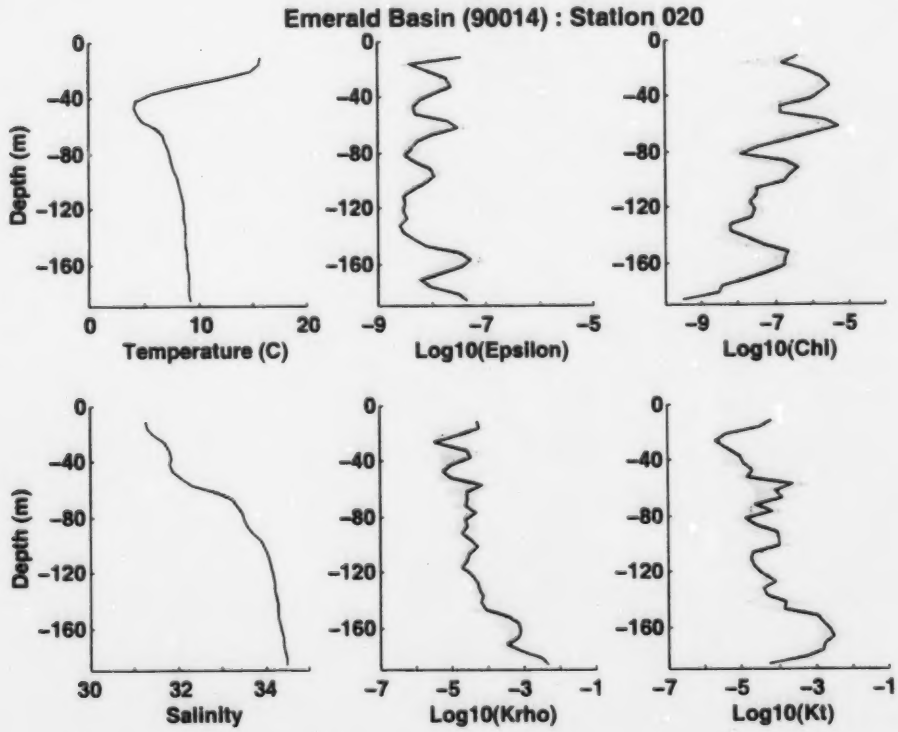
Emerald Basin (90014) : Station 020
Depth (m)
0
-40
-80
-120
-160
0
10
20
Temperature (C)
-9
-7
-5
Log10(Epsilon)
Log10(Chl)
30
32
34
Salinity
-7
-5
-3
-1
Log10(Krho)
Log10(Kt)

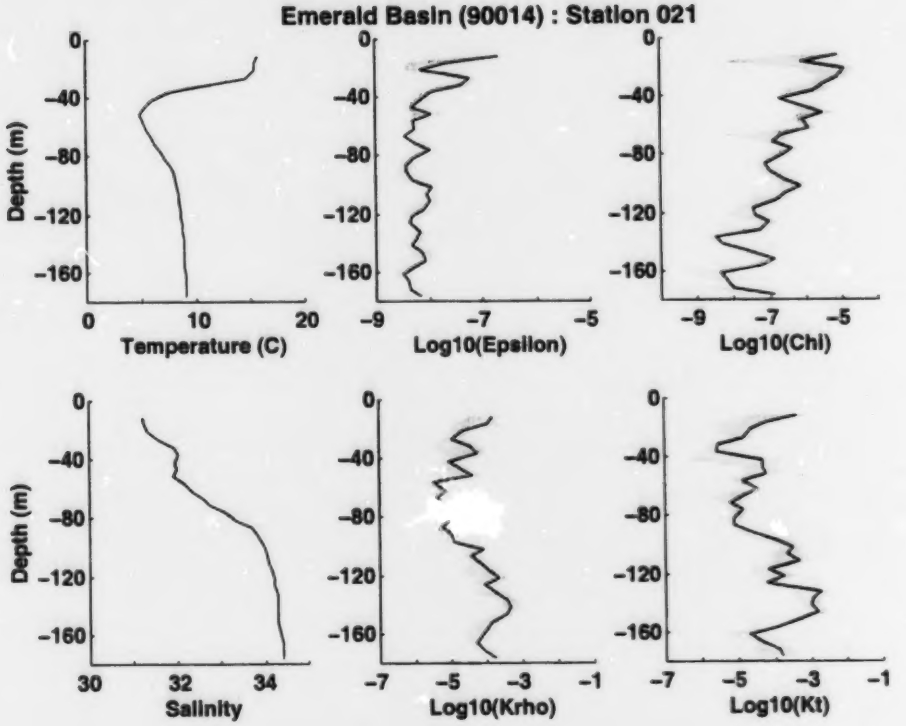
Emerald Basin (90014) : Station 021
Depth (m)
0
-40
-80
-120
-160
0
10
20
Temperature (C)
-9
-7
-5
Log10(Epsilon)
Log10(Chi)
30
32
34
Salinity
-7
-5
-3
-1
Log10(Krho)
Log10(Kt)

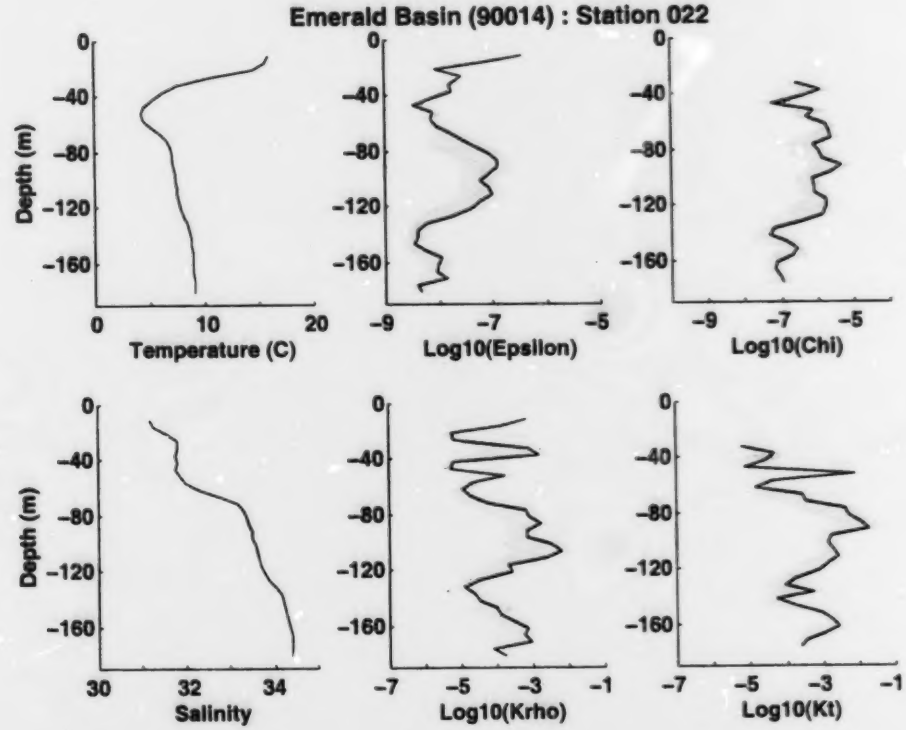
Emerald Basin (90014) : Station 022
Depth (m)
0
-40
-80
-120
-160
0
10
20
Temperature (C)
-9
-7
-5
Log10(Epsilon)
Log10(Chi)
30
32
34
Salinity
-7
-5
-3
-1
Log10(Krho)
Log10(Kt)

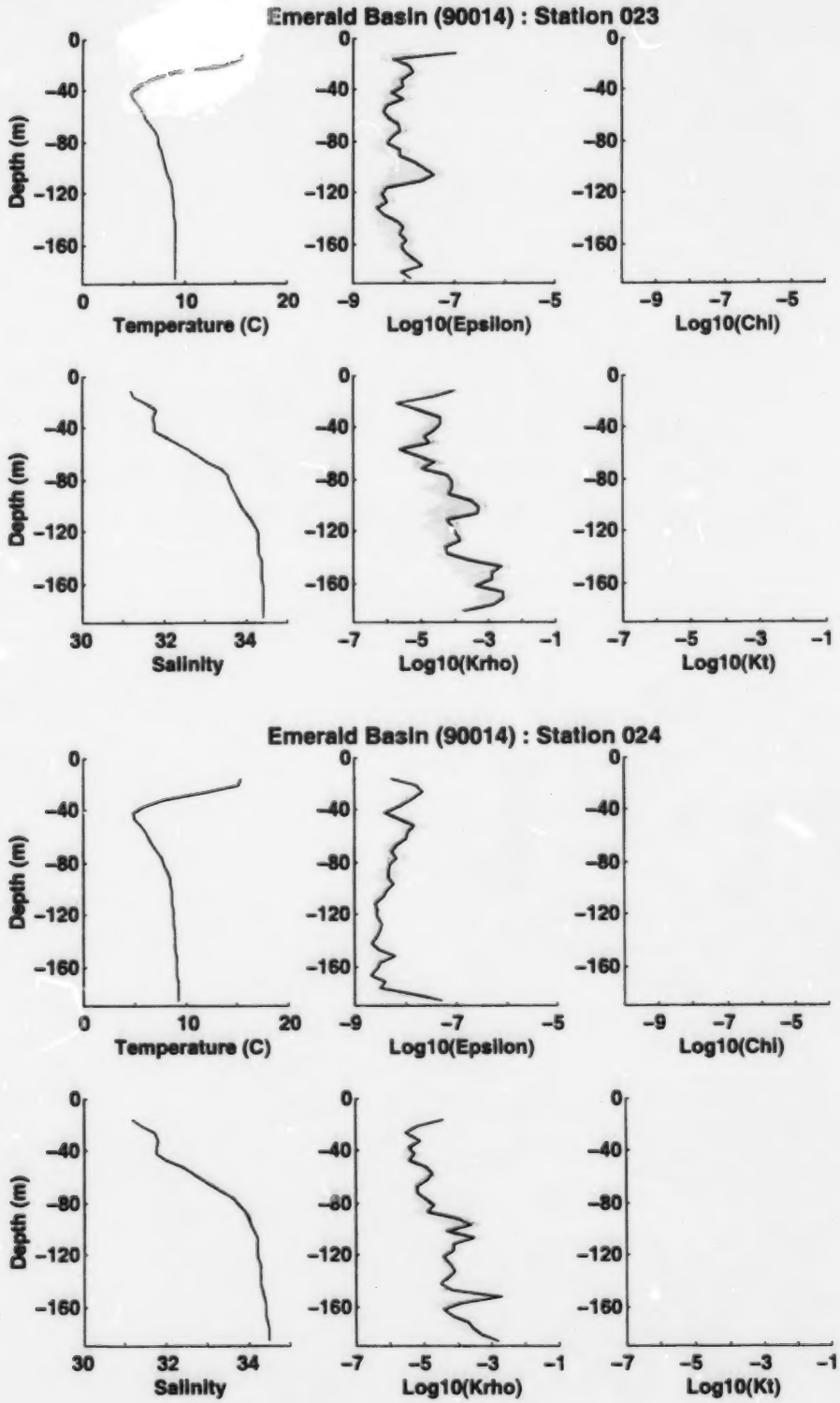
Emerald Basin (90014) : Station 023
Depth (m)
0
-40
-80
-120
-160
0
10
20
Temperature (C)
-9
-7
-5
Log10(Epsilon)
Log10(Chi)
30
32
34
Salinity
-7
-5
-3
-1
Log10(Krho)
Log10(Kt)
Emerald Basin (90014) : Station 024

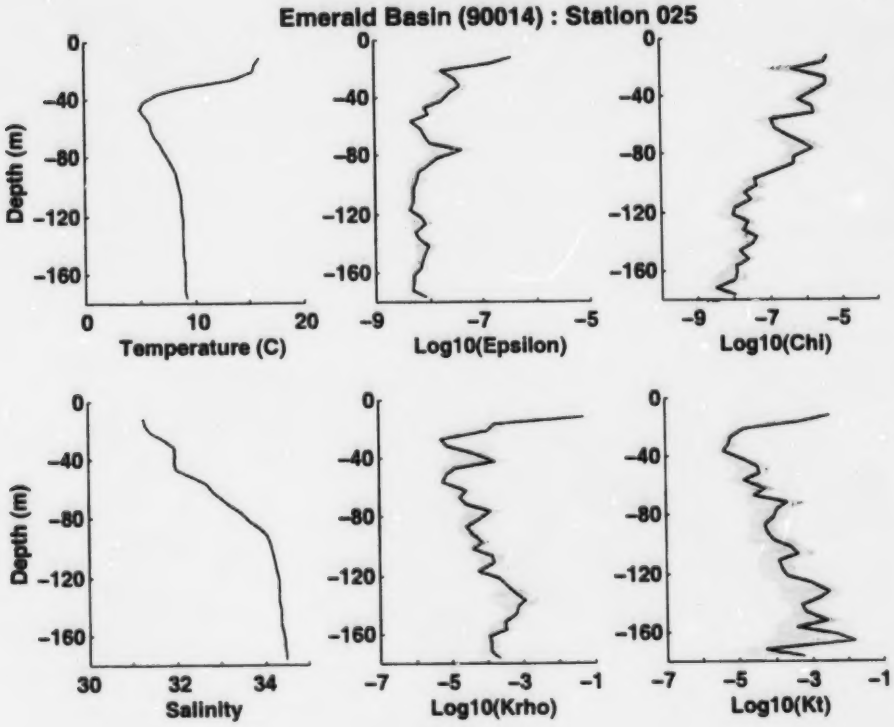
Emerald Basin (90014) : Station 025
Depth (m)
0
-40
-80
-120
-160
0
10
20
Temperature (C)
-9
-7
-5
Log10(Epsilon)
Log10(Chl)
30
32
34
Salinity
Log10(Krho)
Log10(Kt)

Appendix B: ADCP Time Series

An RDI Workhorse ADCP was moored at Station 2 on the Halifax Line for the period 30-Sept – 22 Nov, 2000. This upward-looking instrument was moored at mid-depth (approximately 80 m) in a water depth of 150 m. The ADCP was mounted in a streamline buoyancy float (SUBS) to minimize disturbances from the mean flow. The mooring extended above the ADCP to two SUBS at 14 m depth with Vemco Minilog temperature recorders spaced at 6 m intervals along this section of the mooring. Measurement of current speed and direction were made with the ADCP every 15 minutes in 2 meter depth bins. This appendix includes time series plots of speed and direction from each of the depth bins of the moored ADCP. The plots have been divided into three time periods (30 Sept – 17 Oct; 18 Oct – 4 Nov; 5 Nov – 22 Nov) to allow sufficient resolution in the time axis. The legend in each panel represents the mid-point depth of the bin. The bins above 6.29 m have not been plotted due to the limitations of the ADCP to measure velocities near the ocean surface.

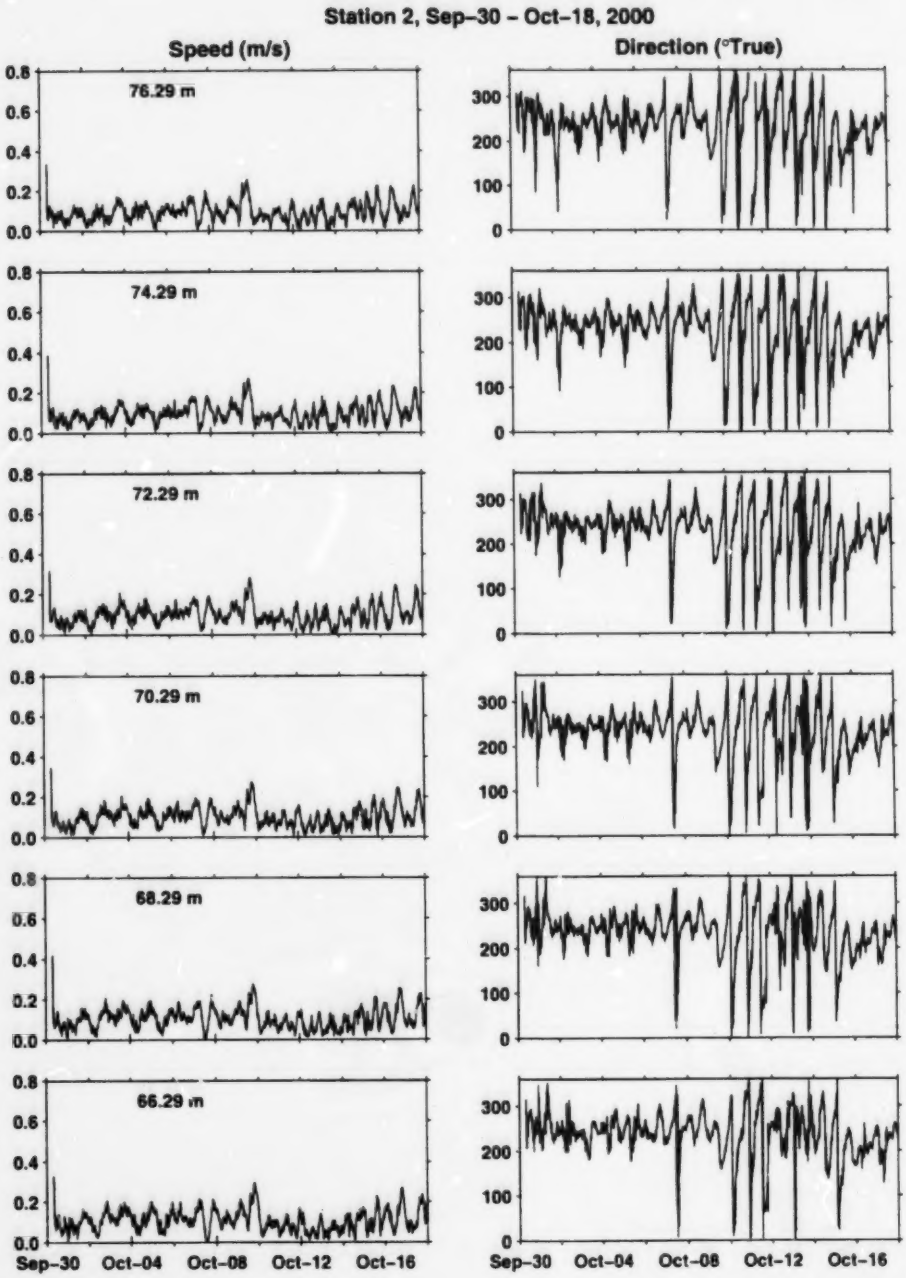
Station 2, Sep–30 – Oct–18, 2000
Speed (m/s)
Direction (°True)
76.29 m
74.29 m
72.29 m
70.29 m
68.29 m
66.29 m
0.0
0.2
0.4
0.6
0.8
0
100
200
300
Sep–30
Oct–04
Oct–08
Oct–12
Oct–16

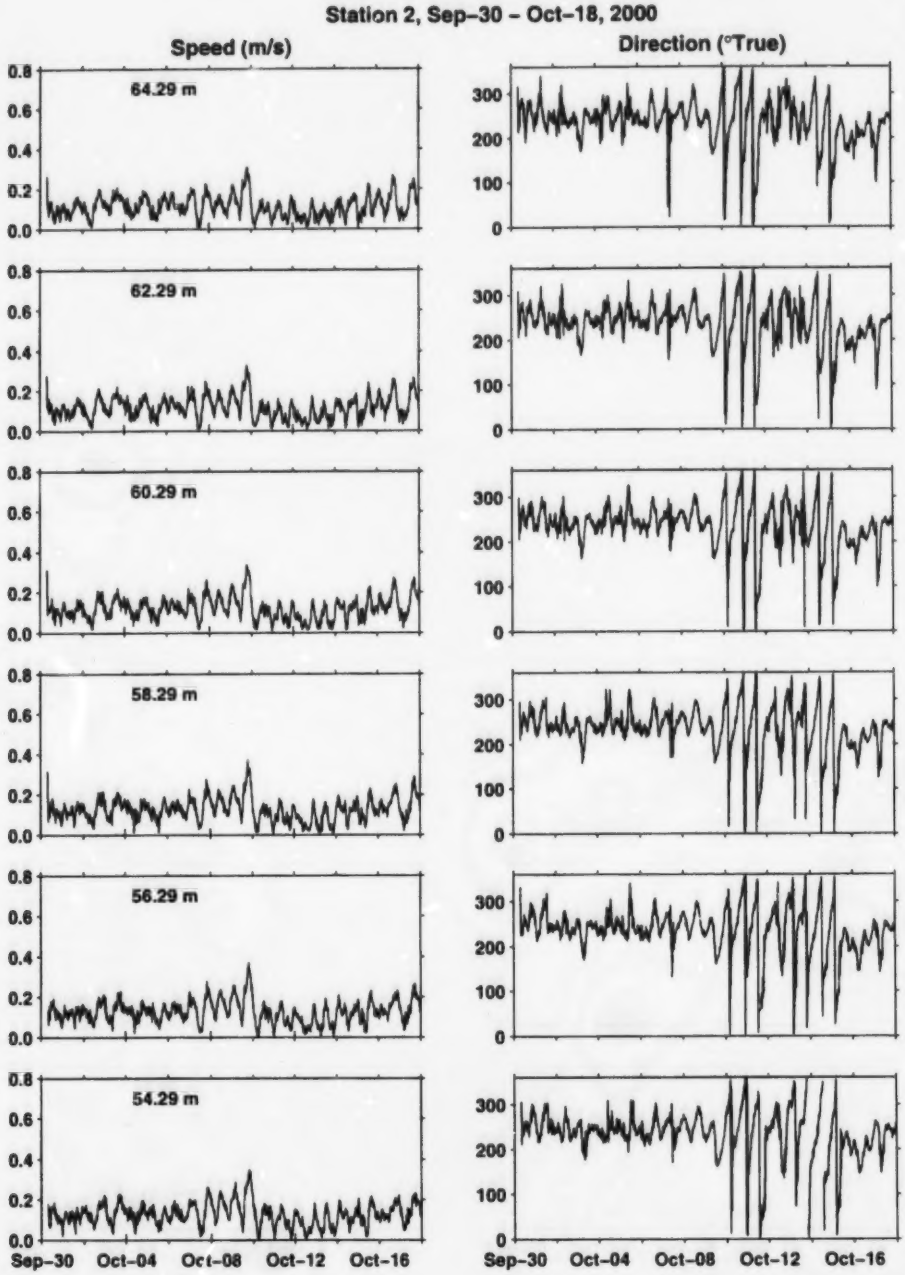
Station 2, Sep–30 – Oct–18, 2000
Speed (m/s)
Direction (°True)
64.29 m
62.29 m
60.29 m
58.29 m
56.29 m
54.29 m
0.0
0.2
0.4
0.6
0.8
0
100
200
300
Sep–30
Oct–04
Oct–08
Oct–12
Oct–16

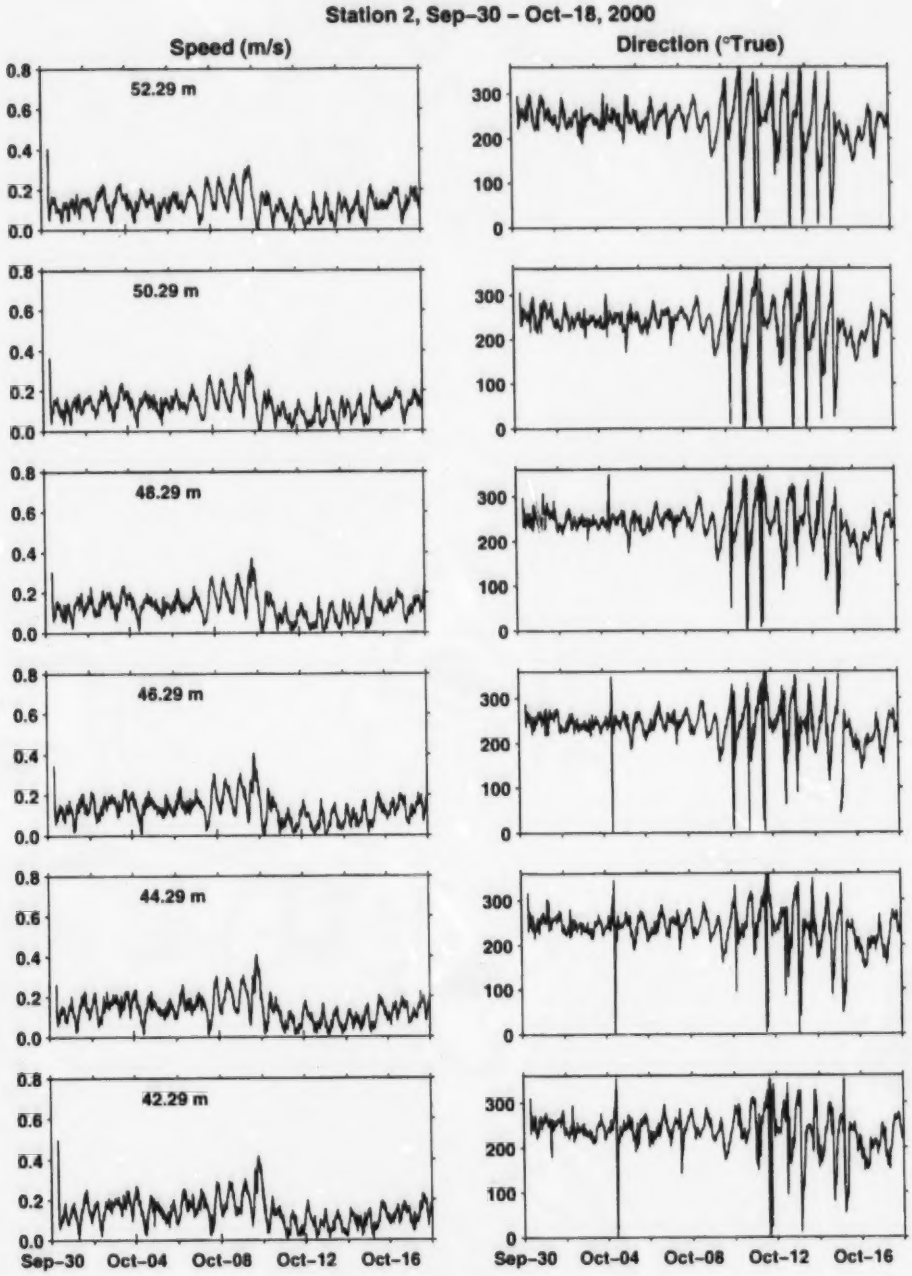
Station 2, Sep–30 – Oct–18, 2000
Speed (m/s)
Direction (°True)
52.29 m
50.29 m
48.29 m
46.29 m
44.29 m
42.29 m
0.0
0.2
0.4
0.6
0.8
0
100
200
300
Sep–30
Oct–04
Oct–08
Oct–12
Oct–16

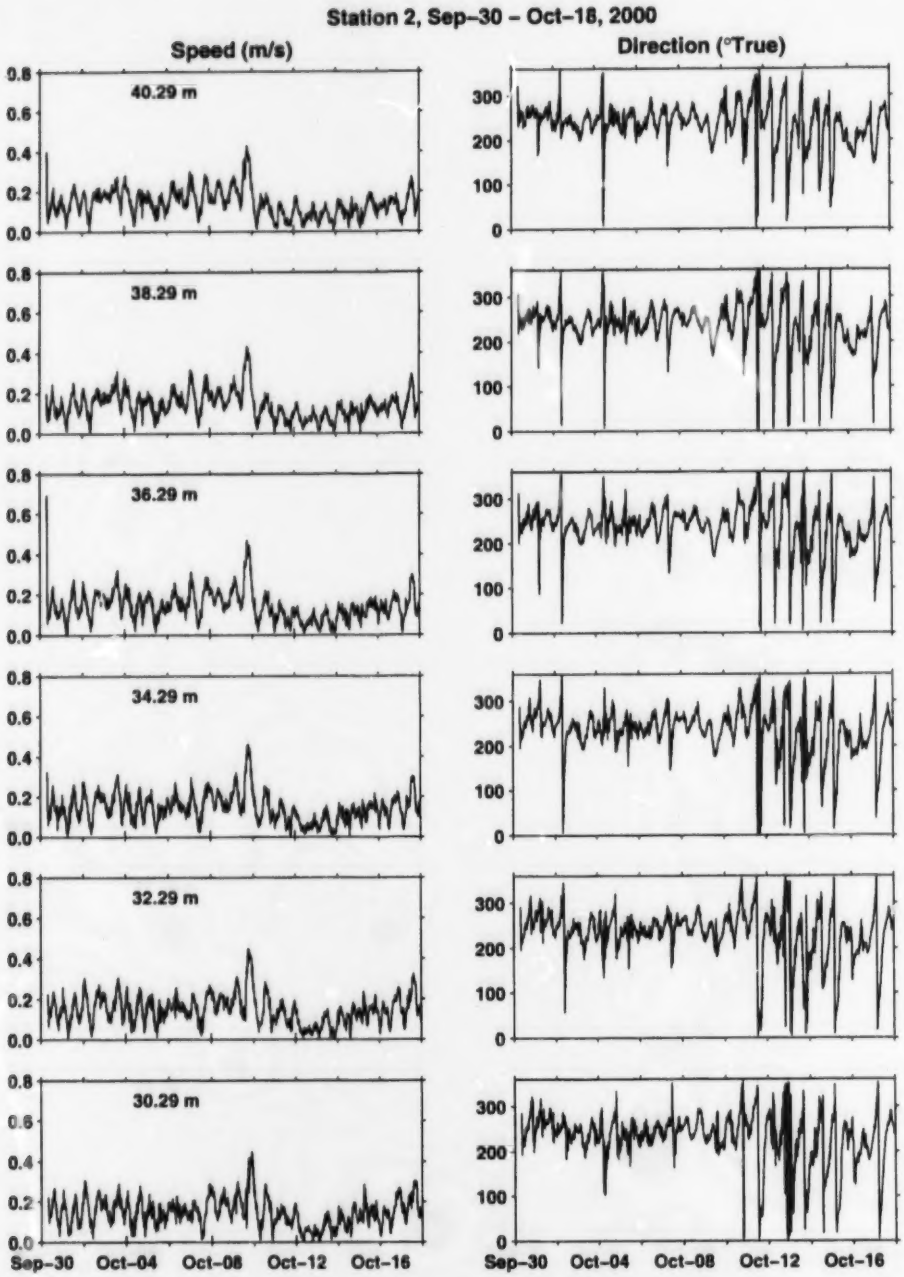
Station 2, Sep–30 – Oct–18, 2000
Speed (m/s)
Direction (°True)
40.29 m
38.29 m
36.29 m
34.29 m
32.29 m
30.29 m
0.0
0.2
0.4
0.6
0.8
0
100
200
300
Sep–30
Oct–04
Oct–08
Oct–12
Oct–16

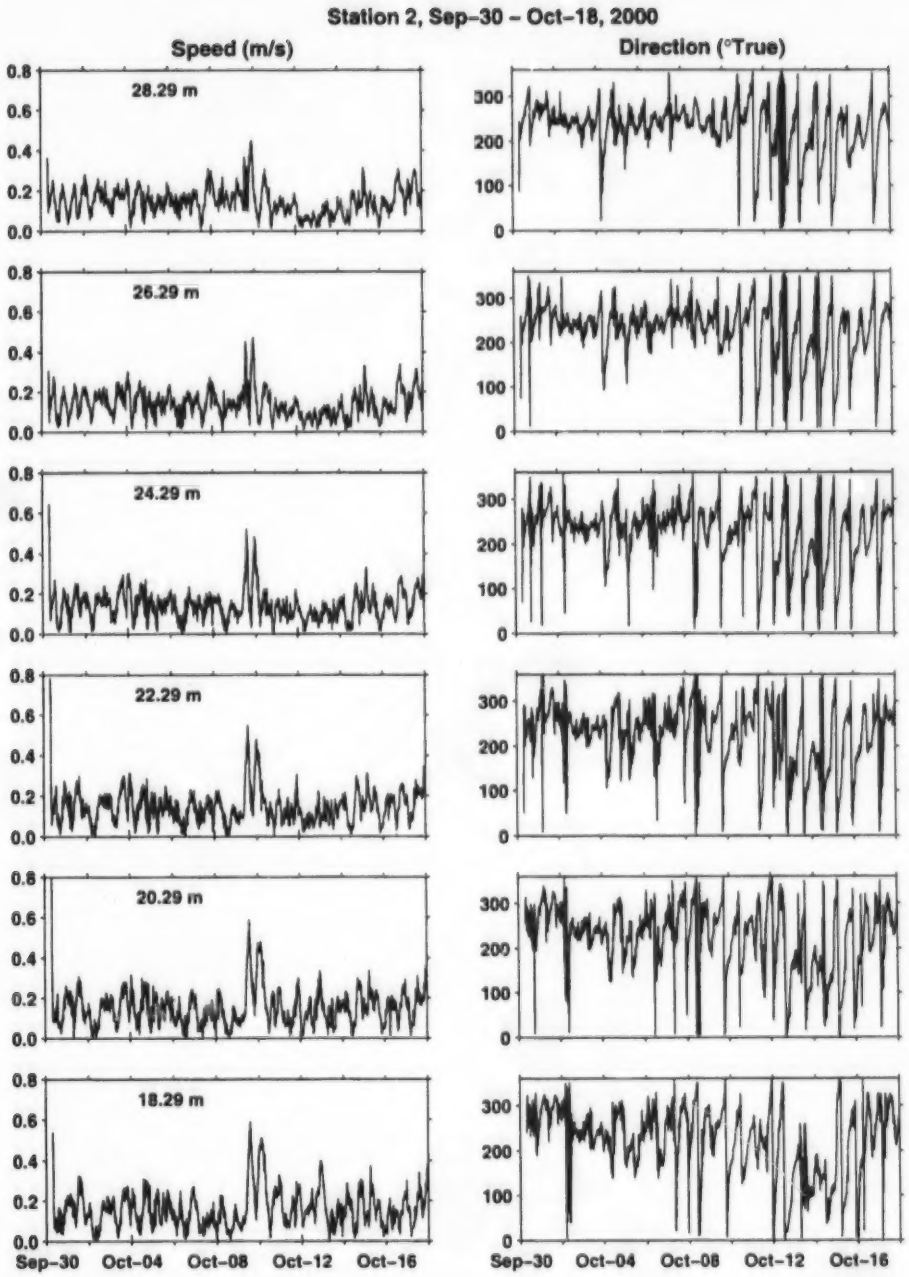
Station 2, Sep-30 – Oct-18, 2000
Speed (m/s)
Direction (°True)
28.29 m
26.29 m
24.29 m
22.29 m
20.29 m
18.29 m
0.0
0.2
0.4
0.6
0.8
0
100
200
300
Sep-30
Oct-04
Oct-08
Oct-12
Oct-16

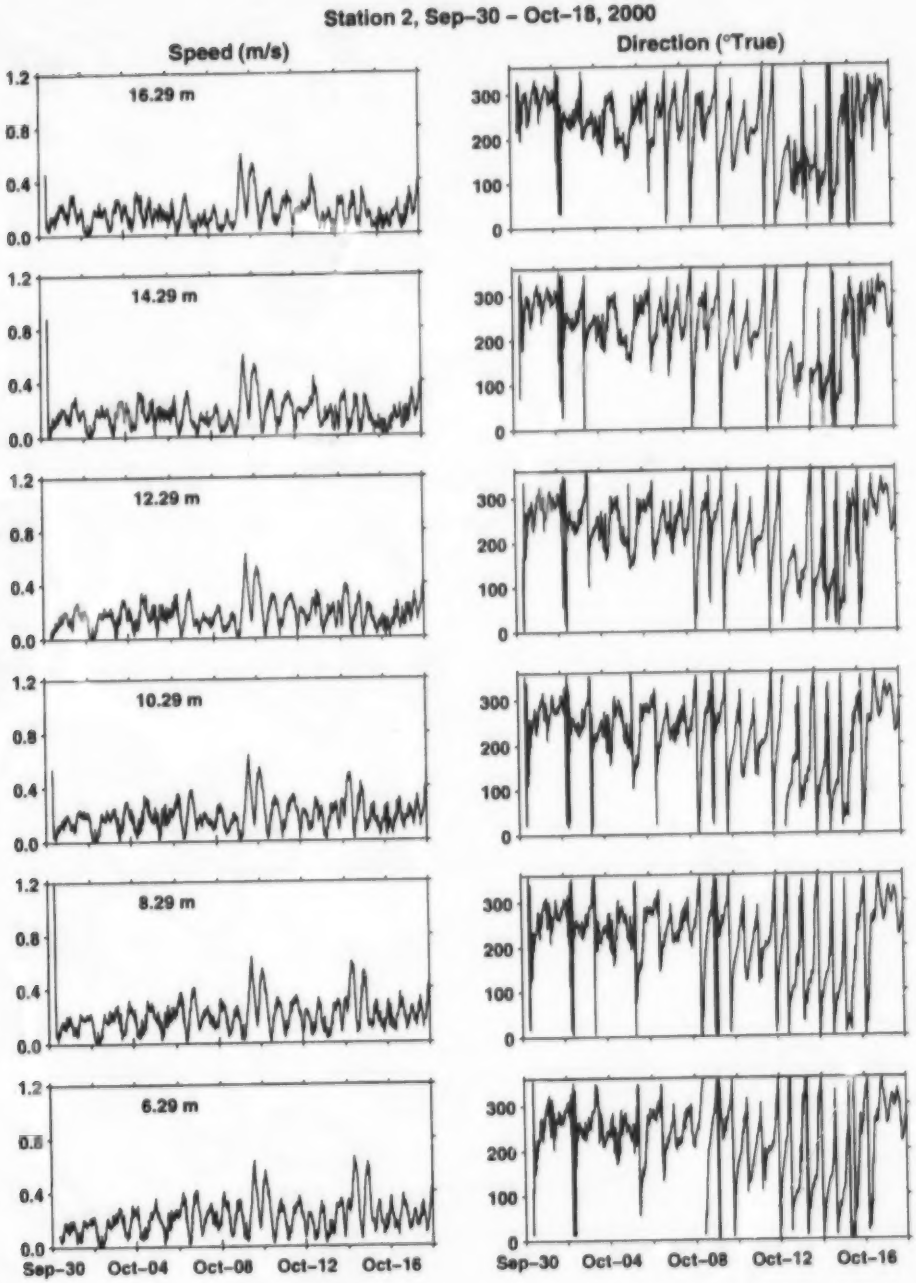
Station 2, Sep–30 – Oct–18, 2000
Speed (m/s)
Direction (°True)
16.29 m
14.29 m
12.29 m
10.29 m
8.29 m
6.29 m
1.2
0.8
0.4
0.0
300
200
100
0
Sep–30
Oct–04
Oct–08
Oct–12
Oct–16

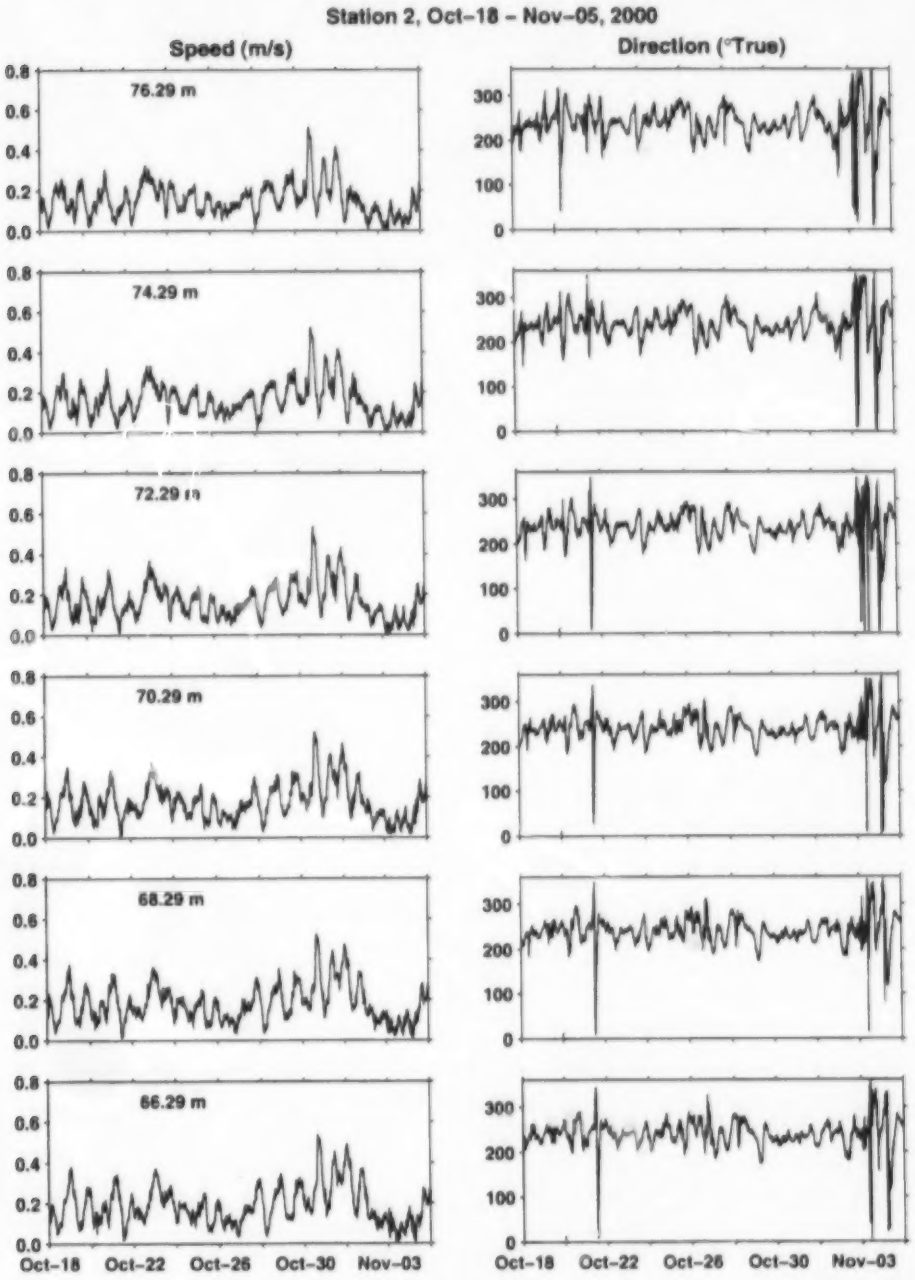
Station 2, Oct-18 - Nov-05, 2000
Speed (m/s)
Direction (°True)
76.29 m
74.29 m
72.29 m
70.29 m
68.29 m
66.29 m
0.0
0.2
0.4
0.6
0.8
0
100
200
300
Oct-18
Oct-22
Oct-26
Oct-30
Nov-03

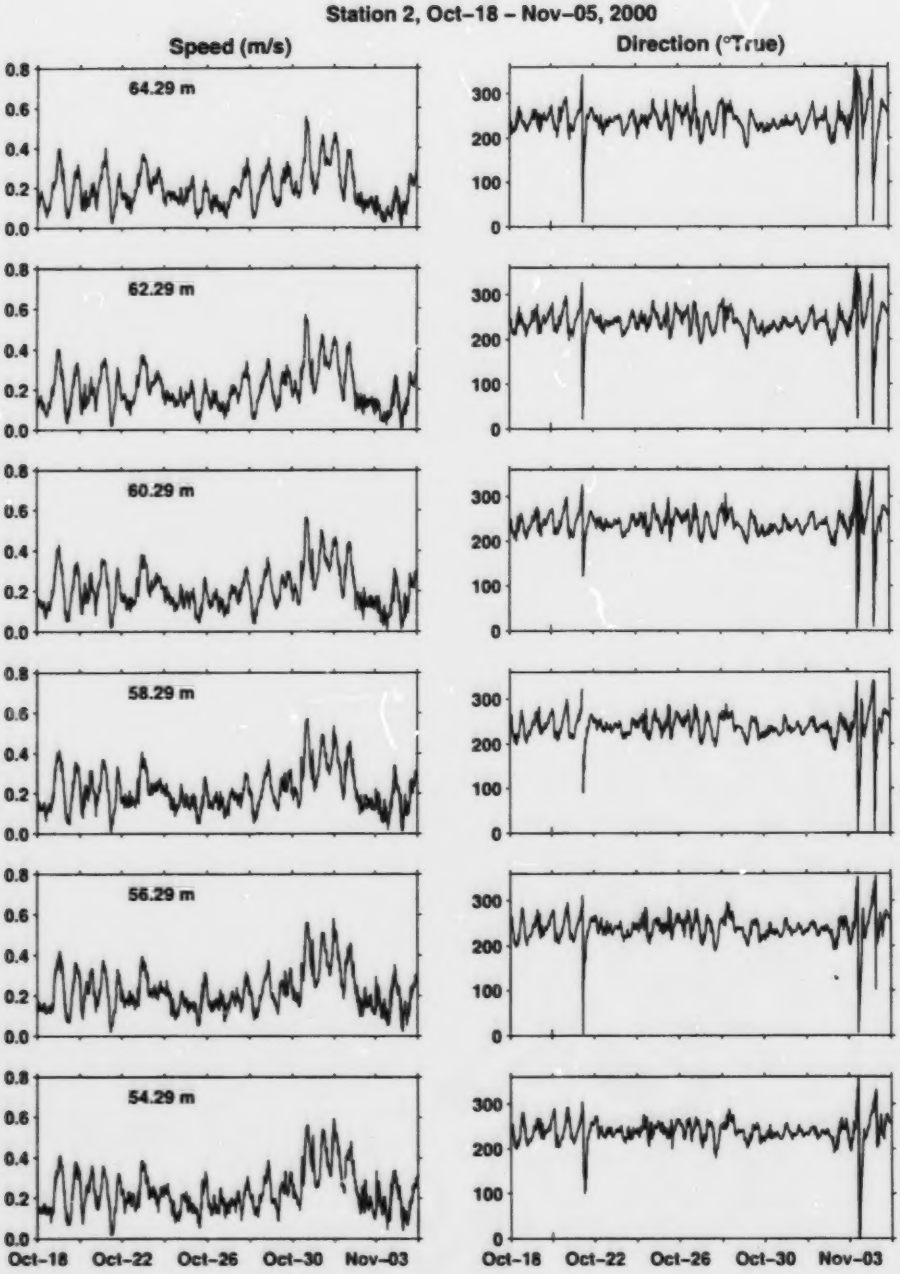
Station 2, Oct-18 – Nov-05, 2000
Speed (m/s)
Direction (°True)
64.29 m
62.29 m
60.29 m
58.29 m
56.29 m
54.29 m
0.0
0.2
0.4
0.6
0.8
0
100
200
300
Oct-18
Oct-22
Oct-26
Oct-30
Nov-03

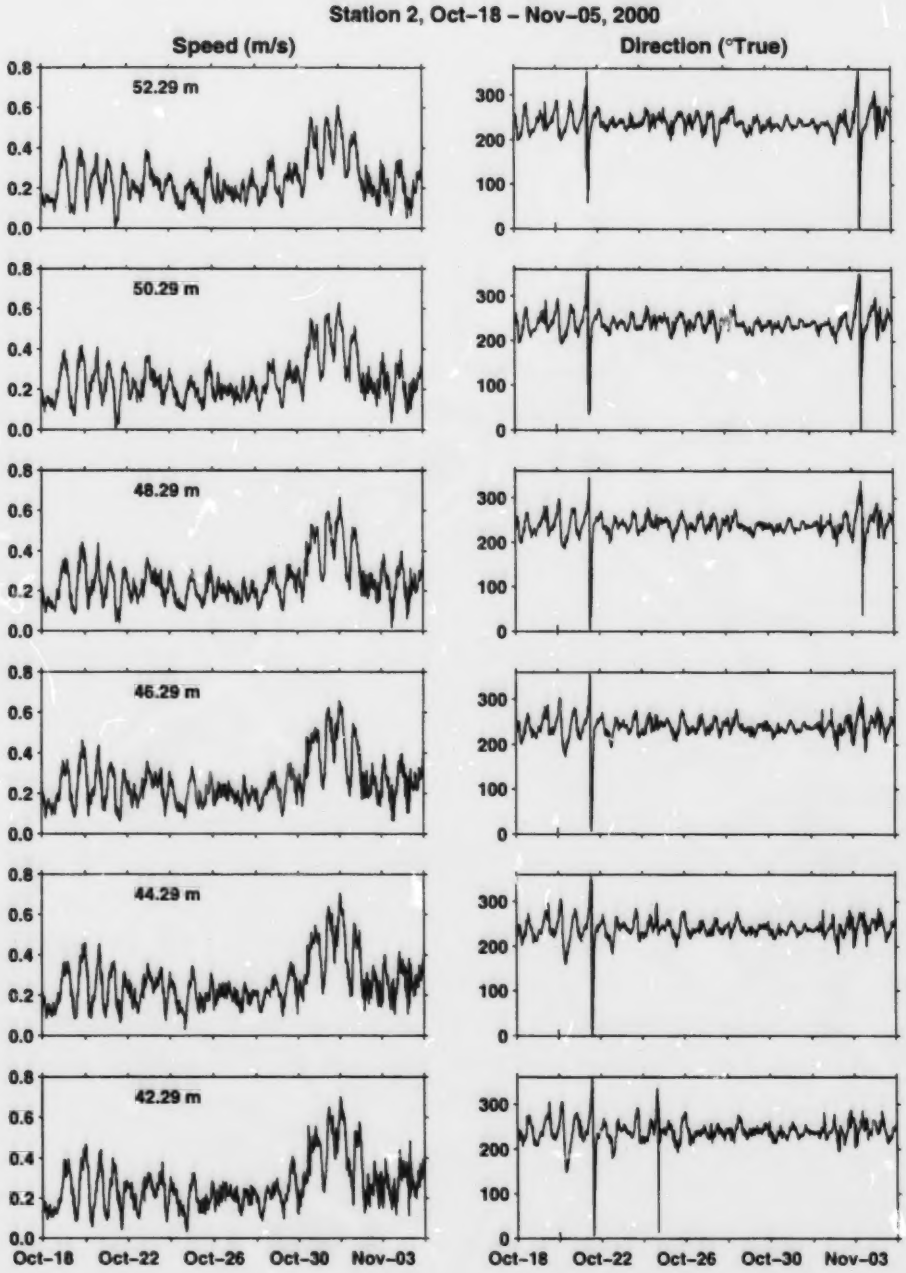
Station 2, Oct–18 – Nov–05, 2000
Speed (m/s)
Direction (°True)
52.29 m
50.29 m
48.29 m
46.29 m
44.29 m
42.29 m
0.0
0.2
0.4
0.6
0.8
0
100
200
300
Oct–18
Oct–22
Oct–26
Oct–30
Nov–03

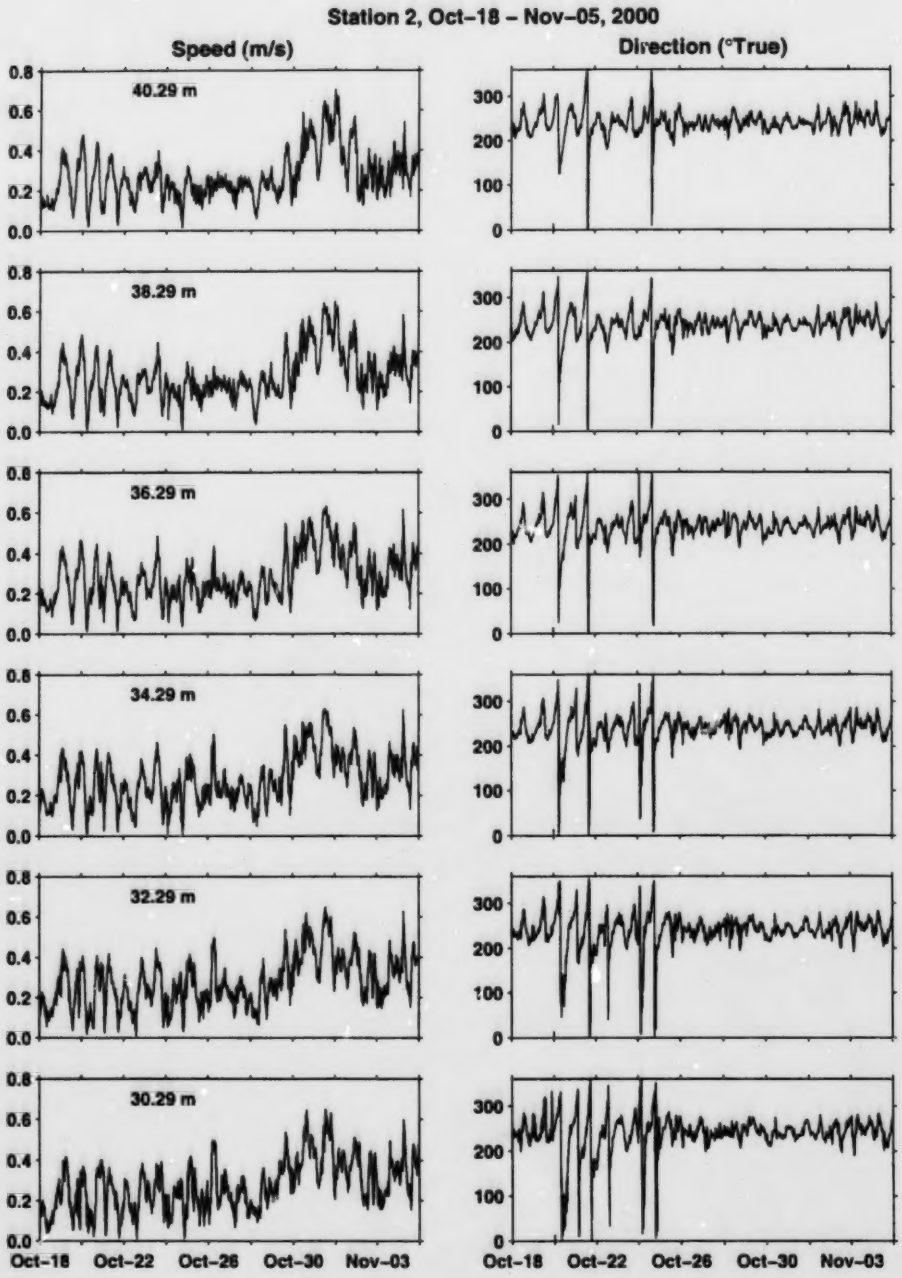
Station 2, Oct–18 – Nov–05, 2000
Speed (m/s)
Direction (°True)
40.29 m
38.29 m
36.29 m
34.29 m
32.29 m
30.29 m
0.0
0.2
0.4
0.6
0.8
0
100
200
300
Oct–18
Oct–22
Oct–26
Oct–30
Nov–03

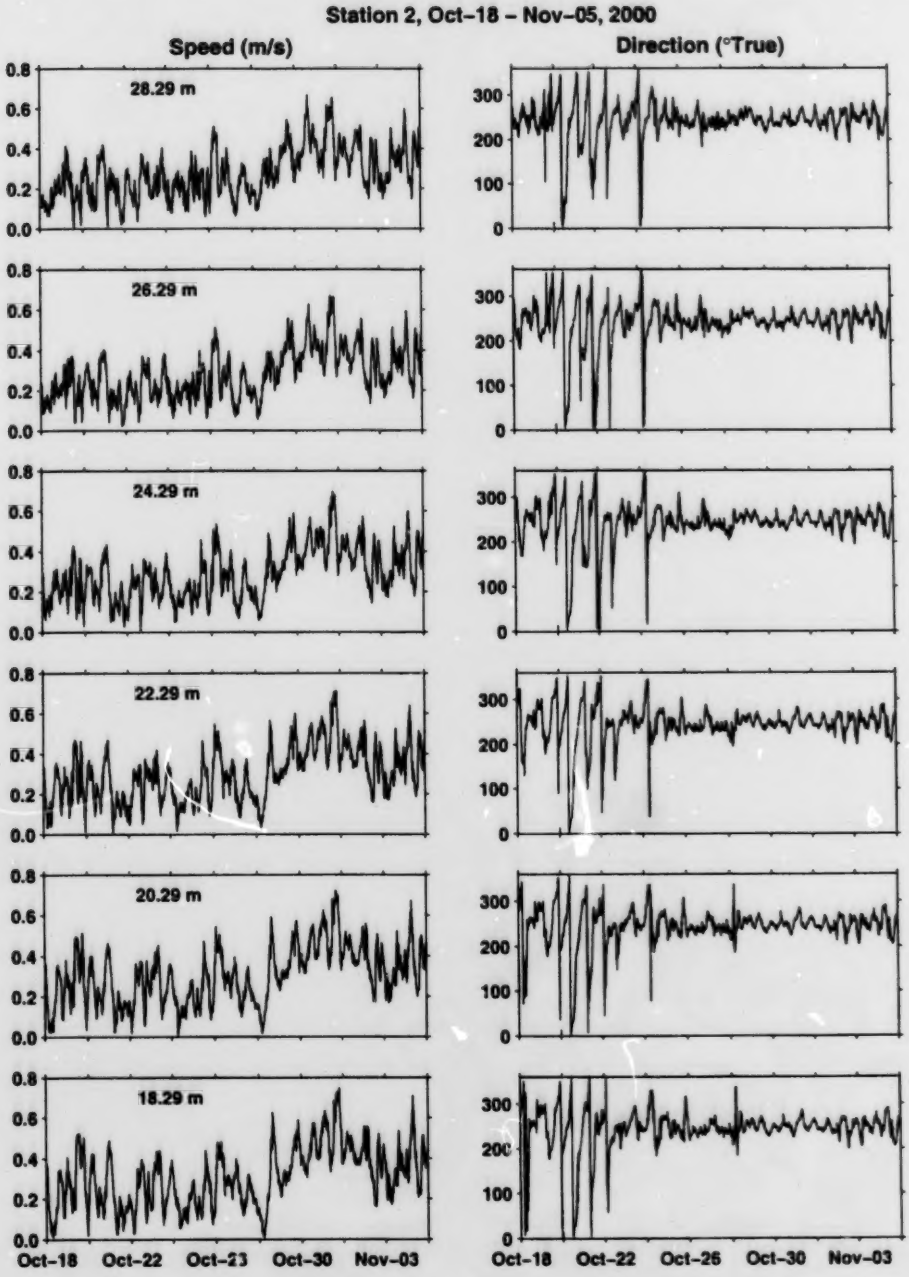
Station 2, Oct-18 – Nov-05, 2000
Speed (m/s)
Direction (°True)
28.29 m
26.29 m
24.29 m
22.29 m
20.29 m
18.29 m
0.0
0.2
0.4
0.6
0.8
0
100
200
300
Oct-18
Oct-22
Oct-23
Oct-26
Oct-30
Nov-03

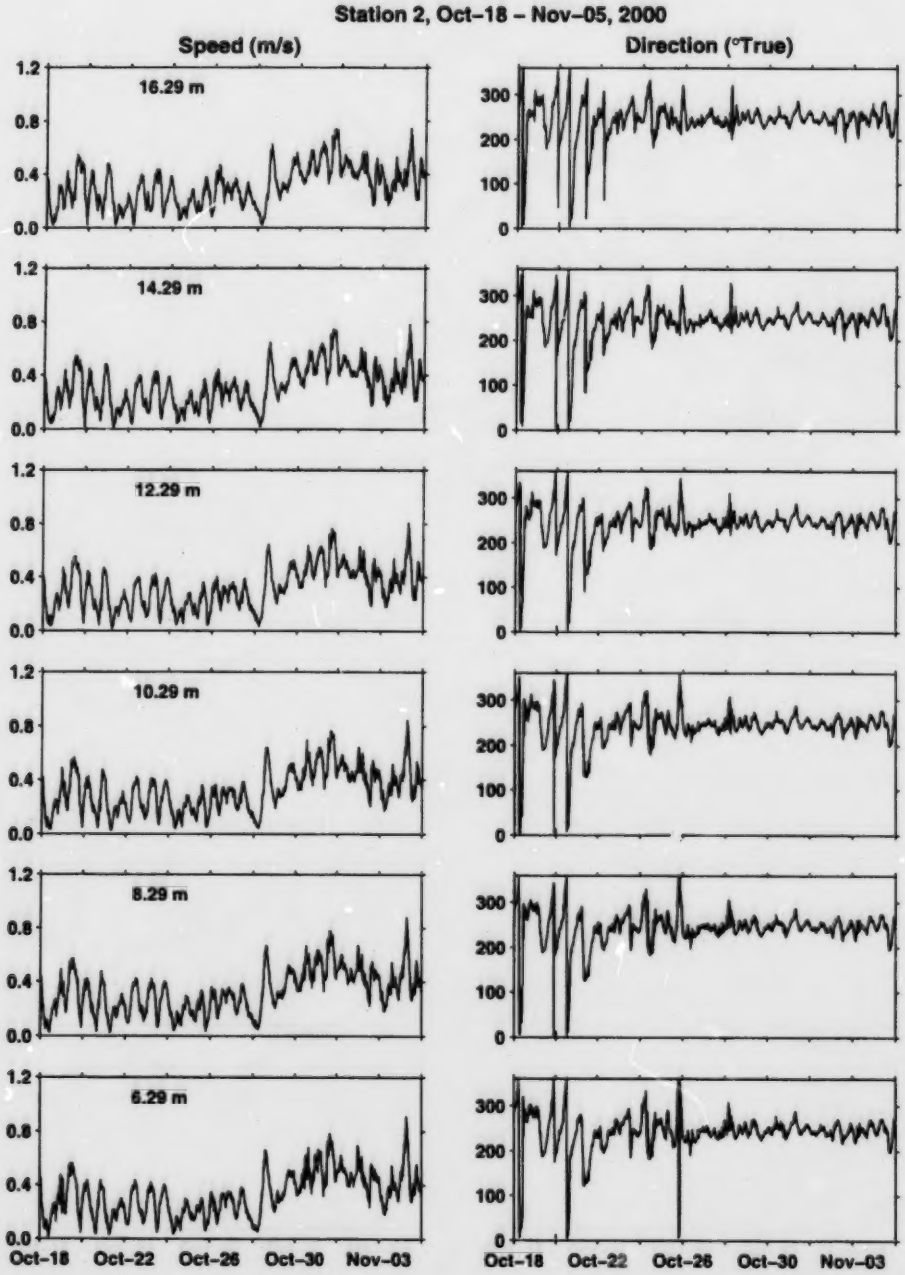
Station 2, Oct–18 – Nov–05, 2000
Speed (m/s)
Direction (°True)
16.29 m
14.29 m
12.29 m
10.29 m
8.29 m
6.29 m
1.2
0.8
0.4
0.0
300
200
100
0
Oct–18
Oct–22
Oct–26
Oct–30
Nov–03

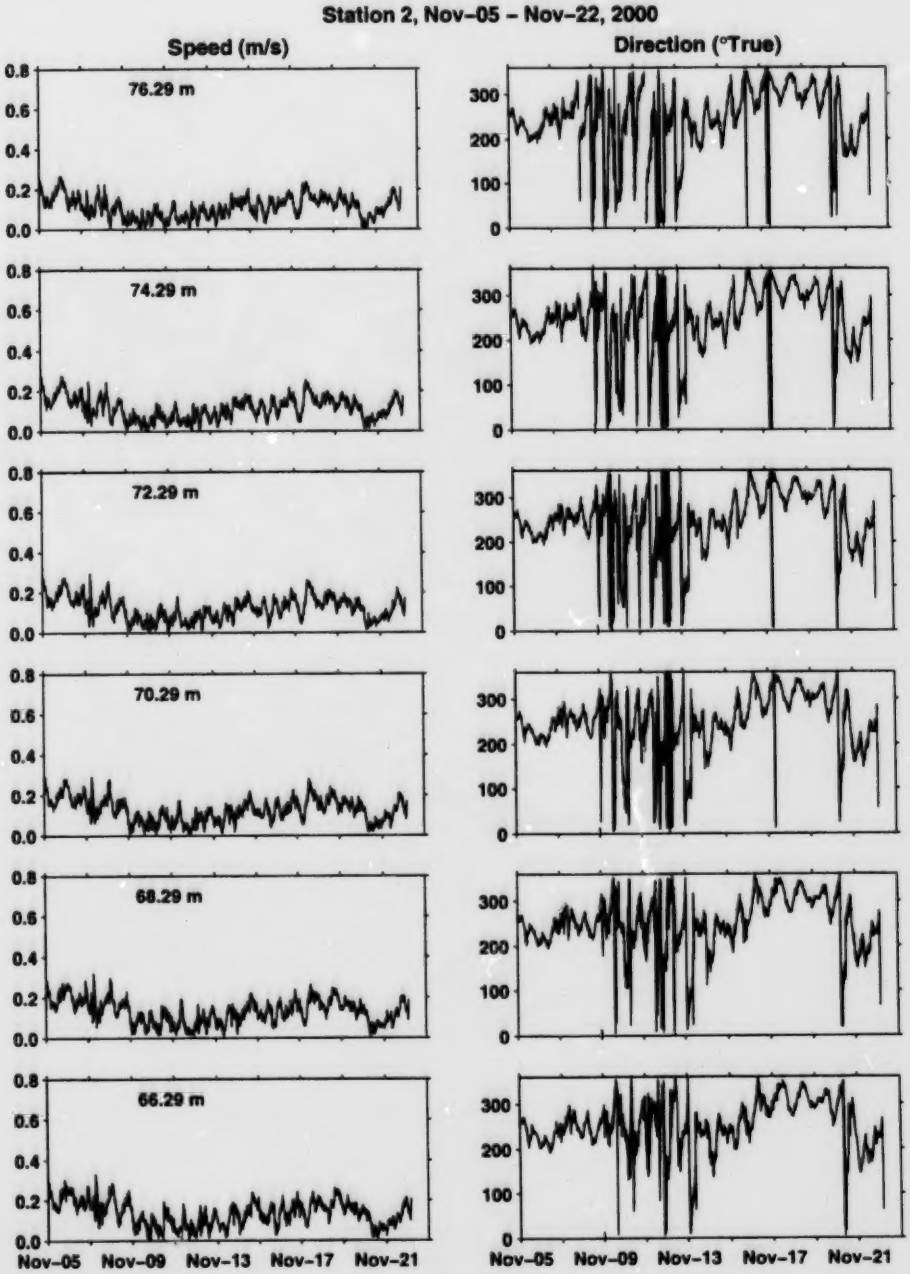
Station 2, Nov-05 – Nov-22, 2000
Speed (m/s)
Direction (°True)
76.29 m
74.29 m
72.29 m
70.29 m
68.29 m
66.29 m
0.0
0.2
0.4
0.6
0.8
0
100
200
300
Nov-05
Nov-09
Nov-13
Nov-17
Nov-21

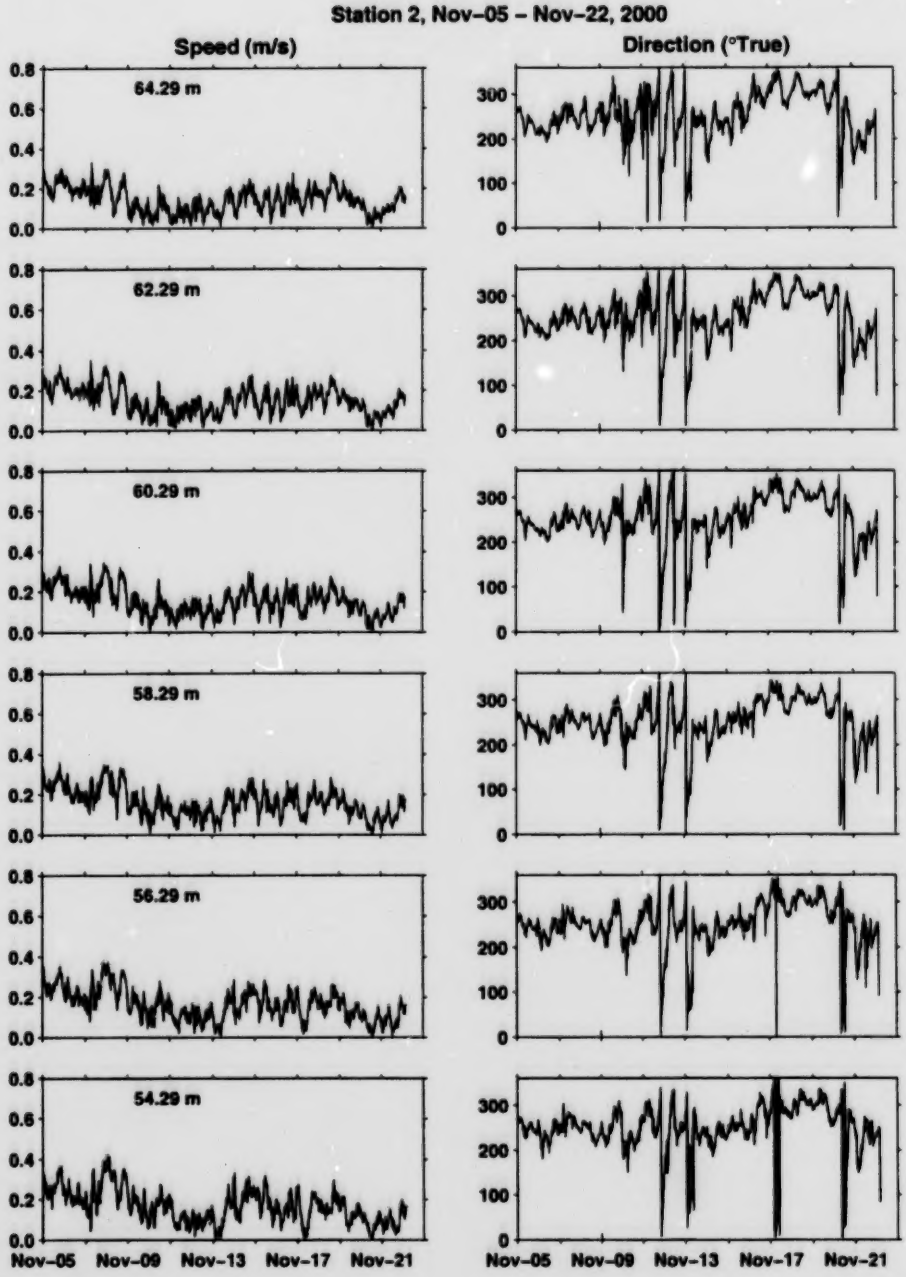
Station 2, Nov-05 – Nov-22, 2000
Speed (m/s)
Direction (°True)
64.29 m
62.29 m
60.29 m
58.29 m
56.29 m
54.29 m
0.0
0.2
0.4
0.6
0.8
0
100
200
300
Nov-05
Nov-09
Nov-13
Nov-17
Nov-21

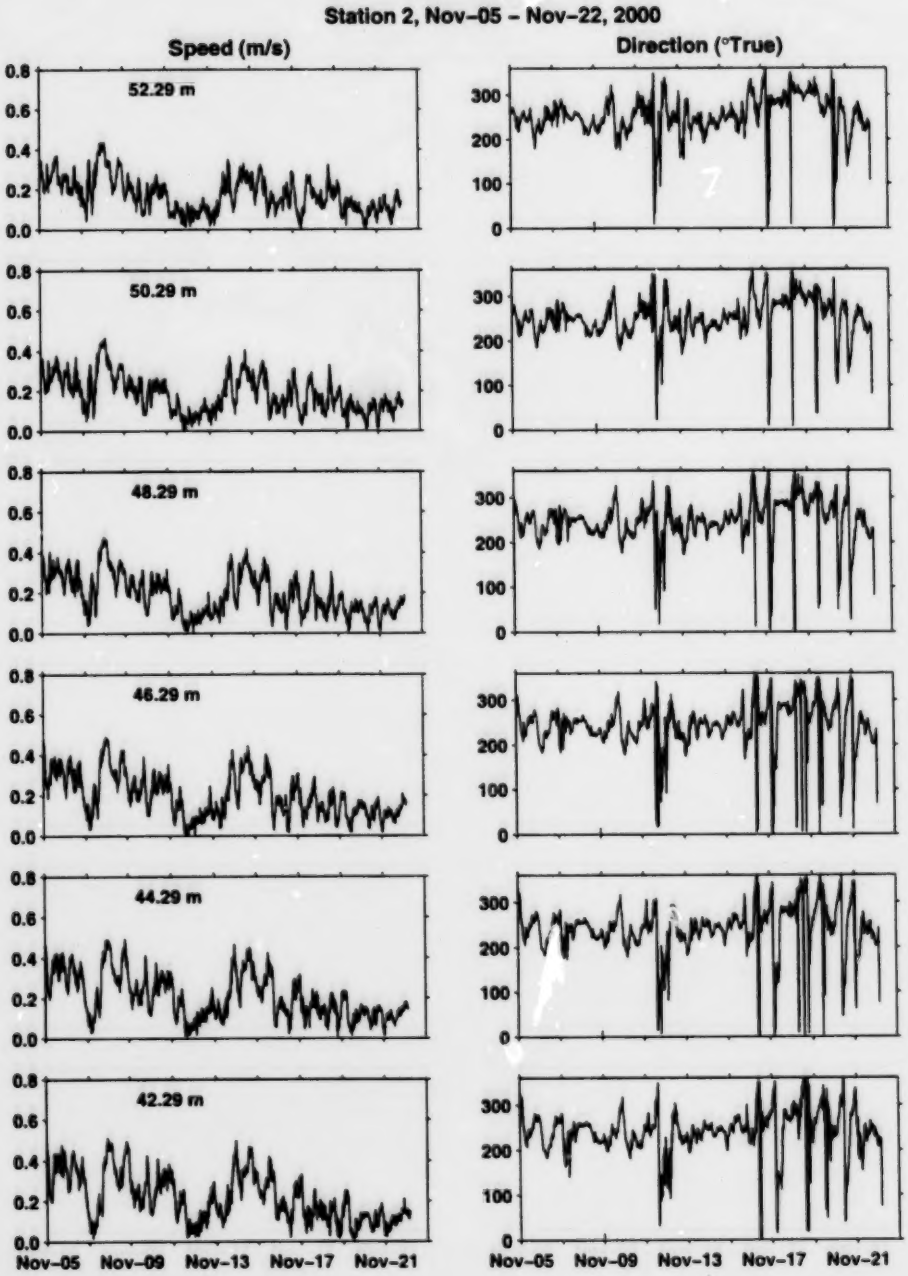
Station 2, Nov-05 - Nov-22, 2000
Speed (m/s)
Direction (°True)
52.29 m
50.29 m
48.29 m
46.29 m
44.29 m
42.29 m
0.0
0.2
0.4
0.6
0.8
0
100
200
300
Nov-05
Nov-09
Nov-13
Nov-17
Nov-21

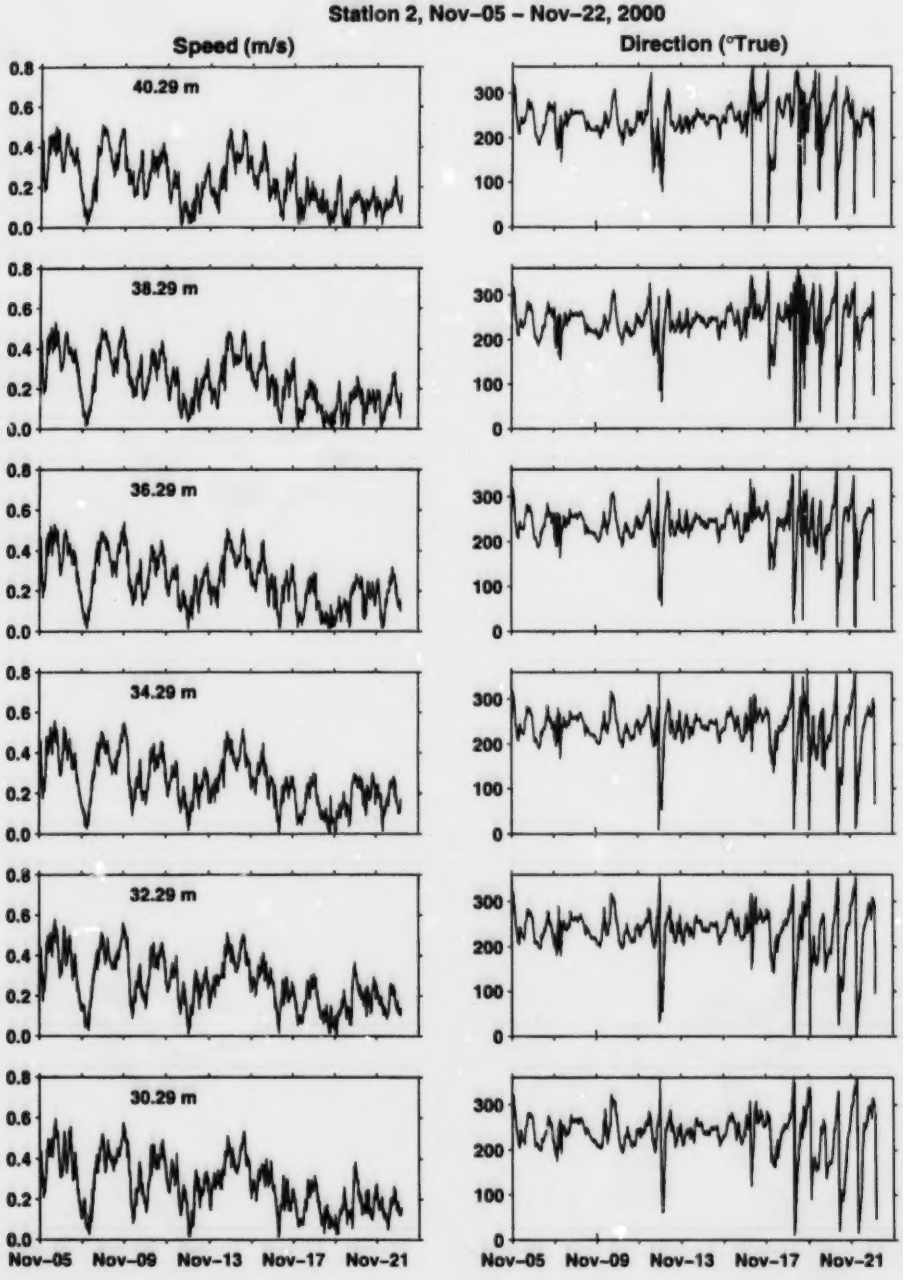
Station 2, Nov-05 – Nov-22, 2000
Speed (m/s)
Direction (°True)
40.29 m
38.29 m
36.29 m
34.29 m
32.29 m
30.29 m
0.0
0.2
0.4
0.6
0.8
0
100
200
300
Nov-05
Nov-09
Nov-13
Nov-17
Nov-21

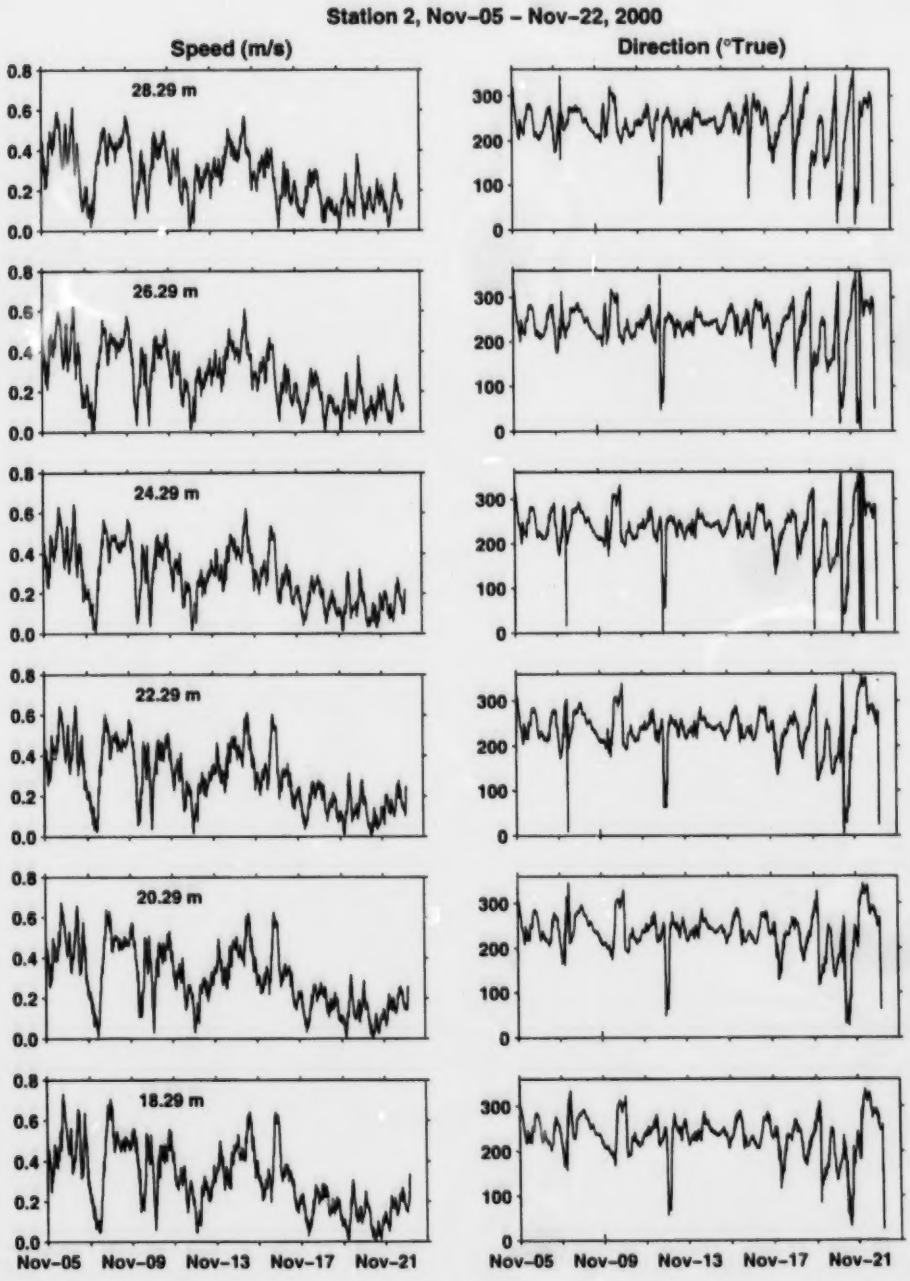
Station 2, Nov-05 – Nov-22, 2000
Speed (m/s)
Direction (°True)
28.29 m
26.29 m
24.29 m
22.29 m
20.29 m
18.29 m
0.0
0.2
0.4
0.6
0.8
0
100
200
300
Nov-05
Nov-09
Nov-13
Nov-17
Nov-21

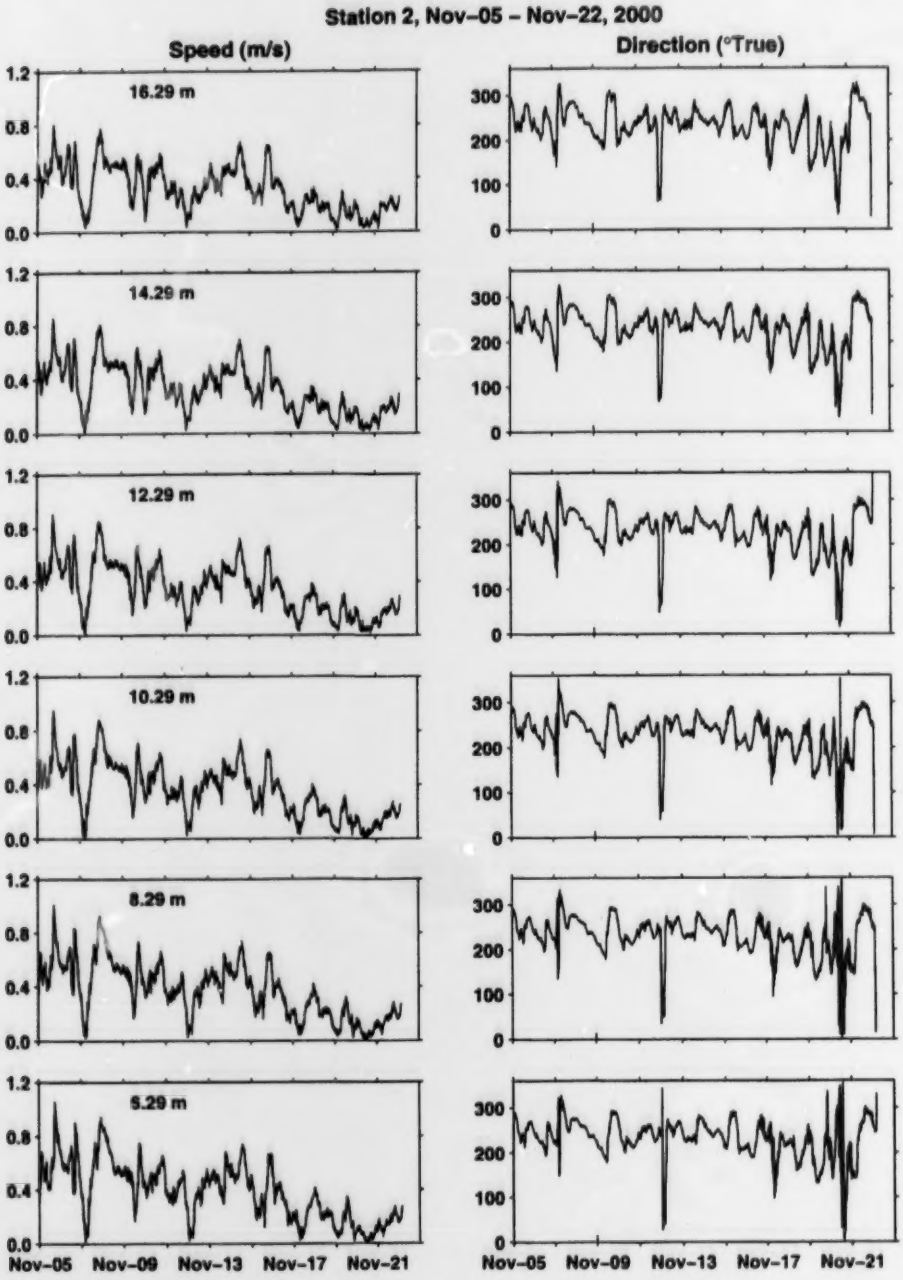
Station 2, Nov-05 – Nov-22, 2000
Speed (m/s)
Direction (°True)
16.29 m
14.29 m
12.29 m
10.29 m
8.29 m
5.29 m
1.2
0.8
0.4
0.0
300
200
100
0
Nov-05
Nov-09
Nov-13
Nov-17
Nov-21